JUN 1-4 1945

VOLUME 101 NUMBER 3

THE ASTROPHYSICAL JOURNAL

AN INTERNATIONAL REVIEW OF SPECTROSCOPY AND ASTRONOMICAL PHYSICS

Founded in 1895 by GEORGE E. HALE *and* JAMES E. KEELER

Edited by

OTTO STRUVE
Managing Editor
Yerkes Observatory of the University of Chicago

S. CHANDRASEKHAR
Associate Managing Editor
Yerkes Observatory of the University of Chicago

PAUL W. MERRILL
Mount Wilson Observatory of the Carnegie Institution of Washington

HARLOW SHAPLEY
Harvard College Observatory
Cambridge, Massachusetts

J. H. MOORE
Lick Observatory
University of California

MAY 1945

THE UNIVERSITY OF CHICAGO PRESS
CHICAGO, ILLINOIS, U.S.A.

May 1945 Vol. 101, No. 3

THE ASTROPHYSICAL JOURNAL

AN INTERNATIONAL REVIEW OF SPECTROSCOPY AND ASTRONOMICAL PHYSICS

Edited by

OTTO STRUVE
Managing Editor

S. CHANDRASEKHAR
Associate Managing Editor

Yerkes Observatory of the University of Chicago

PAUL W. MERRILL
Mount Wilson Observatory of the Carnegie Institution of Washington

HARLOW SHAPLEY
Harvard College Observatory
Cambridge, Massachusetts

J. H. MOORE
Lick Observatory
University of California

With the Collaboration of the American Astronomical Society

Collaborating Editors:

1943-45	1944-46	1945-47
S. B. NICHOLSON Mount Wilson Observatory	JOEL STEBBINS Washburn Observatory	CECILIA H. PAYNE-GAPOSCHKIN Harvard College Observatory
D. B. McLAUGHLIN University of Michigan	A. N. VYSSOTSKY Leander McCormick Observatory	H. N. RUSSELL Princeton University
J. A. PEARCE Dominion Astrophysical Observatory, Victoria	W. W. MORGAN Yerkes Observatory	R. H. BAKER University of Illinois

The Astrophysical Journal is published bimonthly by the University of Chicago at the University of Chicago Press, 5750 Ellis Avenue, Chicago, Illinois, during July, September, November, January, March, and May. ¶The subscription price is $10.00 a year; the price of single copies is $2.00. Orders for service of less than a full year will be charged at the single-copy rate. ¶Postage is prepaid by the publishers on all orders from the United States and its possessions, Argentina, Bolivia, Brazil, Chile, Colombia, Costa Rica, Cuba, Dominican Republic, Ecuador, Guatemala, Haiti, Republic of Honduras, Mexico, Morocco (Spanish Zone), Nicaragua, Panama, Paraguay, Peru, Rio de Oro, El Salvador, Spain (including Balearic Islands, Canary Islands, and the Spanish Offices in Northern Africa; Andorra), Spanish Guinea, Uruguay, and Venezuela. ¶Postage is charged extra as follows: for Canada and Newfoundland, 42 cents on annual subscriptions (total $10.42); on single copies, 7 cents (total $2.07); for all other countries in the Postal Union, 96 cents on annual subscriptions (total $10.96), on single copies 16 cents (total $2.16). ¶Patrons are requested to make all remittances payable to The University of Chicago Press, in United States currency or its equivalent by postal or express money orders or bank drafts.

The following are authorized agents:

For the British Empire, except North America, India, and Australasia: The Cambridge University Press, Bentley House, 200 Euston Road, London, N.W. 1, England. Prices of yearly subscriptions and of single copies may be had on application.

Claims for missing numbers should be made within the month following the regular month of publication. The publishers expect to supply missing numbers free only when losses have been sustained in transit, and when the reserve stock will permit.

Business correspondence should be addressed to The University of Chicago Press, Chicago 37, Illinois.

Communications for the editors and manuscripts should be addressed to: Otto Struve, Editor of THE ASTROPHYSICAL JOURNAL, Yerkes Observatory, Williams Bay, Wisconsin.

Line drawings and photographs should be made by the author, and all marginal notes such as co-ordinates, wave lengths, etc., should be included in the cuts. It will not be possible to set up such material in type.

One copy of the corrected galley proof should be returned as soon as possible to the editor, Yerkes Observatory, Williams Bay, Wisconsin. Authors should take notice that the manuscript will not be sent to them with the proof.

The cable address is "Observatory, Williamsbay, Wisconsin."

The articles in this journal are indexed in the *International Index to Periodicals*, New York, N.Y.

Applications for permission to quote from this journal should be addressed to The University of Chicago Press, and will be freely granted.

Entered as second-class matter, July 31, 1940, at the Post-Office at Chicago, Ill., under the act of March 3, 1879.
Acceptance for mailing at special rate of postage provided for in United States Postal Act of October 3, 1917, Section 1103, amended February 28, 1925.

[PRINTED IN U.S.A.]

THE ASTROPHYSICAL JOURNAL

AN INTERNATIONAL REVIEW OF SPECTROSCOPY AND ASTRONOMICAL PHYSICS

VOLUME 101 MAY 1945 NUMBER 3

THE USE OF INFRARED SPECTRA FOR THE DETERMINATION OF ABSOLUTE MAGNITUDES

P. C. KEENAN* AND J. A. HYNEK†
Washington, D.C.

Received February 14, 1945

ABSTRACT

On infrared spectra taken on a scale of 48 A/mm at the Perkins Observatory it has been found possible to apply the method of spectroscopic absolute magnitudes to stars of type M. Lines of neutral and ionized elements serve as criteria which allow the assignment of luminosity classes Ia (very brilliant supergiants), Ib (ordinary supergiants), II (fainter supergiants), III (giants), and V (dwarfs). The most sensitive feature is the blended line at λ 8514, which is due, at least in part, to a member of a low-lying multiplet of neutral iron.

The luminosity criteria should be useful chiefly in the study of the atmospheres of the cooler components of spectroscopic binaries in which there is a marked difference in temperature between the two members.

The pioneer exploration of stellar spectra in the near infrared region extending from λ 7000 to λ 8700 was carried out in 1934 by Merrill,[1] who charted the principal features found in stars of types B8–M6. Since that time the speed and quality of photographic plates sensitive in the infrared region have been greatly improved; in particular, the Eastman I-N emulsion now has consistently high sensitivity between λ 7500 and λ 8600. With these plates and efficient grating spectrographs, it is possible to obtain infrared spectrograms of late-type stars with exposure times comparable to those needed for the ordinary blue region. Thus the long-wave part of the stellar spectrum is now available for practical use in the comparison of atmospheric characteristics of red stars.

In order to determine the usefulness of this region for the estimation of spectral types and absolute magnitudes, spectrograms of a number of standard stars were obtained by the second writer with the infrared spectrograph on the 69-inch reflector of the Perkins Observatory. The spectrograph employs a grating of 15,000 lines per inch and, as used, was fitted with a 250-mm camera, the combination giving a scale of about 48 A/mm near λ 8000. Most of the spectrograms were taken on Eastman I-N plates, although a few of the brighter stars were photographed also on Eastman IV-N plates in order to take advantage of the higher contrast and finer grain of this emulsion.

* On leave from the Yerkes Observatory for research in connection with the war.

† On leave from the Perkins Observatory to the Applied Physics Laboratory, Johns Hopkins University.

[1] *Ap. J.*, **79**, 183, 1934.

The stars used as standards are listed below in Table 1. In addition to spectral types[2,3] and luminosity classes,[2] estimated absolute magnitudes are included; but it must be kept in mind that for the more luminous stars these are quite uncertain.[4]

Comparison of the spectra of these reference stars showed that the infrared bands of *Ti O* behave consistently with the blue bands and can accordingly be used to assign spectral types through the range M0–M6. The most useful bands are the groups with heads at λλ 7054, 7088, and 7126 for types M0–M3 and the weaker bands at λλ 7743, 7820, 8441, and 8450 for types M4–M7. These bands, which arise from or near the normal level of the *Ti* o molecule, were originally found in the spectra of M-type stars by Merrill[5] and by Bobrovnikoff.[6] The atomic lines from low levels of titanium, etc., also increase in strength with diminishing temperature; but they are not so sensitive and consistent as the bands.

TABLE 1

STANDARD STARS OBSERVED IN THE SPECTRAL REGION λλ 6900–8700 A

Star	Type	Luminosity	M_v
ι Cep	K0	III	0
α Boo	K1	III	− 0.2
ε Aql	K2	III	0
γ Aql	K3	Ib–II	− 3
ε Peg	K3	Ib	− 4
π Her	K3	II	− 2
1 Lac	K3	III	0
λ Her	K3	III	0
ξ Cyg	K5	Ib	− 4
RW Cep	K5–M0	0–Ia	− 6.5
β And	M0	III	0
5 Lac	M0	II	− 2.5
α Sco	M1	Ib	− 4
μ Cep	M2	Ia	− 5.5
α Ori	M2	Ib	− 4
μ Peg	M2	III	0
π Leo	M2	III	0
BD+36°2147	M2	V	+10.5
η Gem	M3	III	− 0.5
R Lyr	M5	III	− 1
HD 182917	M7	III	− 1.5

The problem of estimating luminosities can best be approached by considering first the early M-type stars, among which there are known reference stars ranging in luminosity from dwarfs of the main sequence to the brightest supergiants. In Plate XXVI the spectra of a set of these stars have been arranged in order of decreasing absolute brightness from top to bottom. In the spectral region represented here the bands of atmospheric

[2] Morgan, Keenan, and Kellman, *An Atlas of Stellar Spectra*, Chicago: University of Chicago Press, 1943.

[3] For the M-type stars the system is that of Mount Wilson (Adams *et al.*, *Ap. J.*, **81**, 187, 1935).

[4] The luminosity scale for the M-type stars discussed by Keenan (*Ap. J.*, **95**, 461, 1942) has been modified slightly on the basis of work on the M-type variables at Mount Wilson (Joy, *Ap. J.*, **96**, 344, 1942, and Wilson, *Ap. J.*, **96**, 371, 1942) and on the modulus of the double cluster in Perseus (Bidelman, *Ap. J.*, **98**, 61, 1943, and Morgan, unpublished).

[5] *Bur. Standards, Sci. Papers*, **14**, 487, 1918.

[6] *Ap. J.*, **78**, 211, 1933.

PLATE XXVI

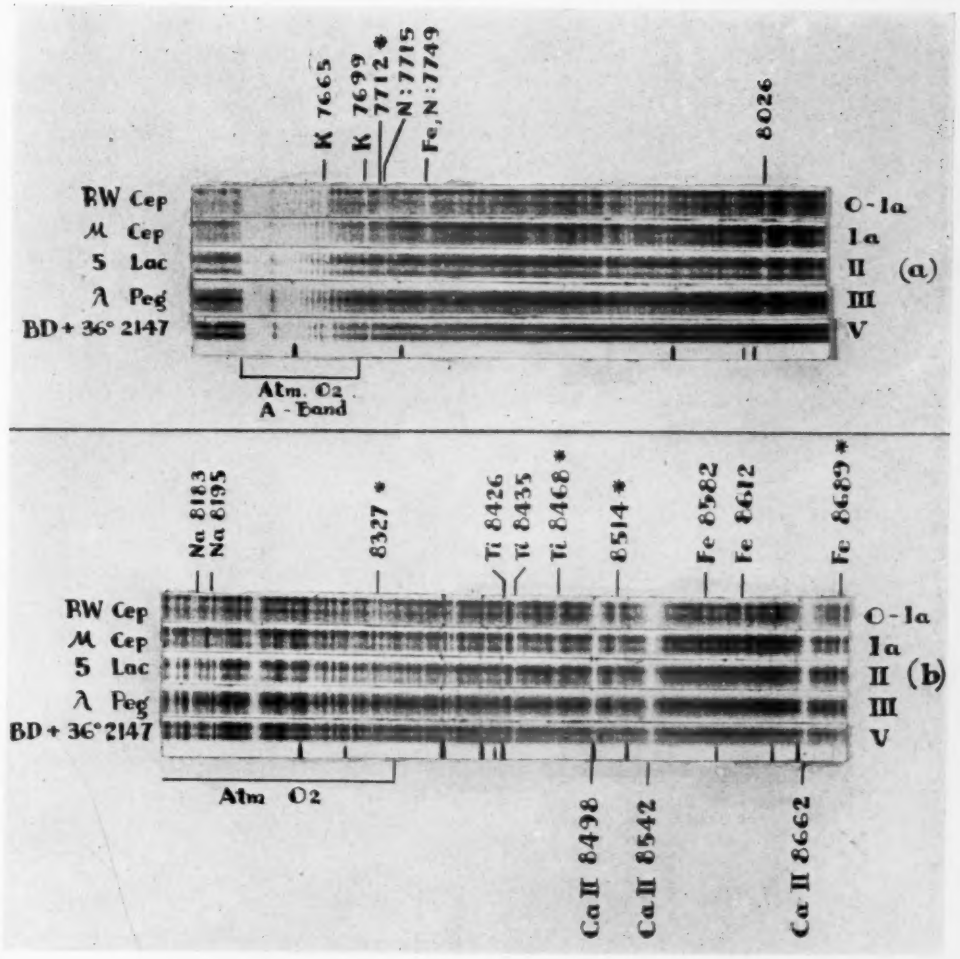

LUMINOSITY SEQUENCE FOR M-TYPE STARS IN THE INFRARED

Lines marked with an asterisk (*) are enhanced in the supergiants

(NOTE: What is indicated as atmospheric band O_2 in the region λ 8200 to λ 8300 is due to water vapor and not to oxygen.)

oxygen and water vapor, indicated in the reproduction, are prominent and hide some of the stellar features. Between them, however, the line spectrum of the stars is practically undisturbed.

Conspicuous in the dwarfs and supergiants are two pairs of lines of neutral potassium and sodium, arising, respectively, from levels of low excitation potential (Table 2). Both pairs lie in the neighborhood of atmospheric bands with which they are partially blended, as indicated in the table. Nevertheless, it can be clearly seen in the reproduction that they pass through a minimum in the giants.

A number of lines of somewhat higher excitation potential, including the strong *Ti* I lines λλ 8364, 8378, 8382–3, 8397, 8412, 8435, and 8548, are markedly stronger in giants than in dwarfs and share the further strengthening which most lines exhibit in passing

TABLE 2

STRONG LINES OF LOW EXCITATION POTENTIAL

λ	Element	E.P. (Volts)	Transition	Blends
7664.907 7698.979	*K*	0.00	$4^2S-4^2P^o$	7665.41 (Atm)
8183.258 8194.836	*Na*	2.09	$3^2P^o-3^2D$	8183.1 (Atm) 8193.7 (Atm)

TABLE 3

INFRARED LINES WHICH STRENGTHEN WITH INCREASING LUMINOSITY

Estimated λ	$I_{\mu\ Cep}$	λ_{Lab}	I_{Lab}	Source	Transition	E.P. (Volts)
7712	1	.....	.....	*Fe* II, *Sm* II, *Mn* I	.....	.....
8327	3s	8327.06	40	*Fe* I	.....	2.2
8468.2	3ns	8468.41	68.5, 20,300	*Fe* I, *Ti* I	.....	2.2
8497.8	15s	8498.06	.....	*Ca* II	$^2D-^2P^o$	1.7
8514.4	5	8514.08	.....	*Fe* I, etc.	.....	2.2
8542.2	25s	8542.13	.....	*Ca* II	$^2D-^2P^o$	1.7
8662.4	15s	8662.17	.....	*Ca* II	$^2D-^2P^o$	1.7
8688.8	5s	8688.63	150	*Fe* I	.....	2.2

from giants to supergiants. The *Fe* I lines λλ 8388, 8582, and 8675 also belong in this group.

Most important for the separation of supergiants from the other stars are a group of lines which are strongly enhanced in passing from low to high luminosities. These lines, several of which are listed in Table 3 and are marked with asterisks in Plate XXVI, arise chiefly from rather low levels of neutral iron or of ions of metals of low ionization potential. The latter are rarer in the red region than in the blue part of the spectrum, since the first excited levels of these ions generally lie several volts above the normal level. There are, however, a few which are favorably situated for observation. With the exception of the members of the infrared *Ca* triplet, they are rather weak in stellar spectra and are usually blended with other lines on spectra of moderate dispersion. Consequently, the identifications in Table 3 are tentative only. The assignment of the atoms chiefly responsible for each line has been made on the basis of the "Multiplet Table" of Charlotte

M. Sitterly,[7] with regard also to the elements found by D. M. Davis[8] to be represented by lines in the blue region of the spectrum of α Sco.

The essential point is that these observed lines, though frequently blends of several lines from different elements, strengthen progressively with increasing luminosity of the star. The strongest and most sensitive is λ 8514, which is indicated on Plate XXVI.[9] In dwarfs and giants λ 8514 is only slightly stronger than λ 8518 of *Ti* I, the line adjacent to the red. In passing to stars of higher luminosity, the *Ti* I line remains at about the same intensity, while λ 8514 strengthens rapidly until in RW Cep it surpasses λ 8435, a blend of two of the strongest *Ti* I lines. The tentative prediction of Merrill[1] that the *Ca* II triplet "may have an interesting relation to luminosity" is fully borne out, as a glance at the reproduction will show. Most of the remaining lines in Table 3 appear only in the brighter supergiants (on spectrograms having a scale of about 50 A/mm) and are of

TABLE 4

INFRARED CRITERIA OF ABSOLUTE MAGNITUDE (TYPES M_0–M_4)

Behavior			Sensitive Lines	Comparison Lines
Dwarfs	Giants	Supergiants		
Strong	Weak	Strong	*K* λ 7664.9 *K* 7699.0 *Na* 8183	λ 7715 Atm 8177
Rather weak	Strong	Strong	8026 *Ti* 8426 *Fe* 8582	....
Very weak	Weak	Rather strong	7712 *Fe* 8327 *Fe-Ti* 8468 8514 *Fe* 8689	7715 Atm 8321 *Ti* 8435 *Ti* 8518, 8435 *Fe* 8675

value chiefly in distinguishing the very brilliant supergiants of luminosity class Ia (RW Cep, μ Cep) from those of class Ib or II (α Ori, 5 Lac).

The enhanced lines are consistently stronger in RW Cep than in μ Cep. This result confirms the conclusion indicated by the lines in the photographic region[4] that, as far as the spectrographic evidence is concerned, RW Cep is more luminous than μ Cep and is one of the intrinsically brightest stars known.

A summary of the luminosity criteria is given in Table 4, where the lines have been grouped according to their behavior. Numerical estimates of relative intensities have not been given, for they will depend upon the dispersion and contrast of the spectrograms. The criteria have been described on the assumption that direct comparisons will always be made with a set of reference stars such as those of Plate XXVI.

[7] We are greatly indebted to Mrs. Sitterly for her kindness in comparing our approximate wave lengths with infrared lines listed in her revised but yet unpublished "Multiplet Table."

[8] *Ap. J.*, **87**, 335, 1938; **89**, 41, 1939.

[9] It is worthy of note that three of the lines which show the strongest enhancement in the supergiants are λλ 8468, 8514, and 8600, which are all members of an *Fe* I multiplet with an excitation potential of 2.2 volts, not greatly different from that of other *Fe* lines which do not exhibit such marked enhancement. The great strength of λ 8514 in RW Cep suggests that the *Fe* line is blended with a line from an unidentified ion.

It is important to keep in mind the limitations in the accuracy of spectroscopic absolute magnitudes. In the infrared the precision will be slightly less than in the photographic region, chiefly because of the smaller number of sensitive lines. The "resolving power" in luminosity estimated from plates of moderate dispersion can be set at about 2 mag. This means that we cannot expect to distinguish reliably between stars differing in absolute magnitude by less than this amount. What can be accomplished, however, is the separation of dwarfs, giants, and supergiants and the division of the supergiants into those that are moderately bright ($M_V = -3$) and those of highest luminosity ($M_V = -6$).

One of the most useful fields of application of the infrared luminosity criteria is the study of the red components of spectroscopic binaries in which the blue region of the spectrum is dominated or disturbed by the light of the hotter component. A notable example of such double stars is VV Cep, the infrared spectrum of which is described in the paper which follows.

THE PRESENCE OF STRONG LINES OF *O* I IN THE INFRARED SPECTRUM OF VV CEPHEI

J. A. HYNEK* AND P. C. KEENAN†
Washington, D.C.
Received February 23, 1945

ABSTRACT

The spectrum of the red component VV Cep was photographed in the region λλ 7200–8700 in October and November, 1944. No emission lines were observed; the absorption lines of the metals had intensities normal for an M2 supergiant and indicated a spectroscopic absolute magnitude (M_v) of −4 or −5.

The only anomalous feature was the great strength of the blended absorption lines of *O* I at λ 7773 and λ 8446. The intensity of these lines was as great as that normally observed in supergiants of types B–F, and physical considerations suggest that the lines are produced by oxygen atoms in the normal atmosphere of the M-type star.

The presence of oxygen atoms in the excited states from which these transitions arise may be due to resonance absorption of the intense ultraviolet diluted radiation from the B-type star near λ 1300. The dimensions of the system are consistent with an energy density sufficient to populate these levels.

In the ordinary photographic region the spectrum of VV Cep is produced by light from both the red and the blue components of the system, the observed radiations from the two being equal near λ 4000. It is only near primary minimum, at intervals of twenty years, that the pure spectrum of the supergiant M-type component can be observed in this region. For this reason, it is important to turn to the infrared spectrum in order to study the atmosphere of the red star throughout the orbital cycle.

In October and November of 1944 two spectrograms of VV Cep, covering the region from λ 7200 to λ 8700, were taken with the 69-inch reflector of the Perkins Observatory by J. A. Hynek and N. T. Bobrovnikoff, respectively. One was taken on an Eastman I-N plate, the other on a IV-N plate; apart from contrast effects, the spectra appear identical. The I-N spectrogram of October 7, 1944, is reproduced in Plate XXVII; for comparison a spectrogram of α Ori is given, since the lines of neutral *Fe*, *Ti*, and the other metals were found to have nearly the same relative intensities in VV Cep as in early M-type supergiants.

The spectral type is close to M2, in agreement with V. Goedicke's estimates from the spectrum in the blue region.[1] The appearance of the lines which were found, in our preceding paper,[2] to be sensitive indicators of luminosity is consistent with a visual absolute magnitude of −4 to −5, since the enhanced lines were found to be slightly stronger than in α Ori or α Sco, (*Ib*), and slightly weaker than in μ Cep, (*Ia*). The closeness of the match with α Ori is apparent in the reproduction.[3]

It will be immediately noticed, however, that there is one striking difference between the two spectra. The blended lines of neutral oxygen at λ 7773 and λ 8446, which are absent (or, if present, barely perceptible) in α Ori, form two of the strongest features in the spectrum of VV Cep. In the latter they have approximately the same strength as in supergiants of types A and F, where they normally reach their maximum development.[4]

* On leave from Perkins Observatory to the Applied Physics Laboratory, Johns Hopkins University.

† On leave from the Yerkes Observatory for research in connection with the war.

[1] *Pub. Mich. Obs.*, Vol. **8**, No. 1, 1939.

[2] *Ap. J.*, **101**, 265, 1945.

[3] The similarity of the blue regions of VV Cep and μ Cep was noticed by Goedicke at the time of primary minimum in 1936 (*op. cit.*).

[4] The variation of the *O* I lines through the spectral sequence can be followed in the reproduction given by Merrill, *Ap. J.*, **79**, 183, 1934, Pl. II. The lines are conspicuously strong in the spectra of α Cyg, β Ori, and ε Aur. They show a marked luminosity effect.

PLATE XXVII

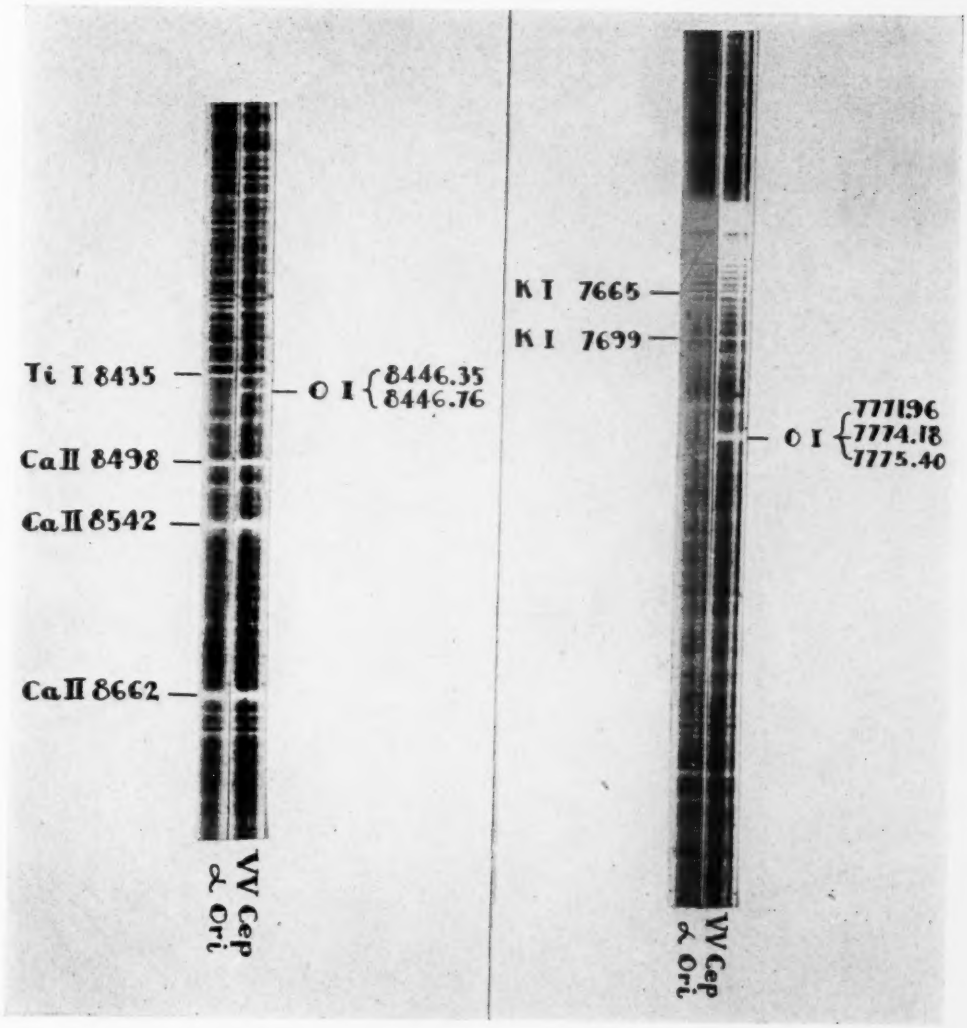

INFRARED SPECTRUM OF VV CEPHEI

UNIV. OF MICH.

Since the *O* I lines are weak or absent in all other late-type stars which have been photographed in the infrared, their strength in VV Cep must be associated with the proximity of the high-temperature (B-type) component of this binary. They cannot be part of the normal spectrum of the B-type star, since its radiation is negligibly small compared to that of the red star in this part of the spectrum. The alternative that the *O* I lines arise from the projection of the B-star's ordinary atmosphere against the disk of the M-type star is improbable because of the low central intensities of these lines; absorption of this strength could be produced only if almost the entire disk of the red star were occulted by the atmosphere of the B-type star. This would be inconsistent with the generally accepted picture of the system according to which the red star has a radius at least one hundred times greater than that of the blue component. Furthermore, the spectrograms were taken not at secondary minimum but more than a year earlier, and no change was noticeable in the interval of seven weeks between exposures.

There remain two possibilities: the excited *O* I atoms responsible for the lines are situated either in the atmosphere of the M-type star or in a diffuse cloud surrounding one or both of the components of the binary system. The absence of even a trace of emission associated with these strong lines (these lines show emission in P Cyg, γ Cass, and ζ Tau) speaks against the second alternative. The evidence from radial velocities is inconclusive

TABLE 1

RADIAL VELOCITIES OF VV CEP FROM INFRARED LINES

PLATE	DATE	VELOCITY (IN KM/SEC)			
		Ti Lines	*Fe* Lines	*Ca* Triplet	*O* I 8446
1169.....	10- 7-1944	−29.4 (7)	−18.7 (4)	−37.7 (3)	−37.7
1189.....	11-25-1944	−25.4 (8)	−20.8 (8)	−31.9 (3)	−53.1

at present, because at the time of observation the system was approaching secondary minimum.

The velocity of the M-type star (predicted from the velocity-curve given by Goedicke) for the epoch of our observation is about −15 km/sec; for the B component, about −25 km/sec. The measures of the present spectrograms of the red component of VV Cep are summarized in Table 1.

The discrepancy between the observed velocities and those predicted for the red star are most readily explained by the known irregularities in its velocity-curve. The systematic differences between the velocities of different elements are possibly an effect of stratification.

On the assumption that the oxygen lines are produced in the atmosphere of the red star, we have the problem of explaining why they have intensities to be expected only in the spectrum of a much hotter star, while the lines of *Ti*, *Fe*, etc., appear with strength normal for an M-type spectrum.

The answer may lie in the combination of two circumstances: the intense radiation of the distant B-type star in the far ultraviolet and the differences between the oxygen and metallic atoms in their potentials of excitation and of ionization. The lower levels of the infrared lines of *Fe* and *Ti* have excitation potentials lying between 1 and 3 volts, and the relative distribution of the atoms among the excited states will be governed entirely by the radiation of the M-type star. The only effect of the B star may be expected to be some decrease in the intensities of all of these lines, since the numbers of neutral atoms will be decreased if there is increased ionization from radiation in the region λλ 1500–1700. Actually, these lines from neutral metals appear to be very slightly weak-

ened, relative to the *Ca* II lines in VV Cep, as compared to α Ori or other similar supergiants (cf. *Ti* I λ 8435 with *Ca* II 8498 in Pl. XXVII).

The situation of the oxygen atoms is essentially different, as can be seen from the Grotrian diagram, of which the lower part is shown in Figure 1. The observed infrared lines originate from the 3^3S^o and 3^5S^o levels, which are 9.11 and 9.48 volts, respectively, above the normal 2^3P level of the neutral oxygen atom. Transitions up to the 3^3S^o level give rise to the ultraviolet triplet λλ 1302-6. These are the ultimate lines of oxygen, since the other low-lying levels, $^1D_2$ and $^1S_0$, are metastable.

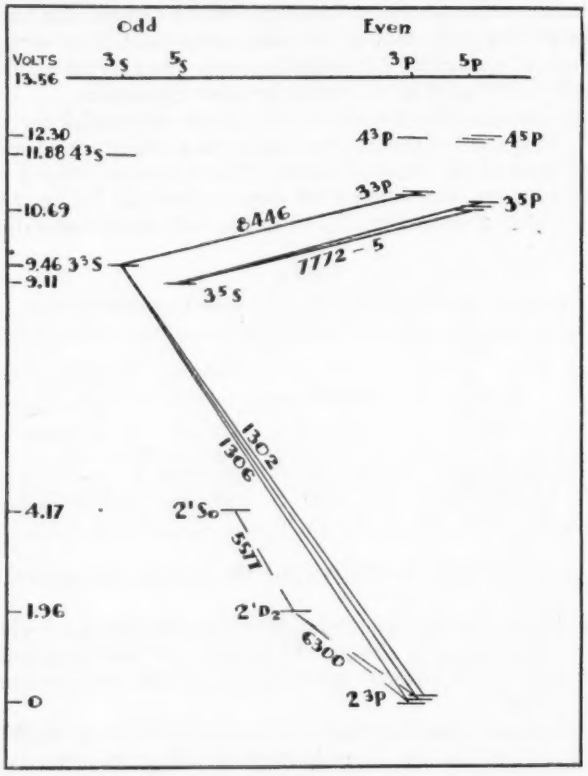

FIG. 1.—Lower energy-levels of *O* I. Permitted transitions are shown by full lines; a few forbidden transitions are included and are shown by broken lines.

If it is assumed that in the atmosphere of the M-type star the energy density of dilute radiation from the B-type star is sufficiently great near λ 1300, the population of the 3^3S^o level will be governed by this radiation quite independently of the radiation of the M-type star itself. When once excited to this state, the atoms will be ready to absorb light at wave-lengths given by the series $3^3S^o - m^3P$, of which the first member is the observed pair at λ 8446, where the intensity of radiation from the red star is high. It will be observed that the other infrared triplet, λλ 7772-5, is the first member of the series $3^5S^o - m^5P$. Since there are no quintet levels lying below 3^5S^o, this level can be reached from below only by the transition $2^3P - 3^5S^o$. Such intercombination lines can be expected to occur in the spectrum of *O* I,[5] and this transition has been observed as the pair of

[5] Condon and Shortley, *The Theory of Atomic Spectra*, p. 218, Cambridge University Press, 1935.

lines at λ 1355.7 and λ 1358.7, having emission intensities approximately one-half those of the permitted triplet lines.[6] In VV Cep the relative intensity of the λ 7774 and λ 8446 blends is very nearly the same as in a normal early-type supergiant, such as β Ori.

To test the reasonableness of this interpretation of the observed spectrum, a rough calculation of the radiation fields can be made on the basis of the orbit derived by Goedicke[1] from spectroscopic and photometric data. Admittedly, the dimensions of the system are quite uncertain, but the general agreement of our independent estimate of the luminosity of the M-type component with the values given by Goedicke suggests that the order of magnitude of the results will not be far wrong. Out of the several possible alternative sets of values given by Goedicke for the relative dimensions and temperatures (allowing for a diffuse atmosphere of the red component) the following were chosen as reasonably consistent with the spectroscopic luminosity results:

Component	T	R
B	18,000° K	13.0 $R\odot$
M2	3,000	1220 $R\odot$

A = semimajor axis = 33 A.U. = 7095 $R\odot$

Consider an atom in the atmosphere of the M-type star. It is assumed to be sufficiently close to the surface so that the relative dilution factor, W_r, for radiation of the red star is $\frac{1}{2}$. The computation is then independent of the radius of this star. Since the M-type star fills a considerable part of the orbit of the system, the atoms in different parts of its atmosphere will be at a wide range of distances from the B-type star. Assume, as a reasonable mean, that this distance is $A - R_M = 6000R\odot$. The ratio of the dilution factors, W_b/W_r, for radiation from the two stars is then 2.7×10^{-6}. In Table 2 the relative contribution of the two stars to the field of radiation surrounding the atom is given for different wave lengths on the assumption that both stars radiate as black bodies.

It is evident that the blue component dominates the radiation field in the far ultraviolet to such a degree that the picture will not be substantially altered by any reasonable changes in the dimensions of the system. The spectral region within which the light from the two stars approximately balances is, however, quite sensitive to the temperature of the B-type star, which may be anywhere between 12,000° and 30,000°. For the crude model assumed above, the intensities from the two stars approximately match near λ 3100, and the radiation of the M-type star is relatively negligible at its own surface for all wave lengths shorter than about λ 2000.

The computed flux of dilute radiation at λ 1300 surrounding the oxygen atoms is 2.9×10^{11} ergs/cm²/sec/cm of wave length. The same energy density of radiation would be found at the surface of a star radiating as a black body at a temperature of slightly less than 5600° K. If the ultraviolet radiation of the stars were actually given by the Planck curve for the star's effective temperature and if the lines at λ 1300 were the only transitions determining the population of the 3^3S level, the intensities of these infrared lines should be the same as in an F7 supergiant, for which the effective temperature is in the neighborhood of 5800°. The close agreement with the intensities of these lines and those in the spectrum of the F0 supergiant ε Aur is therefore of considerable interest. The observed intensities, however, also match those in considerably hotter stars; this is not surprising, since neither of the above assumptions holds true exactly. The essential conclusion to be drawn from this crude calculation is that the absolute intensity of ultraviolet light from the B-type star is of the right order of magnitude to give rise to observable lines.

[6] Hopfield, *Ap. J.*, **59**, 114, 1924.

If the assumption examined in the previous paragraphs proves correct, a more detailed treatment of the problem will be important, for the relative intensities of the lines of different excitation potentials provide a set of conditions relating T_B, T_M, R_B, and A, in addition to the data available to Gaposchkin and Goedicke in their original solutions for the dimensions of the system.

The first need is for a thorough study of the entire red and infrared spectrum of VV Cep in order to compare intensities of lines from as many elements as possible. Among the important lines are the members of the Paschen series of hydrogen. The lines from P13 to the limit of the series fall within the range of the available plates; but other strong absorption features, including the three lines of the *Ca* II triplet, fall at nearly the same wave lengths and prevent the definite identification of the Paschen series in VV Cep. The appearance of the spectrum indicates that they cannot be markedly stronger than in other late-type stars and are not present with intensities comparable to those found in β Ori, α Cyg, or other hot stars. The lack of strengthening in VV Cep is not necessarily surprising but requires explanation.

TABLE 2

RATIOS OF THE RADIATION FLUXES FROM THE BLUE AND RED COMPONENTS AT A POINT IN THE ATMOSPHERE OF THE RED STAR

λ	F_b/F_m	λ	F_b/F_m
1300 A	5.6×10^{7}	3000 A	1.7
2000	1.2×10^{3}	4500	2.3×10^{-2}
2500	24	6000	2.7×10^{-3}

Nitrogen is somewhat analogous to oxygen in its arrangement of energy-levels. The infrared lines, the strongest of which lie at λλ 8680–86 and 8703–18, originate from a $^4P^o$ level which is reached from the normal ^4S level by transitions in the neighborhood of λ 1200. These lines, however, are less easy to observe than the infrared lines of *O* I, for the number of permitted transitions from the *N* I $^4P^o$ level is much greater and none of the lines is comparable in intensity to the strongest oxygen lines.[7] None of the *N* I lines has been detected with certainty on the Perkins spectrograms of VV Cep. The question of whether they show any strengthening in VV Cep, as compared to other late-type stars, can be settled only with spectrograms of higher dispersion.

The interpretations of the strength of the *O* I lines as a result of direct excitation by the radiation of the B-type star leads to the prediction that the oxygen lines should disappear completely during the total phase of primary eclipse (occurring next in 1957), since at that time none of the atoms on the observed side of the M-type star is exposed to direct illumination from the hotter component. Whatever residual excitation occurs would be caused by diffused light. Actually, it is possible that the absorption will be replaced by emission from the illuminated rim—resulting in a selective "flash" spectrum.

If this interpretation is correct, one might expect similar phenomena in related systems like ζ Aur. A plate of this star taken on February 11, 1945, does not show the *O* I lines. At this epoch, however, the B-type star is approaching eclipse (two months prior to ingress) and is unfavorably placed for the excitation of the red star atmosphere that is in the light of sight to the earth. Infrared observations of both the VV Cep and ζ Aur systems at other epochs should prove of considerable interest and will clarify the tentative interpretation of the *O* I lines presented here.

[7] The relative intensity of the *O* I and *N* I lines can be compared in Plate II and Table 2 of Merrill's paper, *Ap. J.*, **79**, 183, 1934.

THE BURRELL TELESCOPE OF THE WARNER AND SWASEY OBSERVATORY

J. J. NASSAU
Case School of Applied Science
Received March 6, 1945

ABSTRACT

In this paper the description of the mounting, optics, and objective prism of the 24-inch Schmidt-type telescope is presented, together with numerical data pertaining to it and its performance.

The program of research and instruction in astronomy at the Warner and Swasey Observatory of the Case School of Applied Science, in Cleveland, Ohio, was considerably advanced recently by the acquisition of a 24-36-inch Schmidt-type telescope. It is intended to present here the essential details and characteristics of this instrument.

In 1919 Mr. Worcester R. Warner and Mr. Ambrose Swasey built and equipped an observatory to serve the basic educational needs of the Case School in astronomy. The principal equipment consisted of a 9½-inch refractor, two transit instruments, a zenith telescope, and the associated recording apparatus, such as precision clocks, chronographs, etc. Later a 3-inch Ross-lens astrographic camera was added.

When an appeal was made in 1939 for funds to enlarge and expand the observatory, many friends were ready to help. Gifts totaling over a quarter of a million dollars were received, principally from persons closely associated with the original founders of the observatory and of the Case School. The additional facilities include a Schmidt-type telescope, a new building to house the telescope, an auditorium and an exhibit hall in memory of Mr. Warner, a library, offices, a photometer room, and a shop. The building was completed in October, 1940, and the telescope was put into operation during the month of November, 1941. The Warner and Swasey Company of Cleveland, Ohio, designed and constructed the mounting and the optical elements of the instrument.

In future publications concerning observations made with this instrument we shall refer to it as the "Burrell telescope," a designation in memory of the late chief engineer of the Warner and Swasey Company.

MOUNTING

The mounting is of the cross-axis type, along the same lines as the large reflectors built by this company (Pl. XXVIII).

Polar axis.—This axis is composed of three castings: a cubical center carrying the declination axis, an upper section provided with radial bearing resting on the north pier-head, and a lower section having a radial and thrust bearing resting on the south pier. The extended portion of the lower section is made of steel forgings pressed into place and carrying the right-ascension driving gear and circles.

Declination axis.—This axis consists of a hollow shaft machined from a forging. It is carried on antifriction bearings of ample capacity for the radial and thrust loads. These bearings are mounted on the center section of the polar axis.

Telescope tube.—The tube is made up of a number of welded-steel sections, $\frac{3}{16}$–$\frac{3}{32}$ inch in thickness. The diameter of the lower section is 4 feet, with the mirror cell bolted to the lower end. The upper section has a diameter of 2.8 feet and supports the correcting lens and a removable dewcap of 17 inches in length. Diaphragms, arranged to prevent inter-reflection, together with ribs extending the length of each section, add to the transverse rigidity of the tube. This construction assures rigid alignment not only between the opti-

cal parts and the plateholder inside the tube but also between them and the guide telescope on the outside.

Mirror cell.—This cell has an over-all diameter of 44 inches. The bottom supports for the mirror consist of three spiders, each having three arms terminating in flat horizontal rings of 6 inches in diameter. The rings are so placed that they support equal portions of the weight of the mirror. The back of the mirror is smooth-ground to avoid excessive friction between the ring pads and the glass. Four side supports provide means for collimating. In order to facilitate handling the mirror, the cell is made in two parts, the inner part being removable to permit the attachment of a lifting band around the circumference of the mirror (Pl. XXIX).

Lens cell.—This cell is mounted in a flanged cell provided with three sets of push-and-pull screws for "squaring." This cell is mounted in a ring provided with collimating screws; three bolts attach the ring to the tube.

The shutters.—There are two shutters inside the tube of the telescope, one just above the mirror and the other just below the lens. Each is made of two cylindrical pieces of metal, which, when open, lie along the inner sides of the tube. One shutter is used primarily to protect the mirror when the telescope is in actual operation, and the other is to control the exposure. Both are operated by hand wheels at the lower end of the tube, close to the guide telescope.

A third shutter has been added for use in cases of short exposure where more accurate timing is necessary. It is a circular, occulting metal sheet 9 inches in diameter, placed just in front of the photographic plate. A lever device at the lower end of the tube actuates it.

Plateholder mounting.—This mounting is supported by four thin vanes attached to the tube 4 feet below the correcting lens. The 2-foot arm which holds the adaptor for the photographic plateholder is pivoted $2\frac{1}{2}$ inches from the intersection of the vanes, which permits swinging the plateholder attachment toward the outside of the tube, as shown by the dotted arc line in Plate XXIX. This enables the observer to change plateholders and to alter the focus without reaching into the tube. Changes of focus are made by a screw-and-slide mechanism. A graduated scale and a large micrometer dial permit direct setting of the focus to 0.001 inch. A clamp-and-latch mechanism aligns the plate accurately in the focal plane after loading.

Circular plateholder (Pl. XXX).—This plateholder is made of aluminum and is designed to accommodate circular glass photographic plates. These flat plates are bent to conform to the spherical focal surface by the curved back plate of the plateholder, which is pressed firmly against the back of the photographic plate and clamped in place. The plateholder has proved highly satisfactory; there has been no breakage at this stage of handling the plates, although more than one thousand plates have been taken. Clips are provided for holding color filters directly in front of the photographic plate.

Guide telescope.—This is a $9\frac{1}{2}$-inch refractor of 123 inches in focal length. The usual right-angle adaptor, eyepieces, and illuminated cross-wires are provided.

Visual observing.—This type of observing may be done on occasion by interposing a 7-inch flat mirror in the convergent light-beam to bring the focal surface to the side of the tube in the manner of the usual Newtonian arrangement. This mirror is mounted in an arm which is ordinarily folded against the inner tube wall (this feature is not shown in Pl. XXIX). By turning a knob on the exterior of the tube the observer may throw the mirror into position for use.

Motions in declination.—Four speeds in declination are provided. For guiding, the speed is 2 minutes of arc per minute of time, and for setting the guide star at the intersection of the cross-wires of the guide telescope the speed is 15 minutes of arc per minute of time. These speeds are obtained by means of a two-speed reversible motor, driving through a gearbox having two trains of gears and a solenoid-operated clutch, arranged so that the same motor may operate either the slow or the quick motions, the quick mo-

PLATE XXVIII

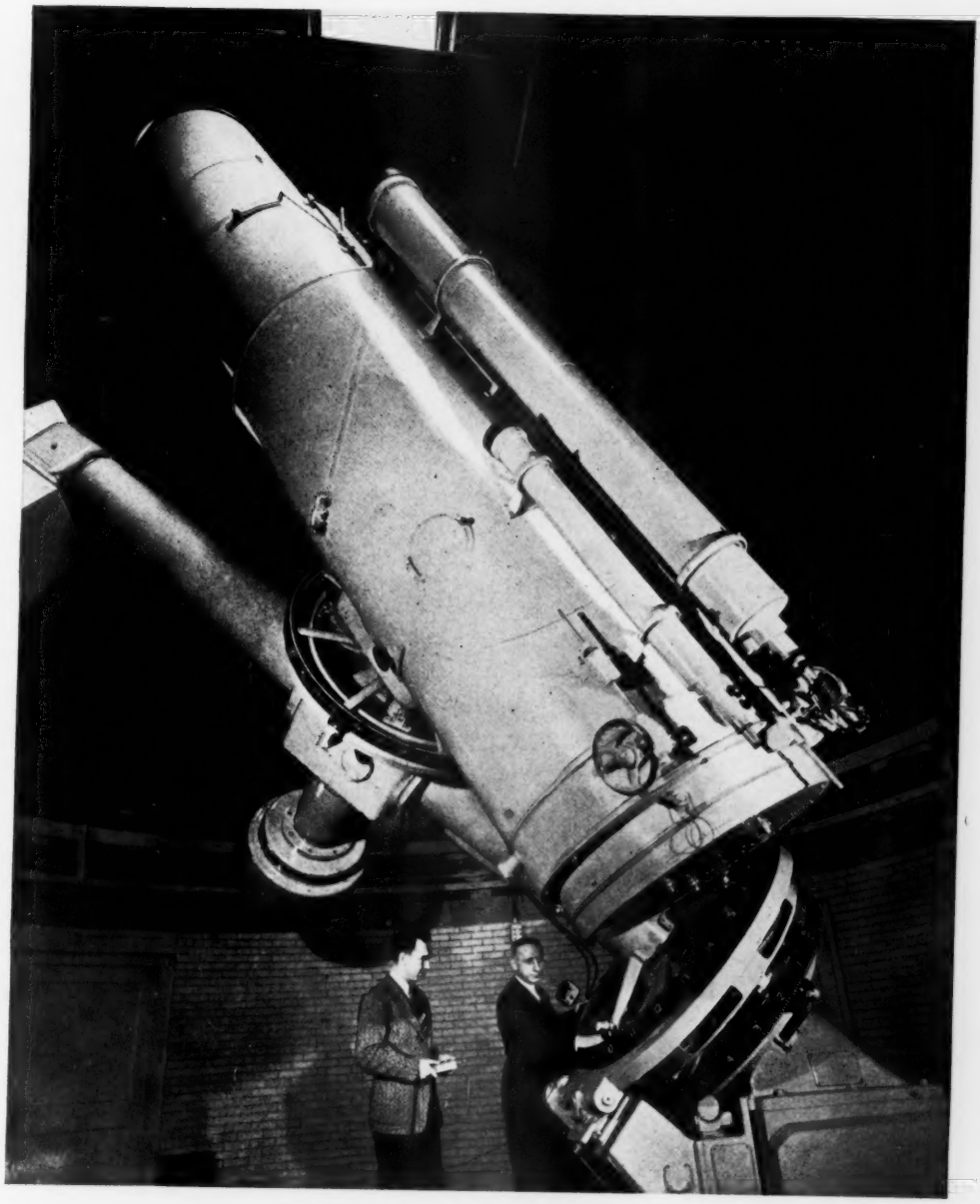

THE 24-INCH SCHMIDT-TYPE TELESCOPE

PLATE XXIX

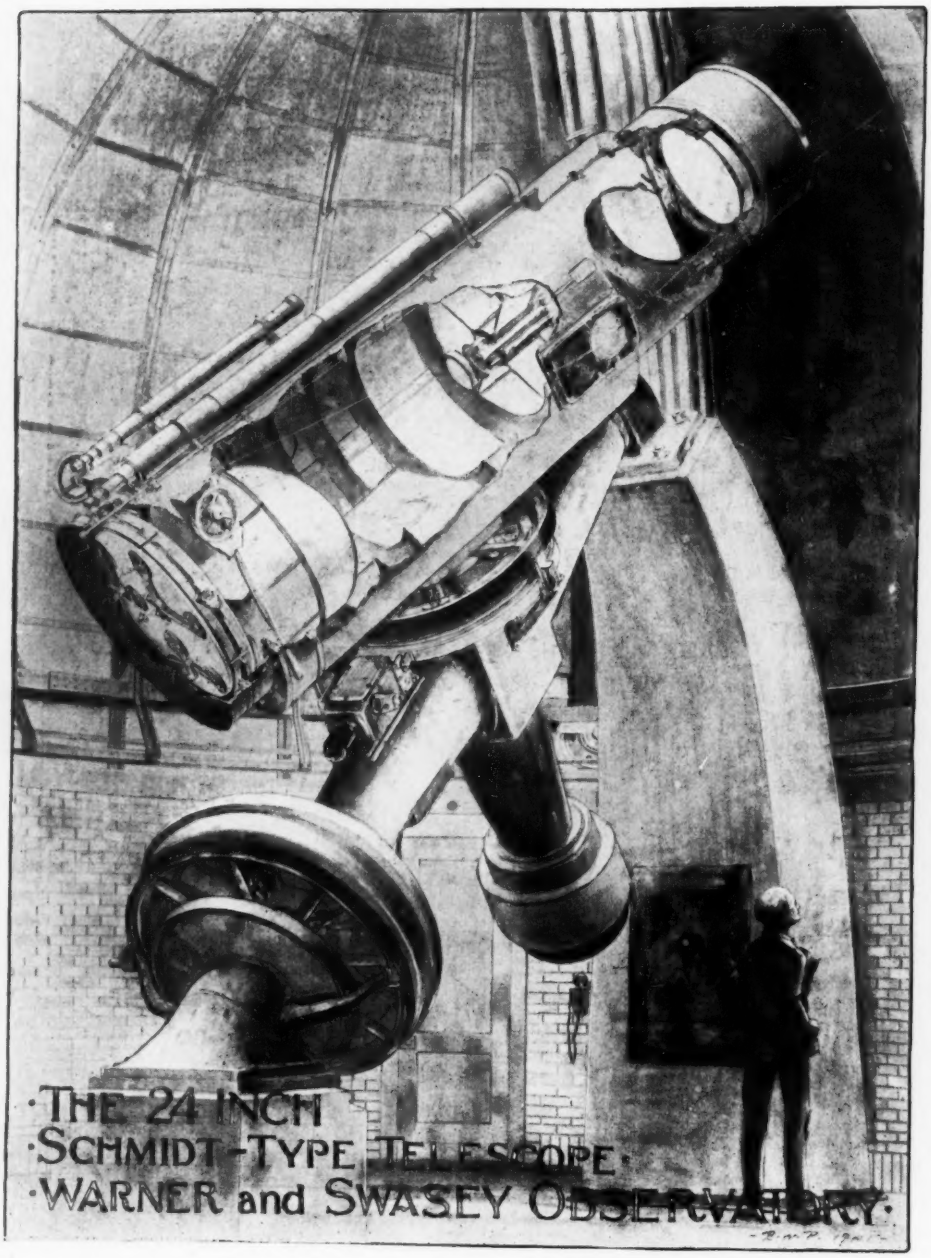

DIAGRAM BY RUSSELL PORTER

PLATE XXX

PLATEHOLDER ATTACHMENT SHOWING PLATEHOLDER OUTSIDE OF TELESCOPE TUBE

PLATE XXXI

PHOTOGRAPH OF A PORTION OF THE NORTH AMERICAN NEBULA (*left*) AND DENEB MADE WITH THE BURRELL TELESCOPE WITH AN EXPOSURE OF 10 MINUTES

The irregular double ellipse just above the nebula is the ghost of Deneb. The long streak is due to the reflection from one of the vanes supporting the plateholder.

tions being 46.0° and 7.6° per minute of time. A clamp with magnetic release connects the driving mechanism to the declination axis.

Motions in right ascension.—The sidereal rate of driving is obtained by the use of a $\frac{1}{16}$-h.p. synchronous motor. As a partial compensation for differential refraction, the rate is slower than the theoretical rate by 1 second of time per hour. A clamp with magnetic release connects the worm wheel to the polar axis when the instrument is driven. The 60-cycle A.C. current provided for the synchronous motor is furnished by the Cleveland Electric Illuminating Company. Its frequency remains sufficiently constant that no guiding is necessary during a 10- or 15-minute exposure.

To increase the efficiency of the telescope, particularly when it is used for the photographing of stellar spectra, a frequency-control device and a frequency regulator are planned and will be secured when war requirements for materials are relaxed.

The two slow speeds in right ascension corresponding to the slow speeds in declination are applied to the driving worm by means of an additional motor. The telescope is also provided with two quick motions in right ascension, one 39.0° and the other 8.5° per minute of time. These motions are achieved by a two-speed motor, driving a spiral pinion which engages a spiral gear mounted on the polar axis. A solenoid-operated clutch release, interposed between the spiral pinion and the motor, leaves the pinion free to turn when the slow motions are in operation.

For both right ascension and declination motions, the clutches and the slow-motion clamps are electrically interlocked so that both quick and slow motions cannot be engaged at the same time. However, both may be released at the same time to permit manual moving of the telescope. This release, which is controlled by a switch near the eye-end of the guide telescope, affords convenient means of rapidly setting the telescope and of adjusting the balance.

The electrical control.—For convenience in setting, the motions referred to above are controlled from portable push-button stations. Push buttons are arranged in two groups, one group for quick motion and circle setting and the other for centering the guide star and guiding. The switches for turning the dome are placed in the box with the first group.

THE DOME

The 28-foot dome is constructed of structural steel covered by insulating material and made waterproof by an outside covering of sheet copper. It is provided with a double shutter opening, 6.5 feet wide, making possible $\frac{1}{2}$-hour exposures at the equator without movement of the dome. Two wind curtains are provided to cover that part of the slit-opening not in use by the telescope. The dome, shutter, and curtains are operated by motors.

OPTICAL PARTS

The 36-inch Pyrex-glass mirror blank.—This blank was manufactured by the Corning Glass Company and is remarkably free from bubbles or other defects. The mirror was ground and polished at the Warner and Swasey Company under the direction of Mr. C. A. Robert Lundin. Its optical surface was then coated with chromium-aluminum by Dr. Robley Williams. After three years the surface shows no sign of loss in its reflecting power.

Correcting lens.—This lens, also made under Mr. Lundin's direction, has a diameter of 24.5 inches. The distance of the depressed zone from the center is 8.48 inches, which fulfils the condition for the minimum amount of glass to be removed to make the aspherical surface of the correcting lens.

Optical testing.—The spherical mirror was tested in the usual manner at the center of curvature. For the testing of the lens the spherical mirror was mounted in a vertical position, with the lens placed at its center of curvature, and a 60-inch-diameter optical flat mirror, placed a few feet beyond the correcting lens for a collimator. The curved surface

of the lens was turned toward the mirror, and a scale 24 inches in length, with the inch divisions well marked, was placed horizontally just in front of the curved side of the lens. A carriage supporting the pin-point light-source and the knife edge was placed at the focus of the lens-mirror system. A diagonal flat, appropriately placed, brought the focus away from the optical axis. For each setting of the carriage the boundaries of the shadowgram were read by means of the scale in front of the lens, thus securing quantitative measures of the diameter of the circle of confusion and means for ascertaining the zone of the correcting lens, which required further figuring. This method of testing was suggested by Dr. James G. Baker. The accepted lens yielded a circle of least confusion of 25μ in diameter with a negligible amount of astigmatism. Numerical details of the optical system are given in Table 1.

TABLE 1

SUMMARY OF NUMERICAL DATA

Mirror (Pyrex):		
Diameter (clear aperture)	36	inches
Thickness at the edge	5.5	inches
Weight	418	pounds
Radius of curvature	167.69	inches
Correcting lens (Vita glass):		
Diameter (clear aperture)	24	inches
Thickness	0.35	inches
Distance of depressed zone from center of lens	8.48	inches
Depth of curve at this zone	0.00054	inches
Distance from mirror to plane of lens (plane surface outside)	168.04	inches
Photographic plate:		
Radius of curvature of plate	84.00	inches
Sagitta of bent plate at center	2.34	mm
Over-all diameter of plateholder	8.56	inches
Diameter of plate	7.75	inches
Clear aperture of plate	7.5	inches
Field	5.16°	
Scale of plate	97.2/mm	
Objective prism:		
Diameter (clear aperture)	24.00	inches
Angle	4°	
Refractive index at 5893 A	1.617	
Dispersion at $H\gamma$	283	A/mm
Length of spectrum from $H\beta$ to $H\epsilon$	3.2	mm

THE 24-INCH OBJECTIVE PRISM

The Bausch and Lomb Company furnished the disk for the 24 inch objective prism. It was manufactured from one piece of dense flint (DF-2) glass weighing 260 pounds, molded to shape in a deep furnace utilizing a pot design to produce the wedge shape. The disk was free from deep striations and air bubbles. The diameter of the finished disk, before being reduced in the optical shop, was 26.75 inches; the thickness varied from 3.0 to 4.3 inches.

The diameter of the finished prism is 24.5 inches, the graduated thickness from 0.75 to 2.5 inches, producing an angle of 4°. The two surfaces were figured flat to within an accuracy of one-tenth of a wave length of sodium light. The annealing of the glass seems to have been excellent. This became apparent from the quality of the spectra secured on first trial, no additional local figuring of the prism being necessary. The spectra (Pl. XXXII) compare favorably with slit spectrograms of low dispersion. Spectral classifica-

PLATE XXXII

OBJECTIVE-PRISM SPECTRA MADE WITH AN EXPOSURE OF 45 MINUTES WITH E-33 EMULSION
Center of field: R.A. = 22^h14^m; d = +55°.5 (1855); size of field $1/2° \times 2/3°$

tion can be made with considerable accuracy, and absolute-magnitude characteristics are readily visible.

The prism-cell mounting is so constructed that when in place it may be easily rotated through any desired angle in a plane perpendicular to the optical axis of the telescope. The cell with the prism forms a symmetrically balanced mass of 150 pounds. A 26-inch, 150-pound ringweight, situated in front of the correcting lens, is first removed from the telescope when the prism is to be mounted; thus any rebalancing of the instrument is avoided. Optical data for the prism are given in Table 1.

Exposure and limits.—With Eastman 103a-O emulsion and 10 minutes' exposure, the limiting magnitude is 18.5. Using Eastman 103G emulsion with a No. 15 Wratten filter and with an exposure of 20 minutes, the limiting photovisual magnitude obtained is 15.5. A No. 22 Wratten filter and Eastman 103-E emulsion with 20 minutes' exposure gave for a limiting red magnitude 16.8 (estimate). Usually plates are developed in a tank with D19 at 65° F. for 5 minutes.

Spectra of stars 0.2 mm wide, of limiting magnitude 12.5, have been obtained with Eastman 33 emulsion and exposure of 30 minutes.

In planning this instrument I am indebted to many friends for inspiration and advice, and it is fitting to express here my sincere thanks to all. Particularly, I wish to thank Dr. Theodore Dunham, Jr., Dr. Walter Baade, and Dr. J. A. Anderson for their generous help during the preliminary stages of planning; Dr. James G. Baker for his generous assistance in the optical tests; Dr. Robley Williams for aluminizing the mirror; and my colleague, Dr. S. W. McCuskey, for his all-round help throughout the duration of the project.

I am deeply indebted to Mr. Charles Stilwell, Mr. Warner Seely, and Mr. William Burger, of the Warner and Swasey Company, for making available for the construction of this instrument all the talent and long experience of the company in the field of telescope-making. Their only concern was to produce an instrument as nearly perfect in its optics, as complete in its design, and as convenient in its operation as was humanly possible. To attain this goal they intrusted Mr. E. N. Jennison with the design of the mounting, Mr. C. A. Robert Lundin with the optics, and Mr. H. L. Cook with the assembling and erection of the telescope, all highly skilful workers and outstanding leaders in their respective fields.

THE MILKY WAY IN MONOCEROS*

BART J. BOK AND JEAN M. RENDALL-ARONS
Harvard College Observatory
Received March 7, 1945

ABSTRACT

The section of the Milky Way in Monoceros, between galactic longitudes 176° and 186°, represents one of the most regular parts of the Milky Way. The present investigation is based on spectral types and colors to $m = 11.5$ and on general star counts to $m = 14.5$. The general absorption in the least-obscured regions is found to be of the order of $A_{pg} = 0.6$ mag/kpc, for distances up to 2000 parsecs. The final results and conclusions are presented in Section VII at the end of the paper. The star densities exhibit nowhere marked increases with increasing distance from the sun. For the stars at large, they are close to unity to a limiting distance of 2500 parsecs. The most notable negative density gradients are found for the F stars. The spectral density-curves indicate that there exist marked variations in the *shape* of the general luminosity function over the first 500 parsecs.

The present paper represents the first of a series on spectral types, colors, and star counts for regions at low galactic latitude not affected appreciably by irregular local obscuration. The section between galactic longitudes 176° and 186° is notable for its uniformity of stellar distribution. If we avoid here the regions south of the galactic circle (where the extensions of the dark nebula in Orion can still be detected) we find nowhere marked regions of local obscuration.

In the next few years students of galactic structure may well wish to pay special attention to the more uniform sections of the Milky Way. The researches of the last fifteen years have made it possible to delineate the more important dark nebulae; and it has further been shown that, for the smooth and relatively unobscured sections of our Milky Way, one may derive from observations of color excesses reliable information concerning the average coefficient of absorption to a distance of 2000 parsecs. In a first attempt at a study of the regular features in the stellar distribution for the nearer portions of our galaxy, we should now concentrate on those regions for which the absorption is probably small and not subject to sizable fluctuations.

The results to be presented here and in some of the papers to follow are based on published and unpublished spectra classified by Miss Cannon, on color indices derived from blue and red photometric comparisons, and on star counts from blue-sensitive plates. Since our work depends to such a large extent on spectral types and color indices, we shall first examine the principal sources of error which affect the analysis of data of this sort.

1. *Systematic errors in spectral classification.*—During recent years it has become more and more evident that most systems of spectral classification are subject to systematic errors, frequently dependent on the apparent magnitude. Miss Cannon's system of classification is probably affected as little as any system by errors of this sort, but even here there has been some indication of the presence of systematic errors depending on apparent magnitude. We have tried to eliminate the effects of such errors by the combination of data for several neighboring spectral subdivisions.

2. *The lack of distinction between giants and dwarfs.*—This represents one of the most serious problems in the use of the HD or HDE spectra of the later spectral types. We have tried to predict the approximate numbers of dwarfs from data on the bright stars and thus to obtain at least approximate information on the distribution of the giants.

3. *Uncertainties in the magnitude and color systems.*—In spite of continuous checking and cross-checking we have found no indications, in the blue or red standard magni-

* A paper presented at the symposium during the dedication of the Observatorio Astrofisico Nacional de Tonanzintla in Mexico, in February, 1942.

tudes, of systematic errors in excess of 0.2 mag. It is believed that the final color indices are in no case affected by systematic errors as high as 0.15 mag.

4. *Errors in the computed absorptions.*—The computed absorptions are subject to error for two additional reasons. The first is that there exists for several spectral types some uncertainty about the value of the average color index for unreddened stars. The errors from this source could hardly be much over 0.1 mag. in the blue-red color system. The second and more serious source of error arises from lack of definite information about the value of the conversion factor from color excesses to total absorptions. We have used the factor 3.0 for our blue-red system, which agrees substantially with the $1/\lambda$-law of scattering, but we realize that future work may make it necessary to use a different value. A comparison between color excesses and galaxy absorptions in intermediate latitudes, however, makes it seem unlikely that the factor is in error by as much as 30 per cent; this is further confirmed by color studies for stars viewed through isolated dark nebulae. Since we have limited ourselves largely to regions of slight obscuration, our computed absorptions should be in error by not more than 0.5 mag.

5. *Errors in absolute magnitudes and dispersions.*—It is extremely difficult to assign average absolute magnitudes and dispersions for each HD spectral class. The establishment of an accurate two-way system of spectral classification, in which the absolute magnitude and spectral class are read off simultaneously, represents one of the most urgent needs. Pending the completion and large-scale operation of such a system, it would, however, be a mistake not to make the best possible use of the available spectral data. For the present investigation the uncertainty in the average assumed absolute magnitudes is large, but we should remember that an analysis based on HD and HDE spectra is already much more accurate than one based on general star counts alone.

If we consider the total effect of these various sources of error, we find that the percentage error of the computed star densities for distances within 1000 parsecs of the sun is generally of the order of 30 per cent and that in extreme cases it may be as high as 50 per cent. It does not seem that at this moment any investigation of galactic structure can claim a higher accuracy, but even with this uncertainty we can decide about the general characteristics of the galactic density distributions in what is generally referred to as the "local system." From the accumulating observations we should soon be able to decide whether our sun is in a region of excessive, average, or subnormal star density with respect to its surroundings.

In a paper presented at the symposium for the dedication of the McDonald Observatory,[1] the stellar distribution for the Milky Way in Monoceros was investigated on the basis of the spectral types, colors, and star counts that were available at that time. We present here the complete data and analysis for the entire section.

I. SPECTRAL TYPES AND COLOR INDICES

Miss Cannon made available to us in advance of publication the HD charts for the section between $\alpha = 6^h22^m$ and 7^h08^m and $\delta = -5°$ to $+3°$. The 1939 paper[1] was largely based on the color indices of 1054 stars in two regions, one centered at $\alpha = 6^h45^m$, $\delta = 0°$, the other at $\alpha = 6^h57^m$, $\delta = +1°$, which together cover an area of 27.8 square degrees. The color indices for these two regions were determined from blue and red polar comparison plates, taken with the 8-inch Ross (IR) camera at the Oak Ridge station of the Harvard Observatory. The blue series were made on Cramer Hi-Speed plates without a filter; the red, on Eastman 1-C special plates with a *ciné*-red filter. Dr. Cuffey and Miss Cherry were responsible for the taking of the plates and for their measurement and reduction. As standards of magnitude, the polar sequence on the International Photographic Scale[2] and the red polar sequence determined by Mrs. Payne-Gaposchkin[3] were used.

[1] *Ap. J.*, **90**, 249, 1939; *Harvard Reprints*, No. 180.

[2] *Trans. I.A.U.*, **1**, 71, 1922.

[3] *Harvard Ann.*, Vol. **89**, No. 5, 1935.

Dr. MacRae, Mr. Fleischer, and Dr. Mowbray took the photometric plates for four more centers. The plates for the six centers, together, provide the material for the determination of color indices and magnitudes for the area of 96 square degrees covered by the *Henry Draper Extension* in this section of the Milky Way. The extremes of galactic longitude and latitude[4] are 176° and 186°, and −4° and +7°. For the four centers of the second group, the blue series were again taken on Cramer Hi-Speed plates; but for the red series, Eastman 103 E plates and a *ciné*-red filter were found to give better results. In addition to the pole, Harvard standard regions C3, C4, and C5 were frequently used as standards. As photographic standards, we used those of Miss Leavitt,[5] corrected according to HB 781; and as photo-red standards, those of Mrs. Payne-Gaposchkin,[6] reduced to the color system of the IR, Eastman 103 E plates, and a *ciné*-red filter. The photo-red magnitude found from Eastman 1-C special plates are on the same color system as those of *H.A.*, Vol. **89**, Nos. 5 and 8, but the magnitudes from the 103 E plates refer to a somewhat longer effective wave length. The color equation of the 103 E system of magnitudes was determined by first plotting the curve relating the scale measurements and the standard magnitudes for the polar stars with color indices <0.40 mag. The magnitudes of the polar stars with C.I. > 1.20 mag. were then read from this curve, and the differences were computed between these magnitudes and those listed in *H.A.*, Vol. **89**, No. 5. The results showed that the magnitudes of *H.A.*, Vol. **89**, No. 5, needed a correction of

$$\Delta m = -0.08 \times \text{C.I.},$$

in order to reduce them to the system of the 103 E plates. This correction was applied to the magnitudes of the standard stars in the drawing of the reduction curves for the standard 103 E plates. All measurements and reductions were carried out by Mrs. Arons. For each center, five blue and five red comparison plates were taken. The total number of color indices available is 2800.

All plates in a series were preferably taken at similar zenith distances; but where it was necessary to apply a correction, we used the formula

$$\Delta m = 0.40 \, (\sec \zeta - 1)$$

for the extinction correction to the blue magnitudes and

$$\Delta m = 0.20 \, (\sec \zeta - 1)$$

for the red magnitudes. All measurements were confined to the central areas of the plates, for which no correction for distance from the center is necessary. The remaining error should not exceed 0.10 mag.

As a check on the consistency of the blue magnitudes for the six IR centers, these magnitudes were intercompared on one of Dr. Baker's star-count plates (see next section) with an exposure time of 30 minutes. This investigation showed that the blue magnitudes in five of the six centers were consistent to within 0.10 mag. but that the blue magnitudes of one region seemed to differ systematically from those for the other centers.

It happened that there was considerable overlap between the IR plates for the region with the questionable magnitudes and a neighboring region for which there was no indication of errors in the photographic magnitudes. The existence of a systematic difference was confirmed by measurements made on the overlapping portions of the IR plates. A comparison between the IR sequence and the sequences used for the star counts also tends to confirm the presence of a small systematic error in the photographic magnitudes of this particular one of the six centers.

[4] All galactic latitudes and longitudes refer to the Harvard pole; $\alpha = 12^h40^m$, $\delta = +28°$.

[5] *Harvard Ann.*, Vol. **71**, No. 4, 1917.

[6] *Harvard Ann.*, Vol. **89**, No. 8, 1938.

The only doubt about the justification for the application of a systematic correction (which at maximum amounts to +0.20 mag. for $m = 10.5$) arises from the good systematic agreement between the average residuals for the five IR plates originally used to derive the standard sequence. We have used the following corrections to the blue magnitudes for the doubtful center:

m_{pg}	Δm	m_{pg}	Δm
9.0	+0.00	10.5	+0.20
9.5	+0.08	11.0	+0.18
10.0	+0.14	11.5	+0.13

These corrections have been applied to the color indices listed in Table 2 for regions 9, 10, 11, and 12. By applying the full correction we may make the color indices for regions 9–12 slightly too red, since the corrections are admittedly the maximum values.

There are no indications for the presence of systematic errors in the photo-red magnitudes; but, because of the lack of red check plates, this result is not too certain; there remains the possibility of systematic errors of the order of 0.10 mag., in the photo-red magnitudes.

II. STAR COUNTS

The plates for the star counts were very generously provided by Dr. R. H. Baker, of the University of Illinois. Ten plates were needed to cover the region between $\alpha = 5^h45^m$ and 7^h15^m, $\delta = -9°$ and $+9°$. The centers of the plates are, on the average, 4° apart; and, since the countable area free from distance correction is close to 60 square degrees, the overlap between the counts from one plate to the next is considerable.

As standards, we used the magnitudes in S.A. 98, which falls well within the region. The magnitudes were taken from *H.A.*, Vol. **101**; and the corrections listed by Seares[7] were used for the reduction to the International Photographic Scale. Because of the considerable overlap from plate to plate, we encountered no difficulties in the transfer of sequences. Even for the plates centered farthest away from S.A. 98, it is unlikely that the standard magnitudes could be in error by as much as 0.2 mag., and the errors are certainly smaller for the nearer plates. Twenty stars were considered a norm for each sequence. The smallness of the systematic errors in the magnitudes was confirmed by a comparison with the standard blue magnitudes for the color program that were obtained by direct polar and C-region comparisons (see preceding section). All photometric calibrations and counts were carried out by Mrs. Arons.

Two checks were made on the accuracy and internal consistency of the counts. First, the counted numbers of stars to different limits of apparent magnitude were compared for all overlapping parts of the plates. It was found that the blue magnitudes used as standards in the star counts and in the work on the colors are generally consistent to within ±0.10 mag. but that a few deviations as large as 0.15 mag. exist. Second, at the conclusion of the program Mrs. Arons recounted for each of the subdivisions A-R (see following section) an area of 4 square degrees. Small corrections were applied to reduce the star counts to one single uniform system.

The absence of an appreciable constant error of counting was proved by a comparison of the star counts for S.A. 98 published by van Rhijn[8] with those for the same center made by Mrs. Arons. For the brighter magnitudes a further check was obtained by comparing the star counts with the results of counts in the same area made in the catalogue of photographic magnitudes for the HDE stars. It may be of interest to mention at this point that the *Henry Draper Extension* is essentially complete to $m_{pg} = 11.5$ in this part of the sky.

The section covered by the star counts was divided into eighteen areas, over each of which the stellar distribution appeared to be reasonably uniform. This division was

[7] *Ap. J.*, **61**, 303, 1925; *Mt. W. Contr.*, No. 289.

[8] *Groningen Pub.*, No. 43, 1929.

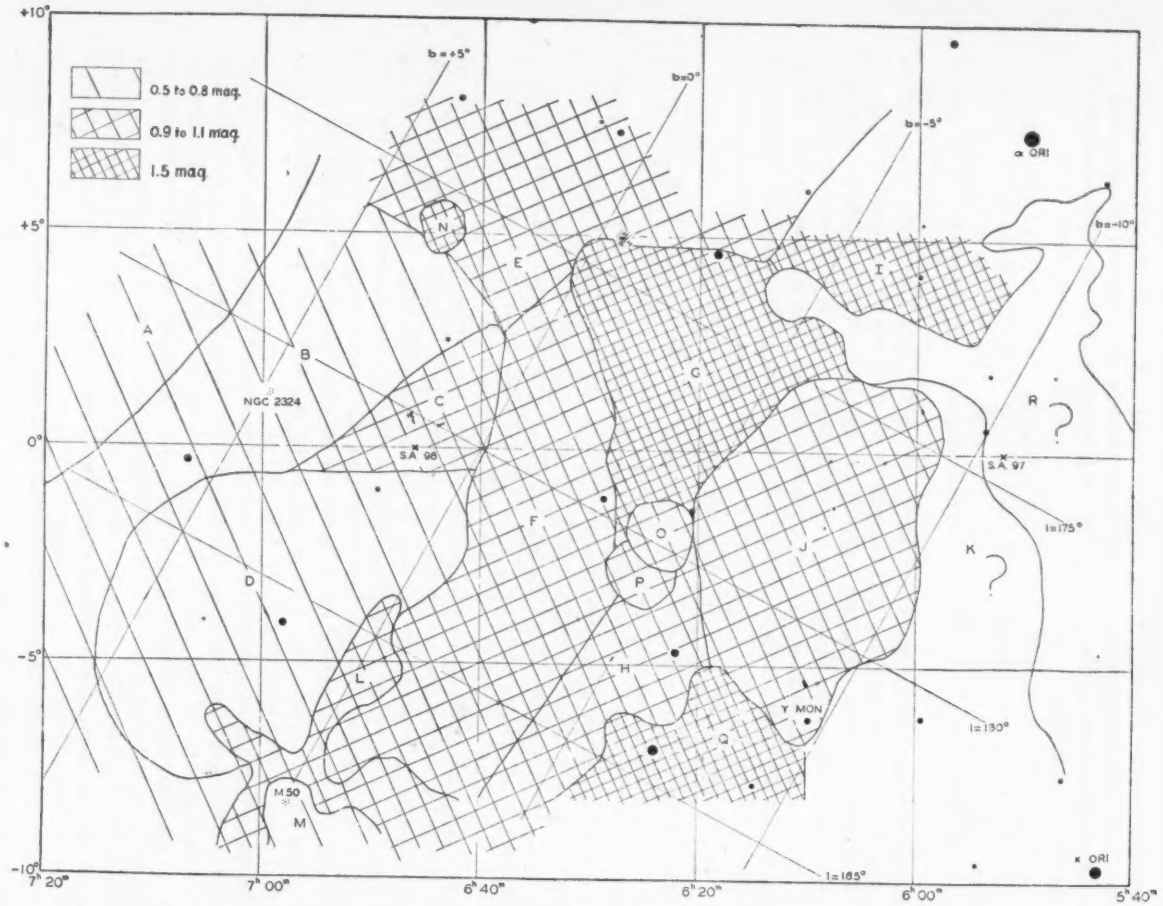

FIG. 1.—The Monoceros region. The capital letters $A, B, C, \ldots . R$ indicate the regions referred to in the text. The shading in these regions gives the derived value of the total photographic absorption at a distance of 1000 parsecs. These shadings have been omitted in K and in R, regions for which the total photographic absorption is not well determined. The positions of some of the more conspicuous stars and clusters and two Selected Areas are shown and for convenience galactic and equatorial co-ordinate nets are included.

made on the basis of the counts to various magnitude limits, from an inspection of long exposure plates reaching to faint limits, and with constant reference to Ross's *Milky Way Atlas*. Figure 1 shows the division in areas *A*–*R*.

In Table 1 we have listed for each area the final values of log $N(m)$, $N(m)$ being the average number of stars per square degree brighter than apparent photographic magnitude m for each particular area.

III. THE ANALYSIS FOR SPACE REDDENING

The spectrum-color survey covers a smaller area than the star-count survey. We felt that it was desirable at first to subdivide the region with known colors and spectral types—which is really the heart of this section of the Milky Way—somewhat more finely than shown in Figure 1. The region with known colors was therefore divided into twenty subregions.

TABLE 1

VALUES OF LOG $N(m)$ FOR PHOTOGRAPHIC MAGNITUDES IN THE MONOCEROS REGION

Area	l	b	8.0	8.5	9.0	9.5	10.0	10.5	11.0	11.5	12.0	12.5	13.0	13.5	14.0	14.5
A	180°	+ 7°	0.25	0.39	0.58	0.84	1.12	1.31	1.49	1.64	1.79	1.98	2.11	2.42	2.49	.....
B	180	+ 5	.48	.69	.80	0.98	1.19	1.38	1.53	1.71	1.85	2.00	2.16	2.45	2.68	2.93:
C	180	+ 2	.38	.73	.69	0.87	1.19	1.43	1.61	1.81	1.95	2.12	2.29	2.48	2.83	.....
D	185	+ 3	.38	.74	.83	0.98	1.19	1.39	1.61	1.79	1.94	2.11	2.28	2.51	2.78	2.99
E	175	+ 3	.....	.....	.73	0.95	1.13	1.32	1.51	1.72	1.88	2.03	2.19	2.40	2.71	.....
F	180	− 3	0.25	.62	.59	0.87	1.11	1.32	1.50	1.69	1.84	1.98	2.15	2.35	2.61	.....
G	175	− 3	.....	.....	.....	0.77	0.93	1.16	1.37	1.56	1.74	1.89	2.05	2.20	2.53	.....
H	183	− 5	.....	.48	.73	0.96	1.20	1.35	1.59	1.70	1.88	2.02	2.19	.....	.....	.....
I	172	− 7	.....	.....	.....	0.73	0.88	1.12	1.30	1.49	1.68	1.84	2.01	2.22	2.55	.....
J	177	− 7	.....	.....	.....	0.68	0.90	1.12	1.33	1.53	1.71	1.86	2.00	2.18	2.60	.....
K	177	−12	.....	.....	.....	0.42	0.77	1.01	1.17	1.37	1.54	1.69	1.87	2.07	2.34	.....
L	183	0	.....	0.49	.46	0.86	1.12	1.35	1.53	1.69	1.84	1.94	2.14	2.34	2.60	2.89:
M	188	0	.....	.....	.91	1.08	1.28	1.48	1.64	1.82	1.92	2.07	2.22	2.41	2.67	.....
N	176	+ 3	.....	.....	.....	1.00	1.21	1.37	1.49	1.62	1.76	1.90	2.05	2.21	2.58	.....
O	180	− 5	.....	.....	.16	0.56	0.87	1.03	1.22	1.41	1.55	1.68	1.83	2.02	2.36	.....
P	181	− 5	.....	.....	.30	0.62	0.83	1.10	1.23	1.40	1.55	1.72	1.84	2.04	2.39	.....
Q	183	− 8	.....	.....	0.02	0.56	0.81	1.09	1.30	1.46	1.51	1.73	1.83	2.03	2.29	.....
R	173	−10	.....	.....	.....	0.50	0.66	0.98	1.19	1.33	1.45	1.59	1.74	1.91	2.21	.....

The data on the color indices and excesses in color areas 1–8 have already been reproduced in the paper presented at the time of the symposium for the dedication of the McDonald Observatory.[1] The resulting color excesses were summarized in Table 2 of that paper. The new material gives similar data for twelve additional regions. The resulting color indices are shown in Table 2 for the stars with spectral types B8–A7 and apparent photographic magnitudes between 10.0 and 11.5.

When the averages for the separate regions were combined, it was found that the results for regions 9–12, 13 and 14, 15–17, and 18–20 were strictly comparable; and in the final analysis we have therefore combined the colors for these areas into single averages. In agreement with the earlier investigation we have assumed the following values for the normal colors of various spectral types:

B8–A0 ..... −0.15 mag.
A1–A7 ..... +0.05

The final color excesses are listed in Table 3.

In spite of the somewhat larger base line of the new color system we are still assuming that a good approximation to the total absorption, K, is obtained from the relation

$$K = 3 \times \text{C.E.}$$

The distances in the last column have been computed from the relation

$$5 \log r = (m - M) + 5 - K .$$

We have assumed throughout that M equals 0.0 for the B8–A0 stars and that M equals +1.2 for the A1–A7 stars.

The total number of early B-type stars for the region was small, but the observed colors of these stars have been taken into consideration in deciding upon the most likely

TABLE 2

MEAN COLOR INDICES IN THE MONOCEROS REGION

Area	9		10		11		12	
l	186°		186°		185°		185°	
b	+5°		+3°		+2°		+1°	
Sp.	B8–A0	A1–A7	B8–A0	A1–A7	B8–A0	A1–A7	B8–A0	A1–A7
m_{pg}								
10.0–10.5	+0.16(10)	+0.20 (7)	−0.01(18)	+0.15(19)	+0.01(21)	+0.04(16)	+0.04(21)	+0.14(14)
10.5–11.0	+ .10(18)	+ .22(16)	+ .08(28)	+ .22(22)	+ .07(30)	+ .10(26)	+ .03(27)	+ .11(22)
11.0–11.5	+0.16(20)	+0.30(24)	+0.18(27)	+0.22(34)	+0.06(31)	+0.17(30)	+0.10(22)	+0.19(32)

Area	13		14		15		16	
l	183°		184°		184°		182°	
b	+1°		−1°		−2°		−2°	
Sp.	B8–A0	A1–A7	B8–A0	A1–A7	B8–A0	A1–A7	B8–A0	A1–A7
m_{pg}								
10.0–10.5	+0.01(7)	+0.09 (9)	+0.02(11)	+0.22 (5)	+0.02 (9)	+0.19 (7)	+0.03(11)	+0.18(10)
10.5–11.0	.00(5)	+ .11 (5)	+ .06(16)	+ .20(18)	+ .09(17)	+ .22(14)	+ .10(15)	+ .24(14)
11.0–11.5	+0.09(5)	+0.23(12)	+0.05(16)	+0.28(17)	+0.31 (9)	+0.20(11)	+0.21(22)	+0.22(26)

Area	17		18		19		20	
l	183°		178°		178°		178°	
b	−4°		−4°		−2°		0°	
Sp.	B8–A0	A1–A7	B8–A0	A1–A7	B8–A0	A1–A7	B8–A0	A1–A7
m_{pg}								
10.0–10.5	+0.05 (9)	+0.24(11)	−0.27(1)	.....	−0.07(18)	+0.09(14)	−0.19 (2)	+0.10 (6)
10.5–11.0	+ .12(11)	+ .22(14)	− .05(1)	.....	+ .04(14)	+ .04(13)	− .04(11)	+ .09(13)
11.0–11.5	+0.28 (8)	+0.33(23)	+0.16(2)	+0.16(4)	+0.17(12)	+0.17(12)	+0.01 (6)	+0.17(16)

values for the interstellar absorption for each area. There are ten stars of spectral class B5 and earlier for which Stebbins, Huffer, and Whitford[9] have measured color indices with the aid of the photoelectric cell and fifty-nine such stars for which our plates yield color indices.

The stars with photoelectric color indices fall almost entirely in regions 17 and 19. The five stars in region 17 indicate no color excess at $r = 400$ parsecs and one amounting to +0.50 on our scale at 2000 parsecs, which is in general agreement with our results in Table 3. The three stars in region 19 are considerably reddened, the average color ex-

[9] *Ap. J.*, **91**, 20, 1940; *Mt. W. Contr.*, No. 621.

cesses on our scale being of the order of +0.50 at $r = 1000$ parsecs. This is larger than the excesses according to Table 3 but, as we shall see presently, is in agreement with our colors for the early B stars.

TABLE 3

COLOR EXCESSES IN MONOCEROS

m_{pg}	B8–A0			A1–A7		
	C.E.	K	r	C.E.	K	r
	Regions 9–12 ($l=185°$, $b=+2°$)					
10.25	+0.20	0.6	850	+0.08	0.2	580
10.75	.22	0.7	1020	.11	.3	690
11.25	+0.37	1.1	1070	+0.17	0.5	790
	Regions 13 and 14 ($l=184°$, $b=0°$)					
10.25	+0.16	0.5	890	+0.07	0.2	580
10.75	.18	.5	1120	.08	.2	720
11.76	+0.22	0.7	1290	+0.11	0.3	870
	Regions 15–17 ($l=183°$, $b=-2°$)					
10.25	+0.18	0.5	890	+0.15	0.5	500
10.75	.25	0.8	980	.18	.5	630
11.25	+0.42	1.3	980	+0.20	0.6	760
	Regions 18–20 ($l=178°$, $b=-2°$)					
10.25	+0.02	0.1	1070	+0.04	0.1	600
10.75	.15	.4	1180	.03	.1	760
11.25	+0.25	0.8	1230	+0.12	0.4	830

The early B's are especially numerous in regions 9–12 and 18–20. In regions 9–12 the average color indices for the stars with spectral types B0–B5 are:

m_{pg}	$\overline{C.I.}$	n
<9.0	−0.21	5
9.0–10.0	+ .02	8
10.0–11.0	+0.09	21

The average unreddened color index for the B0–B5 stars is probably of the order of −0.35 mag., and their mean absolute magnitude close to −2.5. The early-type stars suggest, then, for regions 9–12, a total photographic absorption of the order of 0.6 mag/kpc, in agreement with the value derived from Table 3.

In regions 18–20 the early B stars are quite reddened. For ten stars with apparent magnitudes 9.5–10.5 we find:

Sp.	$\overline{C.I.}$	n
B0	+0.48	2
B3	.53	2
B5	+0.07	6

These data suggest a total photographic absorption of the order of from 1.0 to 1.5 mag/kpc, which is definitely larger than the value in Table 3 but in agreement with the photoelectric colors.

The results on the reddening for the Monoceros–Canis Major region are confirmed, in a general way, by the work of Cuffey[10] on colors in three galactic clusters in Monoceros and Canis Major. One of Cuffey's clusters, NGC 2324, which shows a color excess of 0.30 mag. at a probable distance of 3320 parsecs, falls in region 7 of our color survey.

TABLE 4

TOTAL PHOTOGRAPHIC ABSORPTIONS IN MONOCEROS

Area	$\bar{l}$	$\bar{b}$	A_{pg}	Area	$\bar{l}$	$\bar{b}$	A_{pg}
1–2	180°	0°	1.1 mag/kpc	13–14	184°	0°	0.5 mag/kpc
3–6	181	+3	0.9	15–17	183	−2	1.0
7–8	182	+5	0.4	18–20	178	−2	0.8
9–12	185	+2	0.7				

The second cluster which interests us here, Messier 50, lies directly on the galactic equator 3° south of the southern border of our field. The observed excess of 0.30 mag. at 1210 parsecs agrees well with the averages for regions 13 and 14 in Table 3.

By a combination of the results from various sources we determine the total photographic absorptions as listed in Table 4. The values of A_{pg} refer generally to limiting distances of from 1500 to 2000 parsecs from the sun, depending on the value of the total obscuration. The only regions for which there exists some conflict between the color excesses derived from the A and B stars are regions 18–20. We have here assumed the mean of the value of A_{pg} suggested by the early B's, $A_{pg} = 1.2$ mag/kpc, and that for the B8–A0 stars, $A_{pg} = 0.5$ mag/kpc.

In our discussion of star counts and spectral distributions we have used a somewhat coarser system of subdivision than for the color work. Subdivision *C* of Figure 1 covers regions 1, 2, and 4 and half of 3 and 6; *B* covers 5, 7, and 8 and the remaining parts of 3 and 6; *D* takes in 9, 10, 11, 12, and 13; *F* includes 14, 15, 16, 20, and half of 19; and *G*, 18 and the other half of 19. The small subdivisions *O*, *P*, and *H* all fall in region 17.

The color data lead to the variations of *K* (the average total photographic absorption) with distance from the sun shown in Table 5. The colors of the distant stars in region *C* are apparently generally redder than those of *D*. Since we have already applied the maximum positive correction to the blue IR magnitudes in *D*, it is unlikely that the true reddening is in excess of that listed here. By using the value $A_{pg} = 0.6$ mag/kpc (see next section) in region *D* we are therefore certain that we are applying the maximum allowable absorption correction for this region. The value $A_{pg} = 1.0$ mag/kpc appears to represent an upper limit to the photographic absorption in region *C*.

[10] *Ap. J.*, **94**, 55, 1941.

The star-count data suggest that region F is affected by an obscuring cloud absorbing about 0.3 mag. The resulting extra reddening would be small and is apparently lost in the errors in the color indices. This same cloud covers region G, for which the total absorption will be found to amount to 0.65 mag. from star-count data. This absorption is quite apparent from a comparison between the colors in G and C and D. The colors suggest that the obscuring cloud lies probably at between 500 and 700 parsecs from the sun.

Regions B and H are further away from the galactic equator. For B at $b = +5°$ the absorption amounts to $A_{pg} = 0.6$ mag/kpc to a distance of 1250 parsecs. The small color excess of NGC 2324 suggests that there is little absorption beyond 1500 parsecs in the region, but this needs further confirmation. In region H at $b = -5°$ the color excesses show an average absorption of $A_{pg} = 1.0$ mag/kpc to 1500 parsecs.

TABLE 5

VARIATION OF TOTAL PHOTOGRAPHIC ABSORPTIONS, K, WITH DISTANCE FROM THE SUN (FROM COLOR EXCESSES)

Distance	Region					
	C (180°, +2°)	D (185°, +3°)	F (180°, −3°)	G (175°, −3°)	B (180°, +5°)	H (183°, −5°)
300	0.4	0.1	0.2	0.0	0.3	0.3
500	0.5	0.3	0.4	0.3	.5	0.5
750	0.9	0.5	0.5	1.2	.6	0.7
1000	1.1	0.6	0.6	1.5	.6	0.9
1250	1.3	0.7	0.6	1.5	0.8	1.2
1500	1.6	0.8	1.0	.....	.....	.....
2000	2.0	1.2	2.0	.....	.....	.....

IV. DENSITY ANALYSIS FOR REGION D

We found in the preceding section that, for the area covered by the color survey, the smallest reddening at the galactic equator apparently occurs in region D. Spectral types and color indices are available for an area of 20.7 square degrees in D; and, since these stars all fall between galactic latitude 0° and +5°, we find D an ideal region for a detailed investigation of the variations of star density with increasing distance from the sun.

The photogaphic magnitudes that have actually been used are those corrected for the systematic error discussed in Section I. The absorption characteristics of the region are assumed to be described satisfactorily by the value $A_{pg} = 0.6$ mag/kpc to a limiting distance of 2000 parsecs; because of our correction to the original photographic magnitudes, this coefficient represents an upper limit. The available information on the surface distribution of the stars in D is summarized in Table 6.

The numbers of stars with photographic magnitudes fainter than 8.5 are generally sufficiently large for a satisfactory density analysis, but the total area covered by D is so small that the numbers of brighter stars are too much affected by random fluctuations. We have therefore strengthened the data for the brighter stars in two ways:

1. For the stars with visual magnitudes brighter than 7.0 we have derived values of log $A'(m)$ from a paper by Seydl.[11] The counts represent the averages over all galactic longitudes for the zone with galactic latitude 0° to ±10°; $A'(m)$ is again the number of stars with photographic magnitudes $m - \frac{1}{4}$ to $m + \frac{1}{4}$ reduced to an area of 100 square degrees. The smoothed values of log $A'(m)$ are listed in Table 7.

[11] *Pub. Nat. Obs. Prague*, No. 6, 1929.

2. For the stars brighter than $m_{pg} = 8.5$ special counts were made in the *Henry Draper Catalogue* for the region between $\alpha = 6^h25^m$ and 7^h05^m; $\delta = -7°$ and $+3°$. These counts are reproduced in Table 8.

The values of log $A'(m)$ from these three different sources were plotted against the apparent magnitude for each successive interval of spectral type, and smooth curves were drawn to represent the counts. The final values for log $A'(m)$ are listed in Table 9.

TABLE 6

THE SURFACE DISTRIBUTION OF THE STARS IN REGION *D*
(Total Area = 20.7 Square Degrees)

m_{pg}	Spectra								
	B0–B2	B3–B5	B8–A0	A1–A7	F0–F2	F5–F8	G0–G5	K0–K2	K5–M
<8.0.....	0	5	8	2	2	1	0	5	0
8.0– 8.5....	0	2	15	3	1	0	0	8	0
8.5– 9.0....			24	13	9	1	1	3	3
9.0– 9.5....	1	9	28	10	8	2	2	14	4
9.5–10.0....			41	29	6	3	11	13	5
10.0–10.5....	1	20	64	47	15	10	19	20	8
10.5–11.0....			102	81	20	15	29	32	20
11.0–11.5....	.....	.....	137	96	15	19	28	25	17

TABLE 7

VALUES OF LOG $A'(m)$ FOR THE ZONE $b = 0°$ TO $\pm 10°$, ACCORDING TO SEYDL

Sp.	m_{pg}							
	4.25	4.75	5.25	5.75	6.25	6.75	7.25	7.75
B8–A0.....	9.30	9.68	0.03	0.39	0.70	0.90	.....	.....
A1–A7.....	9.40	9.54	9.78	9.97	0.22	0.46	.....	.....
F0–F2.....	.....	8.90	9.24	9.50	9.80	0.03	.....	.....
F5–F8.....	.....	9.10	9.31	9.50	9.72	9.95	0.20	.....
G0–G5.....	.....	8.97	9.24	9.41	9.66	9.90	0.18	.....
K0–K2.....	.....	.....	9.45	9.67	9.90	0.22	0.50	0.70
K5–M.....	.....	.....	.....	9.02	9.30	9.54	9.75	9.97

The addition of the data in Tables 7 and 8 makes it possible to compute from Table 9 the density distributions from the immediate vicinity of the sun out to the limit of our survey.

Before we can compute the star densities for the stars of spectral types G and later, it is necessary that we attempt somehow to separate the giants from the dwarfs. Because of possible fluctuations in the galactic plane of the numbers of giants at large distances from the sun, it is impossible to depend on average percentages of dwarfs, such as are frequently used in studies for high and intermediate latitudes. Instead we shall try to predict, in various ways, the probable values of $A'(m)$ for the dwarfs alone. Since scarcely any of the dwarfs with photographic apparent magnitudes brighter than 11.5 are beyond 100 parsecs from the sun, we can assume, without too much risk, that the star density in the galactic plane does not vary appreciably for these stars. The predicted numbers have been computed in three different ways:

1. From Seydl's[11] tabulations we find the average numbers of G0–G5, K0–K2, and K5–M stars for $m \leqq 7.0$ for the zone $b = \pm 30°$ to $\pm 70°$. Since the percentages of dwarfs among these stars have been given by van Rhijn and Schwassmann,[12] we can compute the probable numbers of dwarfs for our region. The predicted numbers are represented by a formula of the type

$$\log A'(m)_d = C + 0.60\,(m_{pg} - 8.0)\,.$$

TABLE 8

VALUES OF $A'(m)$ FOR A REGION IN MONOCEROS COVERING 100 SQUARE DEGREES

Sp.	m_{pg}			
	6.75	7.25	7.75	8.25
B8–A0	4	11	18	49
A1–A7	1	0	4	12
F0–F2	0	2	1	3
F5–F8	1	1	0	6
G0–G5	0	0	4	1
K0–K2	1	5	3	4
K5–M	1	0	0	1

TABLE 9

ACCEPTED VALUES OF LOG $A'(m)$ IN REGION D

m_{pg}	Spectra						
	B8–A0	A1–A7	F0–F2	F5–F8	G0–G5	K0–K2	K5–M
4.25	9.30	9.40	.....	.....	.....	.....	.....
4.75	9.68	9.54	8.90	9.10	8.97	.....	.....
5.25	0.03	9.78	9.24	9.30	9.24	9.45	.....
5.75	0.39	9.97	9.50	9.50	9.41	9.67	9.05
6.25	0.70	0.22	9.80	9.72	9.66	9.90	9.28
6.75	0.90	0.46	0.03	9.95	9.90	0.20	9.52
7.25	1.15	0.71	0.30	0.20	0.18	0.50	9.77
7.75	1.45	0.93	0.55	0.43	0.45	0.76	0.07
8.25	1.68	1.15	0.80	0.67	0.75	1.02	0.37
8.75	1.93	1.42	1.05	0.88	1.07	1.33	0.68
9.25	2.13	1.71	1.32	1.13	1.34	1.60	1.03
9.75	2.30	2.03	1.55	1.37	1.65	1.90	1.33
10.25	2.48	2.33	1.77	1.62	1.93	2.05	1.70
10.75	2.68	2.56	2.00	1.83	2.16	2.13	1.81
11.25	2.82	2.70	2.00	2.03	2.26	2.20	2.05

where $C = 0.18$ for the G0–G5 stars and $C = 9.37 - 10$ for the K0–K2 stars. $A'(m)_d$ represents here the average number of dwarfs per 100 square degrees with apparent photographic magnitude $m - \frac{1}{4}$ to $m + \frac{1}{4}$. The number of K5 and M dwarfs proves to be so small as to be negligible for all practical purposes.

2. A study of the percentages of dwarfs in intermediate latitudes for the stars in the Yale zone catalogues[13] shows that at $b = \pm 30°$ the average percentage for $m_{pg} =$

[12] *Zs. f. Ap.*, **10**, 161, 1935.

[13] *Harvard Circ.*, No. 400, 1935.

9.0 − 10.0 is close to 55 per cent for the G0–G5 stars and 10 per cent for K0–K2 stars. We find for the most probable values of C: $C = 0.28$ for the G0–G5 stars and $C = 9.40-10$ for the K0–K2 stars.

3. In the third method the numbers of dwarfs are predicted directly from the luminosity function for G and K stars published by van Rhijn and Schwassmann.[12] Again the basic assumption is made that the star density is equal to unity to the limit of our survey for the dwarf stars. The resulting values of C are: $C = 0.21$ for the G0–G5 stars and $C = 9.54-10$ for the K0–K2 stars.

The agreement between the three different values of C is quite satisfactory. In the following calculations we shall use the formula

$$\log A'(m)_d = 0.25 + 0.60\,(m_{pg} - 8.0)$$

for the G0–G5 dwarfs and

$$\log A'(m)_d = 9.45 + 0.60\,(m_{pg} - 8.0)$$

for the K0–K2 dwarfs. We neglect the dwarfs among the K5–M stars brighter than $m_{pg} = 11.5$ in the galactic plane, their number being too small to be significant. The extreme possible values for C are 0.10 and 0.35 for the G's and 9.40 and 9.60 for the K's. It is unlikely that the predicted numbers of dwarfs could be in error by as much as 20 per cent.

By the use of the above formulae, together with the totals for giants and dwarfs combined from Table 9, we find the probable values of $\log A'(m)_g$ for the giants alone; these are listed in Table 10, together with the corresponding percentages of dwarfs.

The variation of star density with distance from the sun has been computed with the aid of the method of Schalén and Lindblad.[14] The mean absolute magnitudes and dispersions around these means were assumed to have the values given in Table 11. The values listed there are the means per unit volume; the mean values M_m that are used in the Schalén-Lindblad method were computed with the aid of Malmquist's formula.[15] The Malmquist corrections were generally of the order of −1.0 mag.

The computed star densities are given in Tables 12 and 13. In Table 12 we list the densities uncorrected for absorption effects; in Table 13, the corresponding values corrected for a photographic absorption of 0.6 mag/kpc. The densities are expressed as numbers of stars per 1000 parsec^3 as a unit.

The densities in Table 13 represent the most likely values, though we admit that, because of the application of the maximum possible correction to the blue magnitudes, the value $A_{pg} = 0.6$ mag/kpc is decidedly an upper limit. We note that the densities for the B8–A0 stars appear to increase slightly to a maximum of 0.18 at a distance of 200 to 300 parsecs from the sun, that the star density between 500 and 700 parsecs is again very nearly equal to that near the sun, and that the star density drops rapidly between 700 and 1000 parsecs. There is little variation in the star density for the red giants, but a density decrease seems established for the A1–A7 stars. The most striking result is probably the steep negative gradients for the F stars, for which the density at 250 parsecs is one-fourth that near the sun.

We do well, however, at this point to remember the limitations of our analysis as outlined at the beginning of this paper. The density analyses are very sensitive to uncertainties in the assumed values of the mean absolute magnitudes. In the absence of absorption all densities will be doubled if one chooses for the assumed mean absolute magnitude a value less bright by 0.5 mag. without making any change in the assumed dispersion. Since at present the assumed mean absolute magnitudes can be trusted only

[14] See *Uppsala Medd.*, No. 37, 1928.

[15] *Lund Medd.*, Ser. II, No. 22, 1920.

to the nearest half-magnitude, we see that the computed densities may possibly be in error by 50 per cent.

We note further that we must be very careful in the application of the correct value of the Malmquist correction[15] at each apparent magnitude. Frequently the slope of the curve, relating the apparent magnitude, m, and the observed log $A'(m)$'s, decreases as we go to fainter magnitudes. If, in the analysis of the Schalén-Lindblad method, we

TABLE 10

VALUES OF $A'(m)_g$ AND PERCENTAGES OF DWARFS IN REGION D

m_{pg}	G0–G5 Stars		K0–K2 Stars	
	$A'(m)_g$	Percentage of Dwarfs	$A'(m)_g$	Percentage of Dwarfs
4.75	0.08	20	.....	.....
5.25	0.13	23	0.27	3
5.75	0.17	32	0.46	2
6.25	0.30	33	0.76	4
6.75	0.47	40	1.53	3
7.25	0.88	42	3.06	3
7.75	1.56	45	5.6	4
8.25	3.09	45	10.1	4
8.75	6.8	43	20.6	4
9.25	11.9	46	38.2	4
9.75	24.7	40	76	4
10.25	40	53	106	5
10.75	66	55	122	10
11.25	40:	80:	133	16

TABLE 11

MEAN ABSOLUTE MAGNITUDES AND DISPERSIONS

Sp.	M_0 (pg)	σ
B8–A0	+1.0	±1.0
A1–A7	2.0	1.0
F0–F2	3.5	1.2
F5–F8	4.5	1.2
gG0–gM	+2.0	±1.0

apply then a single average Malmquist correction, we are in effect using too bright a value of M_m for the faint apparent magnitudes; and the densities for large distances will then come out smaller than the actual values. By following this procedure we might derive erroneous negative density gradients.

In cases where it is difficult to apply Malmquist corrections because of irregularities in the (m, log $A'(m)$) curves, it is generally preferable to do the analysis with the aid of an (m, log π) table for each spectral interval. It is not difficult to construct the basic (m, log π) tables so that the densities, found by trial and error, represent the average numbers of stars per unit volume of 1000 parsec^3 at each distance. In this method it is not necessary to compute the Malmquist corrections, since these are automatically accounted for in the construction of the basic tables.

With respect to the results of Table 13, we may doubt the reality of the excess density for the B8–A0 stars at 200 to 300 parsecs, but the drop in star density beyond 700 parsecs seems too large to be accounted for by uncertainties in the analysis or other sources

TABLE 12

SUMMARY OF STAR DENSITIES (NUMBER OF STARS PER 1000 PARSEC^3) IN MONOCEROS REGION *D*
(No Absorption Correction)

d	SPECTRA				
	B8–A0	A1–A7	F0–F2	F5–F8	gG0–gM
50	0.12	0.43	1.3	3.5	0.25
100	.12	.35	0.83	1.9	.25
150	.13	.27	0.65	1.2	.23
200	.14	.22	0.47	0.8	.22
300	.14	.20	0.28	.....	.18
400	.12	.18	0.15	.....	.16
500	.10	.15	.....	.....	.12
600	.08	.12	.....	.....	0.09
700	.07	0.09	.....	.....	.....
800	.06	.....	.....	.....	.....
900	.05	.....	.....	.....	.....
1000	0.04	.....	.....	.....	.....

TABLE 13

SUMMARY OF STAR DENSITIES (NUMBER OF STARS PER 1000 PARSEC^3) IN MONOCEROS REGION *D*
(Corrected for $A_{pg}=0.6$ Mag/Kpc)

d	SPECTRA				
	B8–A0	A1–A7	F0–F2	F5–F8	gG0–gM
50	0.12	0.43	1.3	3.3	0.27
100	.15	.34	0.93	1.9	.27
150	.16	.32	0.76	1.2	.28
200	.18	.27	0.55	0.8	.27
300	.18	.28	0.28	.....	.25
400	.17	.27	.....	.....	.23
500	.15	0.23	.....	.....	0.19
600	.13	.....	.....	.....	.....
700	.13	.....	.....	.....	.....
800	.10	.....	.....	.....	.....
900	.08:	.....	.....	.....	.....
1000	0.06:	.....	.....	.....	.....

of error. The negative density gradient for the A1–A7 stars is slight, but in all probability real. The rapid drop in star density for the F stars is too large to be accounted for by errors of any sort. Finally, for the red giants there is little indication of the presence of large variations in star density over a distance of 500 parsecs. It seems unlikely that the remaining uncertainties would be sufficiently large to change the character of the above general conclusions.

V. THE CHANGES IN THE LUMINOSITY FUNCTION

For all analyses of general star counts we are forced to make use of an assumed general luminosity function. Not only is our knowledge of this function for the vicinity of the sun far from complete; but we have come to realize, more and more, that it may vary considerably as we proceed outward from the sun. The existence of such variations for the directions of the galactic polar caps is well established, and their approximate values have been derived. Until recently very little information was available on the variations in the galactic plane. From spectral data, such as those analyzed in the preceding section, however, it is possible to study these variations directly, and we shall attempt to do so for the direction of region *D* in Monoceros.

The star densities of Table 13 are used as a basis for the calculations. With the aid of the mean absolute magnitudes and dispersions of Table 11 we can compute the contribution to the general luminosity function made by the stars of successive spectral classes at each distance. By adding the numbers for the spectral subdivisions we can

TABLE 14

CHANGES IN THE GENERAL LUMINOSITY FUNCTION FOR REGION *D* IN MONOCEROS
(Values of log $\varphi'(M)$)

M_{pg}	*d* (PARSECS)					
	Van Rhijn	50	100	200	300	500
−0.5	.....	8.18	8.20	8.26	8.23	8.15
0.0	8.38	8.52	8.53	8.56	8.57	8.46
+0.5	.....	8.88	8.86	8.85	8.83	8.72
+1.0	9.04	9.12	9.08	9.04	9.02	.....
+1.5	.....	9.34	9.26	9.17	9.15	.....
+2.0	9.47	9.48	9.40	9.26	.....	.....
+2.5	.....	9.62	9.51	9.30	.....	.....
+3.0	9.56	9.72	9.54	9.30	.....	.....
+3.5	.....	9.82	9.61	9.34	.....	.....

obtain the number of stars, $\varphi'(M)$, between absolute photographic magnitudes $M - \frac{1}{4}$ and $M + \frac{1}{4}$ per 1000 parsec^3 at various distances from the sun. We have reproduced these figures in Table 14. For comparison we have added the values of $\varphi'(M)$ according to van Rhijn's standard function,[16] corrected to refer to the same interval in absolute magnitude and unit volume.

We note that there exists a satisfactory agreement between the standard function and that derived from our material at a distance of 100 parsecs from the sun. The only marked excess of our numbers over those represented by the standard function occurs at $M = 0$; apparently, we find here for near-by regions an excess in the number of A stars over the average included in the standard function.

As we proceed outward, the shape of the general luminosity function changes appreciably. The values of log $\varphi'(M)$ at $M = 0.0$ remain steadily in excess of the standard value, but the log $\varphi'(M)$ values at $M = +2.0$ and $+3.0$ are well below the standard values at 200 parsecs from the sun. Table 14 also shows clearly how very limited is the information on changes in the luminosity function that can be derived from spectral data complete to the eleventh or twelfth apparent magnitude. We shall need accurate spectral classifications to at least the fourteenth magnitude before we can be

[16] *Groningen Pub.*, No. 47, Table 6, 1936.

gin to investigate changes in the luminosity function to distances of 1000 parsecs with any degree of completeness.

VI. THE ANALYSIS OF THE STAR COUNTS

The data on the star counts have already been given in Table 1. For purposes of analysis it is desirable to have also available the values of $A(m)$, the average numbers between $m - \frac{1}{2}$ and $m + \frac{1}{2}$ per square degree of the sky. The adopted values of $A(m)$, computed from slightly smoothed values of $N(m)$, are printed in Table 15. We shall now proceed to analyze these $A(m)$'s in detail. For a brief résumé of conclusions the reader is referred to the summary at the end of the paper.

1. *Regions* C *and* D.—The two fields at $b = +2°$ are close to the galactic equator; and the absorption coefficient there seems to be, on the average, equal to $A_{pg} = 0.7$ mag/kpc. With this value for the absorption assumed to hold to a distance of 2500

TABLE 15

ADOPTED VALUES OF $A(m)$ IN MONOCEROS

Area	l	b	9.0	10.0	11.0	12.0	13.0	14.0
A	180°	+ 7°	4.28	13.5	25.2	49.8	119	296
B	180	+ 5	4.87	13.4	29.6	53	157	500
C	180	+ 2	5.56	18.4	36.1	69	199	601
D	185	+ 3	5.26	15.0	35.8	68	202	624
E	175	+ 3	5.51	12.4	30.0	56	133	466
F	180	− 3	4.89	13.5	28.0	49	123	457
G	175	− 3	.....	8.9	20.9	40.4	95	297
H	183	− 5	3.77	10.2	22.3	37.8	111	161
I	172	− 7	.....	7.0	17.9	39.0	97	359
J	177	− 7	.....	7.9	21.4	32.4	90	360
K	177	−12	.....	7.5	13.2	26.7	68	229
L	183	0	5.24	14.7	30.6	42.9	119	361
M	188	0	8.0	16.5	33.7	54.6	140	318
N	176	+ 3	.....	12.9	18.2	37.8	91	392
O	180	− 5	.....	7.1	13.3	28.5	52	243
P	181	− 5	2.85	7.7	13.9	26.9	58	280
Q	183	− 8	.....	8.2	16.5	24.3	55	169
R	173	−10	1.34	6.3	12.3	16.6	45	151

parsecs, we can now proceed to analyze the general star counts for these regions, and also the published star counts[8] for S.A. 98, which falls in region C. Because of the lack of information about the changes in luminosity for distances beyond 500 parsecs, we shall use the standard (m, log π) table for $b = 2°$ from the paper by Bok and MacRae presented at the symposium of the New York Academy of Sciences on "The Fundamental Properties of the Galactic System."[17] The density analysis with the aid of the (m, log π) table, corrected for absorption, yields the average densities listed in Table 16.

The star densities in Table 16 show an excess within 500 parsecs of the sun; but beyond that, to the limit of 2500 parsecs for which our absorptions are more or less valid, we find a constant average star density very nearly equal to that near the sun. Because of the considerable variations in the shape of the general luminosity function in the galactic plane which were brought to light in the preceding section, it is not simple to interpret the densities of Table 16. The incipient decrease in the star density for the F stars (Table 13) apparently does not persist to great distances—or, at least, does not affect similarly the densities for the G and K dwarfs. A careful study of the distributions of the F, G, and K dwarfs between $m = 11.0$ and $m = 15.0$ for this part of the sky promises to yield exceedingly interesting results.

[17] *Ann. N.Y. Acad. Sci.*, **42**, 219, 1941.

2. *Regions* G, F, *and* E.—These three regions are at the same low latitudes as regions *C* and *D*. The deficiencies in the $A'(m)$'s, therefore, strongly suggest the presence of a dark nebula of nonuniform density, with a small absorbing power in *F* and *E* and a somewhat larger one in *G*. The general star counts in *F* and *E* are very similar; and since no color excesses are available in *E*, we shall limit our analysis to *F* and *G*, making the tacit assumption that the results for *F* apply in general to *E*.

From the deficiencies in $A(m)$ for *G* we find that the total photographic absorption of the extra dark nebula amounts to 0.65 mag. The general star counts suggest that the dark nebula is relatively close to the sun, but the total area covered by the nebula is too small to yield a dependable value for its distance. We have found previously (see Table 5) that the color excesses show that the stars beyond 600 parsecs from the sun are abnormally reddened by an amount corresponding very nearly to the total absorption found from the star counts. The numbers of stars are rather small in *G*, and random fluctuations in the counted numbers render it inadvisable to make an elaborate distance analysis from the numbers of stars of successive intervals of spectral class. The deficiencies are apparently mostly in the B8–A0 stars; the later A's and the G–M stars are deficient beyond $m = 10.0$, and the F's show little effect even at 11.0. The spectral-distribution data place the dark nebula at a distance of roughly 500 parsecs from the sun.

TABLE 16

AVERAGE DENSITIES CORRECTED FOR A_{pg}=0.7 MAG/KPC FROM GENERAL STAR COUNTS

Distance	Region *D*	S.A. 98	Distance	Region *D*	S.A. 98
<100.....	1.5	1.0	< 630.....	1.0	1.2
158.....	1.5	1.2	1000.....	1.0	1.0
251.....	1.5	1.5	1580.....	1.0	1.0
400.....	1.0	1.5	2510.....	.....	1.0

The total photographic absorption of the dark nebula affecting *F* is only 0.30 mag. from the star-count data. The effects of this small absorption do not appear clearly in the color excesses, but the similarity of the spectral distribution curves in *G* and *F* make it seem likely that the distance of the nebula is 500 parsecs or slightly less. It seems reasonable to suppose that the dark nebulae overlying *G*, *F*, and *E* are all part of the same system and that we may assign an average distance of 500 parsecs to this nebula. The nebula is probably a part of the system of dark nebulae associated with the bright nebula in Orion.

3. *Regions* L *and* M.—Both regions are comparatively small in area. Region *L*, which lies along the galactic equator, is one of star deficiency. It should naturally be compared with *D* and *F*. The run of the star counts in *L* agrees very closely with that in *F;* and we conclude from the $A(m)$'s in Table 16 that, overlying region *L*, in addition to a general absorption $A_{pg} = 0.7$ mag/kpc, there is present a dark nebula absorbing between 0.3 and 0.5 mag. at a distance of the order of 500 parsecs.

The deficiencies in region *M* are (with the exception of that for $m = 14.0$) less than in region *L*. Region *M* is toward the edge of our counted region; but the counts, so far as they go, indicate that the distribution of stars and dark material to a distance of 2000 parsecs does not differ markedly from that for *D*.

4. *Regions* B *and* A.—These two fields at $b = +6°$ and $+8°$ fall in the relatively unobscured regions north of the galactic circle. No galaxy counts are available at these latitudes, but at $b = +10°$ an average photographic absorption of the order of 1.0 mag. is suggested. The colors in *B* show that the absorption in this field is probably represented best by $A_{pg} = 0.6$ mag/kpc to a limiting distance of 1500 parsecs; Cuffey's color

data for NGC 2324 render it unlikely that there is much absorption beyond 1500 parsecs for this direction.

The (m, log π) tables for $b = 6°$ and $b = 8°$ by Bok and MacRae[17] were corrected for $A_{pg} = 0.6$ mag/kpc to limiting distances of, respectively, 1500 and 1200 parsecs. The computed average densities are found to be very nearly equal in both fields. In judging these densities we should keep in mind that they are expressed in terms of the average densities at corresponding heights above the galactic plane in the direction of the galactic pole and that the usual drop in star density with increasing distance from the galactic plane has already been taken into account. The densities are:

Distance	Density	Distance	Density
63	1.5	400	1.0
100	1.5	630	0.8
158	1.5	1000	0.8
250	1.5	1580	0.8

Again we find an excess for the regions within 400 parsecs of the sun. The deficiency beyond 500 parsecs seems well established by the counts, but we should remember that the densities are rather sensitive to the assumed value for the absorption coefficient for these directions. The deficiencies would disappear if the total absorption were increased by 0.5 mag. A careful study of the distributions of faint galaxies for the region between $l = 180°$ and 190° and $b = +5°$ and $+15°$ would be well worth while.

5. *Regions* J, H, *and* Q.—These three regions are south of the galactic plane at the same distance from the galactic circle as B and A. Color indices and excesses are available for H, in which field the observed excesses suggest an average value $A_{pg} = 1.0$ mag/kpc to 1500 parsecs.

A comparison between the star counts in H and B suggests that in H we have, in addition to the same general absorption that overlies B, a dark nebula absorbing 0.7 mag. at a distance of not more than 500 parsecs from the sun. Because of the lack of a sufficient number of stars brighter than $m = 10.0$, it is impossible, from the general counts alone, to fix the distance of this nebula more carefully. The absence of appreciable color excesses for the A1–A7 stars with $m = 9.5$ to 10.5, together with the appreciable excesses for the B8–A0 stars with $m = 9.5$ and fainter, makes it very likely that the dark nebula is at 400–500 parsecs from the sun.

The counts in J show a somewhat smaller deficiency with respect to B and A than did those in H. The average absorption of the dark nebula is of the order of 0.5 mag.; but, because of lack of spectral and color data, we can say little more than that it is within 500 parsecs of the sun. Region Q falls at almost the same galactic latitude as does A; the deficiencies in $A(m)$ are large, and the total absorption of the dark nebula here amounts to nearly 1.0 mag.

6. *Regions* R *and* K.—Lack of data on spectra and colors makes it very difficult to say anything definite about these two fields. We are further hampered by the lack of a suitable comparison field north of the galactic circle at the same latitudes (9° and 11°). Also, the apparent absence of galaxies shows that we have here a rather heavily obscured region. Region R (in which division falls S.A. 97) is apparently most obscured and the counts here seem to demand a dark nebula with a total absorption of approximately 1.0 mag.

7. *Remaining regions.*—Region N is a small patch, somewhat obscured, in E; the excess absorption is less than 0.5 mag. Regions O and P are both very small. The counts and colors show that in all probability the absorption characteristics in these fields resemble those in H very closely. Region I is at the edge of the counted area. Apparently the stellar distribution and the structure of the obscuring material in I do not differ materially from what we have already found for G.

VII. RESULTS AND CONCLUSIONS

The investigation deals with the study of stellar distribution for a region of the Milky Way in Monoceros, where the surface distribution of the stars is quite uniform. The analysis is based on spectral types (HDE) and color indices for an area of 100 square degrees and star counts for 400 square degrees. It is found that the computed star densities are subject to uncertainties of the order of 30 per cent of their values because of errors arising from difficulties in the classification of spectral types, photometric errors, errors in the derived absorptions, and lack of information about mean absolute magnitudes and dispersions around these means.

The basic data are given in Table 1 (see Fig. 1) and Table 2. The main results of the analysis are the following:

1. Reddening is present in the apparently unobscured regions of the Milky Way between $l = 178°$ and $l = 188°$, the average coefficient of absorption amounting to $A_{pg} = 0.6$ to 1.0 mag/kpc to a distance of 2000 parsecs.

2. Star counts and observed color excesses suggest the presence of extended regions of obscuration south of the galactic equator. The total absorption is slight, varying between 0.3 and 1.0 mag. The obscuration is probably caused by the low-latitude extensions of the Orion dark nebulae and is apparently located at 400–500 parsecs from the sun.

3. The regions at $b = +6°$ to $+8°$ are comparatively clear, with an average $A_{pg} = 0.6$ mag/kpc to limiting distances of 1500–1200 parsecs.

4. The density analysis for a region of minimum obscuration near $l = 185°$, $b = +2°$ (see Table 13), shows that—

a) The densities of the B8–A0 stars are either the same or slightly in excess of those for the vicinity of the sun to $r = 500$ parsecs and then drop to one-half the value near the sun at $r = 1000$ parsecs;

b) The densities of the A1–A7 stars drop to 60 per cent of that near the sun at $r = 500$ parsecs;

c) Steep negative gradients are exhibited by the F0–F2 and F5–F8 stars (density 25 per cent) of that near the sun at $r = 250$ parsecs;

d) The densities of the gG0–gM stars are almost constant over the first 500 parsecs, with a tendency to decrease.

5. The star counts to $m = 14.5$ in the clear regions, combined with the available data in S.A. 98 to $m = 18.0$, show that for $l = 180°$, $b = 0°$, the average star density for the vicinity of the sun is in excess by 20–50 per cent with respect to the prediction by the standard luminosity function of van Rhijn and that the average density for $r = 1000$ to 2500 parsecs is close to unity.

6. The spectral density curves show further that the general luminosity function for the direction $l = 185°$, $b = +2°$, exhibits pronounced variations in shape over the first 500 parsecs (see Table 14).

THE STELLAR DISTRIBUTION FOR TWO SOUTHERN FIELDS*

BART J. BOK AND FRANCES W. WRIGHT
Harvard College Observatory
Received March 7, 1945

ABSTRACT

The present paper is a continuation of the investigation for the Milky Way in Monoceros, published in the preceding paper. The fields are at $l = 261°$, $b = +1°$ (S.A. 193), and at $l = 249°$, $b = +1°$ (Field II). Selected Area 193 is apparently free from obscuration to a distance of 1600 parsecs, where as in Field II the average absorption to 1200 parsecs amounts to $A_{pg} = 0.5$ mag/kpc. The final results and conclusions are presented in Section VI at the end of the paper. The star densities in Field II are similar to those in the Monoceros field. The same holds for S.A. 193 with the exception that for this field the early B stars do not exhibit any marked decrease of space density with distance from the sun. Further evidence is presented for the existence of marked changes in the *shape* of the general luminosity function within 200–500 parsecs from the sun.

During the last years of her life Miss Cannon spent much time and effort on the classification of the spectra of faint Milky Way stars in Carina and Centaurus. Since it is extremely important that we should obtain magnitudes and colors for most of these stars, the observers at the Boyden Station, under the direction of Dr. Paraskevopoulos, have taken, in recent years, many photometric series of plates for this part of the sky. A special star-count program is intended to supplement the work on the colors, magnitudes, and spectra of the brighter stars.[1] Because of world conditions, it may be many years before we shall be able to complete the collection of the necessary plate material for the entire area, and we have therefore decided to measure the available plates for those areas for which enough material has already accumulated. The measurement and reductions were all done by Miss Wright, who collaborated with Bok in the analysis. The carrying-out of the research was made possible in part by a grant from the Draper Fund of the National Academy of Sciences.

We shall report here the results for two centers, the first being S.A. 193 at $\alpha = 11^h24^m$, $\delta = -60°$ ($l = 261°$, $b = +1°$), and the second, a field at $\alpha = 10^h13^m$, $\delta = -56°$ ($l = 249°$, $b = +1°$). The bright nebula near η Carinae lies about halfway between these two centers, at $l = 254°$, $b = 0°$. Selected Area 193 falls in the rich but fairly uniform section of the Milky Way between the Carina nebula and the Southern Coal Sack ($l = 270°$, $b = 0°$). Field II falls in a uniform region directly west of the Carina nebula. In spite of the close proximity of the Carina nebula, the stellar distribution for this center differs rather markedly from that around the Carina nebula, or S.A. 193. The surface distribution of the stars in Field II is remarkably uniform, but the surface density of the stars is there very much less than for the section between $l = 252°$ and $l = 270°$. A comparative study of S.A. 193, the region near η Carinae, and Field II promises to be very interesting.

The colors for S.A. 193 have been investigated by Dr. and Mrs. Gaposchkin,[2] who found there a surprising preponderance of stars with negative color indices. The work by the Gaposchkins was done before Miss Cannon's spectra had become available. Because of the presence of systematic errors in the Potsdam spectral classes,[3] Mrs. Gaposch-

* A paper presented at the symposium held during the dedication of the Observatorio Astrofisico Nacional de Tonanzintla in Mexico, in February, 1942.

[1] *Trans. I.A.U.*, **6**, 282, 1938.

[2] *Ap. J.*, **90**, 321, 1939; *Harvard Reprints*, No. 181, 1939; also "Harvard Mimeo. Ser.," Vol. 2, No. 3, 1936.

[3] Cf. Vyssotsky, *Ap. J.*, **93**, 425, 1941.

kin did not attempt a complete density analysis; but her results for S.A. 193 show clearly that the light of distant stars in this region is not appreciably reddened.

I. Color Indices and Space Reddening

The total number of available color indices in S.A. 193 is 732; that for Field II, 333. In each case we have covered an area of 6 square degrees.

The photographic magnitudes for S.A. 193 were determined from two 30-minute plates with the 3-inch Ross camera (RB) and from two 10-minute exposures with the 8-inch Bache camera (B). The photo-red magnitudes were determined from two 120-minute and two 15-minute exposures with the 24-inch Bruce camera (A). As standards, the Gaposchkin photographic and photo-red magnitudes[4] for S.A. 193 were used. The magnitudes were measured only on the central portions of the plates free from distance correction. The only correction that was applied to the magnitudes was one for color equation to reduce the photographic magnitudes of the late-type stars measured on the RB plates to the International Photographic system. Grating images were found useful for the measurement of the magnitudes of the brightest fifteen stars in the field.

The system of the photographic and photo-red magnitudes used here is, of course, the same as that in the study of the Gaposchkins, since both are based on the same standard sequences. Further checks of this standard sequence will be possible when the Carina-Centaurus programs are completed, but the plates that are available lead us to believe that the system of colors should agree to within 0.20 mag. with the blue-red system for the C regions at $+15°$.

The probable error of an average final photographic magnitude is of the order of ± 0.06 mag.; that of a final photo-red magnitude, of the order of ± 0.08 mag. The average probable error of the color indices in this investigation is therefore close to ± 0.10 mag.

The color indices in Field II were obtained in very much the same way. The blue magnitudes were measured on one 60-minute and two 30-minute RB plates, calibrated with the aid of a transferred sequence from S.A. 193, and two 10-minute plates taken with the 10-inch Metcalf (MF) telescope in series with the standard regions E4 and F2. The magnitudes were all consistent, with the sole exception that a small correction was applied to the standards in E4. The red magnitudes were found from one 15-minute and two 20-minute A plates and two 15-minute MF plates; S.A. 192 served as a standard. Small corrections for extinction were applied, but there was no need to consider distance corrections in any part of the program.

The results of the color analyses are summarized in Tables 1 and 2. The numbers in parentheses directly following each average are the numbers of contributing stars. The most striking effect in both tables is the preponderance of negative color indices among the early-type stars of all magnitudes.

There always remains, especially for far southern declinations, the possibility of systematic errors in the photometric system. We shall therefore inspect first the average color indices of those stars for which the excesses, if present at all, would be expected to prove rather small. We list for that purpose in Table 3, side by side, the normal colors for Harvard spectral types adopted by Mrs. Gaposchkin[2] in her study of red indices in southern Selected Areas and some averages for S.A. 193 and Field II.

Table 3 shows, first of all, that the averages for S.A. 193 and Field II are remarkably similar. A comparison between the observed averages and the normal colors indicates that, especially for the faintest stars, the observed colors allow a maximum positive correction of, at most, $+0.20$ mag. This result, however, is uncertain because of possible small systematic errors in the spectral classes and, further, because of lack of information concerning percentages of dwarfs and average true color indices for unreddened regions.

[4] *Harvard Ann.*, Vol. 89, No. 9, 1937.

The data on the color excesses of the early-type stars are summarized in Table 4. The spectral classes and the assumed true color indices are at the head of the table. The entries are the color excesses derived from Tables 1 and 2 and, in parentheses, the numbers of stars contributing to each average.

TABLE 1

OBSERVED COLOR INDICES IN S.A. 193
($l=261°$, $b=+1°$)

Sp.	m_{pg}						
	8.00–8.49	8.50–8.99	9.00–9.49	9.50–9.99	10.00–10.49	10.50–10.99	11.00–11.49
B0	−0.18(1)	−0.30(1)	−0.14(1)	−0.43(3)	−0.27(2)	.....	−0.15(1)
B2	−0.36(1)	.....	−0.30(1)	.....	−0.30(1)	.....	.....
B3	.....	−0.60(4)	−0.55(3)	−0.30(6)	−0.20(2)	+0.19(1)	.....
B5	−0.53(1)	−0.36(1)	−0.44(4)	−0.45(5)	−0.35(9)	−0.32(6)	−0.23(1)
B8–A0	−0.44(6)	−0.37(11)	−0.35(28)	−0.32(42)	−0.30(63)	−0.39(90)	−0.26(90)
A1–A2	−0.05(1)	−0.03(2)	+0.21(2)	−0.15(3)	−0.14(9)	−0.28(18)	−0.11(23)
A3–A7	.....	+0.01(1)	+0.09(2)	+0.16(2)	0.00(3)	−0.11(12)	−0.08(24)
A8–F2	.....	+0.14(1)	+0.37(2)	+0.29(4)	+0.09(5)	−0.16(2)	−0.28(2)
F5–F8	.....	+0.16(3)	+0.21(1)	+0.48(2)	+0.35(6)	+0.36(2)	+0.33(7)
G0–G5	.....	+0.95(2)	+0.82(1)	+0.73(4)	+0.60(11)	+0.87(9)	+0.77(15)
K0–K2	+1.32(2)	+1.27(4)	+1.21(6)	+1.33(3)	+1.20(8)	+1.39(11)	+1.11(15)
K5 and later	+1.37(1)	+1.56(3)	+1.95(1)	+2.04(3)	+1.75(5)	+1.89(6)	+1.74(11)

TABLE 2

OBSERVED COLOR INDICES IN FIELD II
($l=249°$, $b=+1°$)

Sp.	m_{pg}						
	8.00–8.49	8.50–8.99	9.00–9.49	9.50–9.99	10.00–10.49	10.50–10.99	11.00–11.49
B0	.....	.....	.....	.....	.....	+0.46(1)	.....
B2	.....	−0.26(1)	.....	.....	.....	.....	.....
B3	.....	.....	.....	.....	.....	.....	.....
B5	−0.39(1)	.....	.....	−0.11(2)	.....	.....	.....
B8–A0	−0.14(8)	−0.36(7)	−0.10(8)	−0.14(15)	−0.12(25)	−0.16(42)	−0.19(32)
A1–A2	.....	.....	−0.08(4)	+0.13(6)	+0.07(11)	−0.08(18)	−0.18(4)
A3–A7	.....	.....	+0.11(3)	+0.28(1)	+0.06(2)	−0.09(21)	−0.07(4)
A8–F2	+0.53(2)	+0.10(1)	+0.23(2)	+0.52(1)	+0.40(6)	+0.22(7)	−0.03(1)
F5–F8	.....	+0.47(1)	.....	+0.39(1)	+0.67(3)	+0.29(6)	−0.01(1)
G0–G5	+1.10(1)	+1.15(1)	+0.82(2)	+0.54(2)	+0.33(2)	+0.60(6)	+0.13(3)
K0–K2	.....	+1.44(4)	+1.27(4)	+1.23(2)	+1.30(10)	+1.45(9)	+1.56(2)
K5 and later	.....	.....	+2.11(1)	+1.94(2)	+1.98(5)	+1.77(10)	+1.81(9)

We shall first analyze the excesses for S.A. 193. We note from Table 2 that in S.A. 193 all excesses for the B8–A0 and A1–A2 stars come out negative. Their average is not far from −0.20 mag.; and, in order to reduce them to zero on the average, we shall have to apply the maximum correction of +0.20 mag. allowed by the colors of the late-type stars. We therefore reach the conclusion that in S.A. 193 the B8–A2 stars down to the limit of 11.5 show no sign of space reddening and that interstellar reddening does not

affect the colors of the stars up to a distance corresponding to a value of the modulus $m - M = 11.0$. The corresponding distance amounts to 1600 parsecs. This conclusion is confirmed very nicely by the observed color excesses for the B3 and B5 stars for which $m - M < 11.0$.

TABLE 3

AVERAGE COLOR INDICES IN S.A. 193 AND FIELD II COMPARED TO NORMAL VALUES

Sp.	Normal Colors		S.A. 193		Field II	
	Main Sequence	Giants	m=9.0 to 10.0	m=11.0 to 11.5	m=9.0 to 10.0	m=10.5 to 11.0
A1–A2	+0.05	.....	0.00	−0.11	+0.05	−0.08
A3–A7	+0.20	.....	+0.12	−0.08	+0.15	−0.09
A8–F2	+0.28	.....	+0.32	−0.28:	+0.32	+0.22
F5–F8	+0.45	+0.80	+0.39	+0.33	+0.39	+0.29
G0–G5	+0.70	+1.00	+0.75	+0.77	+0.68	+0.60
K0–K2	+1.05	+1.50	+1.25	+1.11	+1.26	+1.45

TABLE 4

OBSERVED COLOR EXCESSES IN S.A. 193 AND FIELD II

Sp.	B0	B2	B3	B5	B8–A0	A1–A2
Normal C.I.	−0.50	−0.45	−0.35	−0.20	−0.10	+0.05
m_{pz}	S.A. 193					
8.0– 9.0	+0.26(2)	+0.09(1)	−0.25(4)	−0.24(2)	−0.29(17)	−0.09(3)
9.0–10.0	+ .14(4)	+ .15(1)	− .03(9)	− .25(9)	− .23(70)	− .06(5)
10.0–11.0	+ .23(2)	+0.15(1)	+0.28(3)	− .14(15)	− .25(153)	− .28(27)
11.0–11.5	+0.35(1)	.....	.....	−0.03(1)	−0.16(90)	−0.16(23)
	Field II					
8.0– 9.0	.....	.....	.....	.....	−0.14(15)	.....
9.0–10.0	.....	.....	.....	+0.09(2)	− .03(23)	0.00(10)
10.0–11.0	+0.96(1)	.....	.....	.....	−0.05(67)	−0.07(29)

The more distant stars in S.A. 193 show, however, very definite signs of space reddening. We assume the following values for the mean absolute magnitudes:

B0 = −4.0 B3 = −2.2
B2 = −3.0 B5 = −1.6

These agree closely with those suggested by Stebbins, Huffer, and Whitford.[5] We find, after the application of the correction of +0.20 mag. to the excesses of Table 4, that the average excess for $m - M = 11.8$ equals +0.17, for $m - M = 12.6$, +0.37; and for

[5] *Ap. J.*, **90**, 209, 1939; *Mt. W. Contr.*, No. 617.

$m - M = 14.0, +0.40$. The uncertainties for the absolute magnitudes for the small number of stars involved render it inadvisable to analyze these data any further, but we conclude that for S.A. 193 space reddening does definitely set in beyond a distance of 1600 parsecs and that it amounts to +0.40 mag. at a distance of 3000–4000 parsecs.

The total photographic absorption equals probably three times the blue-red color excess. The color data at hand suggest that for S.A. 193 there is little or no absorption (less than 0.5 mag.) for distances up to 1600 parsecs. Apparently, some absorption exists between $r = 1600$ parsecs and $r = 4000$ parsecs, but the average coefficient is probably not more than 0.5 mag/kpc. Because of the application of the maximum allowable correction of +0.20 mag. to all observed colors, this coefficient is an upper limit.

The data for Field II are rather meager in comparison, since so very few early B stars enter in Table 4. We shall, in this case, have to depend almost exclusively on the B8–A0 stars. If we assume that the measured color indices require no correction for systematic error, we can conclude from Table 4 that no perceptible reddening effects are present in Field II up to a distance of 1600 parsecs. If, instead, we assume that the colors require

TABLE 5

VALUES OF $A'(m)$ FOR A REGION OF 100 SQUARE DEGREES CENTERED AT S.A. 193

Sp.	m_{pg}			
	7.27	7.75	8.25	8.75
B8–A0	35	30	87	197
A1–A7	6	8	13	35
F0–F2	1	1	9	17
F5–F8	1	2	5	15
G0–G5	0	1	9	12
K0–K2	1	3	16	21
K5–M	1	1	7	9

the maximum admissible correction suggested by Table 3, we find that the excess for the B8–A0 stars at $m_{pg} = 11.0$ will be, at most, +0.20 mag. The corresponding total absorption would then be of the order of 0.6 mag. at a distance of 1200 parsecs. The colors for the B8–A0 stars indicate, therefore, a maximum photographic absorption of 0.5 mag/kpc for Field II.

Very little can be said about the photographic absorption beyond $r = 1200$ parsecs in Field II. The very few stars that are observed (see Table 2) suggest the presence of considerable reddening at greater distances, but it would be unwise to attempt an estimate from the few scattered colors of early B stars.

II. DENSITY ANALYSES FOR S.A. 193

We found in the preceding section that the stellar distribution in S.A. 193 is apparently unaffected by interstellar absorption to a limiting distance of 1200 parsecs. It is, therefore, a simple matter to compute the variations in space density with increasing distance from the sun.

The data on the surface distribution of the fainter stars in an area of 6 square degrees have already been reproduced in Table 2, where the numbers in parentheses represent the total numbers of stars for separate intervals of apparent magnitude and spectral class. For the brighter stars we have proceeded in very much the same way as for the Monoceros region. The data for the surface distribution of the stars brighter than 7.0 mag. are those of Table 7 of the preceding paper. We reproduce in Table 5 the data on the surface distribution of the HD stars with apparent magnitudes between 7.0 and 9.0.

The final smoothed log $A'(m)$ curves were obtained from diagrams in which the log $A'(m)$ values from the three different sources were plotted against the apparent photographic magnitudes. The adopted values of log $A'(m)$ are listed in Table 6.

TABLE 6

ACCEPTED VALUES OF LOG $A'(m)$ IN S.A. 193

m_{pg}	SPECTRA						
	B8–A0	A1–A7	F0–F2	F5–F8	G0–G5	K0–K2	K5–M
4.25	9.30	9.40	.....	.....	.....	.....	.....
4.75	9.65	9.57	8.91	9.08	8.94	.....	.....
5.25	0.02	9.77	9.20	9.28	9.20	9.42	.....
5.75	0.35	0.00	9.50	9.50	9.45	9.68	9.05
6.25	0.65	0.23	9.79	9.73	9.68	9.94	9.28
6.75	0.95	0.47	0.07	9.95	9.93	0.20	9.52
7.25	1.28	0.75	0.35	0.18	0.20	0.48	9.77
7.75	1.62	1.02	0.63	0.41	0.47	0.78	0.02
8.25	1.97	1.27	0.92	0.70	0.77	1.09	0.50
8.75	2.28	1.51	1.23	0.98	1.10	1.41	0.95
9.25	2.55	1.77	1.52	1.22	1.38	1.68	1.35
9.75	2.80	2.03	1.78	1.47	1.67	1.90	1.63
10.25	3.02	2.28	1.88	1.67	1.93	2.09	1.90
10.75	3.25	2.53	1.82	1.87	2.18	2.26	2.15
11.25	3.50	2.78	1.50	2.10	2.48	2.41	2.37

TABLE 7

ACCEPTED VALUES OF LOG $A'(m)_g$ IN S.A. 193

m_{pg}	G0–G5 STARS		K0–K2 STARS	
	log $A'(m)_g$	Percentage of Dwarfs	log $A'(m)_g$	Percentage of Dwarfs
4.75	8.84	22	.....	.....
5.25	9.08	25	9.40	2
5.75	9.30	28	9.67	2
6.25	9.51	33	0.02	3
6.75	9.72	38	0.23	3
7.25	9.98	40	0.47	3
7.75	0.23	43	0.77	3
8.25	0.53	43	1.08	3
8.75	0.88	40	1.40	3
9.25	1.15	42	1.67	3
9.75	1.43	44	1.88	4
10.25	1.65	47	2.07	5
10.75	1.86	52	2.23	7
11.25	2.16	52	2.37	10

The separation of giants and dwarfs for the G–M stars was effected in the same way as for the Monoceros field.[6] The results are given in Table 7.

For the computation of the star densities we used the values of M_0 and σ as listed in Table 11 of the preceding paper. The computed star densities, expressed in the numbers

[6] See the preceding paper.

of stars per 1000 parsecs^3 as a unit, are given in Table 8. No corrections for absorption were applied.

The most striking result of Table 8 is that it is very similar to Table 13 for the Monoceros field. There are no significant differences between the density gradients in the two fields. We may have here a real condensation of B8–A0 stars, which reaches its maximum

TABLE 8

SUMMARY OF STAR DENSITIES IN S.A. 193
(Numbers of Stars per 1000 Parsecs^3; A_{pg}=0.0 Mag/Kpc)

d	SPECTRA				
	B8–A0	A1–A7	F0–F2	F5–F8	gG0-gM
50	0.12	0.45	1.5	3.2	0.30
100	.13	.35	1.3	2.2	.25
150	.16	.30	0.9	1.4	.26
200	.16	.28	0.6	1.0	.25
300	.16	.22	0.3	.....	.24
400	.16	.19	.....	.....	.22
500	.15	.16	.....	.....	.19
600	.13	0.15	.....	.....	0.17
700	.12	.....	.....	.....	.....
800	.12	.....	.....	.....	.....
900	.11	.....	.....	.....	.....
1000	0.11	.....	.....	.....	.....

TABLE 9

COUNTED NUMBERS OF STARS FOR AN AREA OF
50 SQUARE DEGREES CENTERED ON FIELD II

SP.	m_{pg}			
	7.25	7.75	8.25	8.75
B8–A0	4	24	31	46
A1–A7	0	3	6	20
F0–F2	0	2	5	9
F5–F8	1	1	2	8
G0–G5	0	5	5	14
K0–K2	3	4	13	15
K5–M	0	1	3	1

density at between 200 and 500 parsecs from the sun, where the star density exceeds that for the vicinity of the sun by more than 30 per cent. At a distance of 100 parsecs from the sun the density of the B8–A0 stars is, in contrast to our results for Monoceros *D*, about equal to that for the immediate vicinity of the sun. The slight negative gradients for the densities of the A1–A7 stars and the red giants and the steep negative gradients for the F's are again in marked contrast to each other.

III. DENSITY ANALYSES FOR FIELD II

The density analyses for Field II proceed along the same lines as those for S.A. 193 and the Monoceros field. Again we use the data of Table 7 of the preceding paper as

representative of the distribution of the stars brighter than $m = 7.00$. The distribution of the stars between the seventh and ninth magnitudes is shown in Table 9. The counts refer to an area of 50 square degrees, centered upon Field II. In the choice of this area, care was taken not to have it cover the rich regions near η Carinae; the square lies between galactic longitudes 246° and 253° and latitudes −3° and +4°.

TABLE 10

ACCEPTED VALUES OF LOG $A'(m)$ FOR FIELD II

m_{pg}	SPECTRA						
	B8–A0	A1–A7	F0–F2	F5–F8	G0–G5	K0–K2	K5–M
4.25	9.30	9.30	.....	.....	.....	.....	.....
4.75	9.70	9.55	8.90	9.10	8.95	.....	.....
5.25	0.05	9.78	9.20	9.32	9.18	9.38	8.75
5.75	0.38	0.00	9.50	9.54	9.40	9.64	9.05
6.25	0.70	0.22	9.78	9.76	9.62	9.92	9.30
6.75	1.00	0.44	0.04	9.98	9.88	0.21	9.55
7.25	1.25	0.68	0.30	0.20	0.18	0.51	9.80
7.75	1.57	0.96	0.60	0.45	0.52	0.83	0.08
8.25	1.80	1.22	0.90	0.70	0.90	1.14	0.38
8.75	2.00	1.50	1.20	0.95	1.22	1.45	0.75
9.25	2.20	1.80	1.42	1.20	1.40	1.72	1.12
9.75	2.40	2.08	1.67	1.45	1.58	1.92	1.50
10.25	2.61	2.38	1.90	1.70	1.74	2.10	1.90
10.75	2.82	2.70	2.10	1.97	1.90	2.21	2.20

TABLE 11

ACCEPTED VALUES OF LOG $A'(m)_g$ FOR FIELD II

m_{pg}	G0–G5 STARS		K0–K2 STARS	
	log $A'(m)_g$	Percentage of Dwarfs	log $A'(m)_g$	Percentage of Dwarfs
4.75	8.85	22	.....	.....
5.25	9.04	27	9.36	2
5.75	9.23	32	9.63	2
6.25	9.42	38	9.90	4
6.75	9.64	42	0.20	3
7.25	9.94	42	0.50	3
7.75	0.31	38	0.82	3
8.25	0.73	32	1.13	3
8.75	1.06	30	1.44	3
9.25	1.18	40	1.70	3
9.75	1.26	53	1.97	3
10.25	1.18	74:	2.08	5
10.75	.....	.....	2.17	8

Table 10 gives the final smoothed values of log $A'(m)$ from the three different sources combined. The separation of giants and dwarfs for the G–M stars was effected in the same manner as for the Monoceros field. The results are given in Table 11.

The star densities were again computed with the aid of the values for M_0 and σ listed in Table 11 of the preceding paper. The results are in Tables 12 and 13. The entries in

Table 12 are the densities computed for the case of no absorption. In Table 13 the densities were corrected for the absorption of 0.5 mag/kpc suggested by the color data.

A comparison between Table 13 of the preceding paper and Tables 8 and 13 of the present paper shows that there exists a great deal of similarity between the star densities

TABLE 12

SUMMARY OF STAR DENSITY IN FIELD II

(Numbers of Stars per 1000 Parsecs^3; No A_{pg} Applied)

d	SPECTRA				
	B8–A0	A1–A7	F0–F2	F5–F8	gG0-gM
50	0.12	0.45	1.4	3.5	0.30
100	.13	.35	1.1	2.3	.27
150	.15	.27	0.8	1.6	.27
200	.16	.24	0.7	1.0	.26
300	.16	.24	0.4	.....	.24
400	.16	.24	.....	.....	.20
500	.14	.22	.....	.....	.15
600	.11	0.19	.....	.....	0.12
700	.09	.....	.....	.....	.....
800	.08	.....	.....	.....	.....
900	.07	.....	.....	.....	.....
1000	0.06	.....	.....	.....	.....

TABLE 13

SUMMARY OF STAR DENSITY IN FIELD II

(Numbers of Stars per 1000 Parsecs^3; Corrected for A_{pg}=0.5 Mag/Kpc)

d	SPECTRA				
	B8-A0	A1–A7	F0–F2	F5–F8	gG0-gM
50	0.13	0.47	1.4	3.5	0.30
100	.14	.35	1.2	2.4	.29
150	.18	.30	1.0	1.8	.30
200	.19	.29	0.9	1.1	.31
300	.21	.32	0.5	.....	.30
400	.21	.34	.....	.....	.24
500	.18	.31	.....	.....	0.20
600	.16	0.28	.....	.....	.....
700	.15	.....	.....	.....	.....
800	.12	.....	.....	.....	.....
900	0.11:	.....	.....	.....	.....

in Monoceros *D*, S.A. 193, and Field II. In all three fields the B8–A0 stars show an initial increase in average density, large enough, probably, to be real, followed by a decrease. But, whereas in Monoceros *D* the density at 1000 parsecs is decidedly less than that for the vicinity of the sun, we find for S.A. 193 and Field II an average star density for the B8–A0 stars again almost equal to that for the solar neighborhood.

The red giants in all three cases show almost constant density over the first 500 parsecs, with an indication of a gradual drop in average density; the gradient is least for Field II, steepest for S.A. 193, and intermediate for the Monoceros field. The F stars

behave similarly in the three fields; there is apparently no escape from a rapid decrease in the star density for these stars.

IV. The Distribution of the B0–B5 Stars

It is of interest to compare the distribution of the early B stars for the field in Monoceros, S.A. 193, and Field II. The relevant data are reproduced in Table 14. The Monoceros numbers represent the total for regions *C*, *D*, and *F* of the preceding paper.

The large number of early-type stars in S.A. 193 is quite noticeable. According to Seydl's tabulations,[7] we observe, on the average, two B0–B2 stars and seven B3–B5 stars between $m_{pg} = 4.5$ and m_{pg} 5.5 per 500 square degrees near the galactic circle. In the absence of absorption, and for constant average space density, we should then expect about three B0–B2 stars and ten B3–B5 stars between $m_{pg} = 8.0$ and m_{pg} 9.0 for the area of 6 square degrees covered by S.A. 193. Since absorption is present in S.A. 193 for distances beyond 1600 parsecs, we conclude from Table 14 that the observed numbers of B0–B5 stars are compatible with a constant star density equal to that for the vicinity of the sun up to a limit of 2500 parsecs.

TABLE 14

Observed Distribution of Early B Stars

m_{pg}	Monoceros (67 Square Degrees)		S.A. 193 (6 Square Degrees)		Field II (6 Square Degrees)	
	B0–B2	B3–B5	B0–B2	B3–B5	B0–B2	B3–B5
8.0– 9.0.....	1	5	3	6	2	1
9.0–10.0.....	5	23	5	18	0	1
10.0–11.0.....	2	33	3	18	1	0

Quite the reverse is true for the fields in Monoceros and Field II. Even if we consider that for Monoceros A_{pg} may be as high as 0.8 mag/kpc and that in Field II $A_{pg} = 0.5$ mag/kpc, we find that the numbers predicted for constant density are several times larger than the observed ones; and we conclude that the reality of negative density gradients for the B0–B5 stars at $l = 185°$ and $l = 249°$ is established. These results, together with the observed high frequency of early B stars in the region of η Carinae[8] at $l = 254°$, make it seem likely that the region of constant density of the early B stars has a sharp boundary near $l = 252°$.

When we compare these results with those obtained for some other sections of the Milky Way, especially with those investigated by Schalén, Wernberg, and Wallenquist, we find that the star densities drop sharply as we move away from the sun for $l = 73°$ and $l = 135°$. In Cygnus we find a very slight decrease at $l = 40°$. In the direction of the Sagittarius and Scutum clouds, low densities are observed at 1000 parsecs from the sun; but for the Scutum region, the space densities of the early B's at 2000 parsecs are again quite high.

V. The Changes in the Luminosity Function

The values of log $\varphi'(M)$ were computed by the same procedure as was followed in the construction of Table 14 of the preceding paper. Because of the similarity in density-curves for the various spectral classes in the three regions, it is not surprising that there

[7] *Pub. Nat. Obs. Prague*, No. 6, 1929.

[8] *Harvard Reprints*, No. 77, 1932.

appears to be considerable resemblance between Tables 15 and 16 of the present paper and Table 14 of the Monoceros paper.

It may be of interest to compare these results with data in the changes in the general luminosity function that may be derived for other sections of the Milky Way from spectra and magnitudes determined by Swedish astronomers. Two investigations by Schalén[9,10] provide the necessary data for fields in Cygnus and in Auriga. For a region in Cepheus we have the material of Wernberg,[11] and for the Sagittarius cloud we have made use of Wallenquist's[12] spectral data. Since for most of these fields we have little information on the densities of the A stars within 200 parsecs of the sun and since existing surveys tell us little about the densities for the F stars beyond this distance, we shall limit ourselves here to the computation for every field of the value of log $\varphi'(M)$ for the distance of 200 parsecs from our sun.

TABLE 15

CHANGES IN THE GENERAL LUMINOSITY FUNCTION FOR S.A. 193
(Values of log $\varphi'(M)$)

M_{pg}	d (PARSECS)					
	Van Rhijn	50	100	200	300	500
−0.5	.....	8.18	8.11	8.18	8.15	8.15
0.0	8.38	8.53	8.50	8.52	8.49	8.43
+0.5	.....	8.90	8.85	8.82	8.78	8.69
+1.0	9.04	9.15	9.09	9.03	8.97	.....
+1.5	.....	9.37	9.29	9.18	9.10	.....
+2.0	9.47	9.53	9.45	9.28	.....	.....
+2.5	.....	9.65	9.56	9.32	.....	.....
+3.0	9.56	9.75	9.64	9.36	.....	.....
+3.5	.....	9.83	9.72	9.40	.....	.....

TABLE 16

CHANGES IN THE GENERAL LUMINOSITY FUNCTION FOR FIELD II
(Values of log $\varphi'(M)$)

M_{pg}	d (PARSECS)					
	Van Rhijn	50	100	200	300	500
−0.5	.....	8.20	8.18	8.25	8.30	8.23
0.0	8.38	8.57	8.53	8.59	8.62	8.54
+0.5	.....	8.91	8.87	8.89	8.90	8.82
+1.0	9.04	9.16	9.11	9.10	9.10	.....
+1.5	.....	9.38	9.30	9.26	9.23	.....
+2.0	9.47	9.53	9.45	9.36	.....	.....
+2.5	.....	9.66	9.56	9.43	.....	.....
+3.0	9.56	9.76	9.65	9.47	.....	.....
+3.5	.....	9.84	9.72	9.50	.....	.....

[9] *Uppsala Medd.*, No. 37, 1928.

[10] *Ibid.*, No. 55, 1932.

[11] *Uppsala Ann.*, Vol. 1, No. 4, 1941.

[12] *Bosscha Ann.*, Vol. 5, No. 5, 1939.

For the region in Cygnus, we deduce from Schalén's colors, and from the photoelectric colors of Stebbins, Huffer, and Whitford,[13] that at $l = 41°$, $b = +1°$ to $+3°$, the absorption is very nearly equal to $A_{pg} = 1.0$ mag/kpc. For the region in Cepheus, $l = 70°$ to $75°$, $b = 0°$ to $-3°$, studies by Wernberg and Miss Risley[14] indicate an average value $A_{pg} = 0.33$ mag/kpc. For the Sagittarius region we assume from the colors of Stebbins, Huffer, and Whitford that in Wallenquist's Region II the absorption is represented by $A_{pg} = 1.0$ mag/kpc.

The results are collected in Table 17. The figures in the last column represent the general luminosity function of van Rhijn,[15] which represents the best available reference curve for the vicinity of the sun.

We have not included in our survey Schalén's material for the Scutum cloud,[16] but from the data at hand it seems that the values of log $\varphi'(M)$ for Scutum resemble those for the Sagittarius region.

TABLE 17

THE GENERAL LUMINOSITY FUNCTION AT 200 PARSECS FROM THE SUN FOR VARIOUS DIRECTIONS IN THE GALACTIC PLANE, COMPARED WITH VAN RHIJN'S STANDARD FUNCTION VALUES OF LOG $\varphi'(M)$

M	Field and Galactic Longitude							
	Cygnus 40°	Cepheus 73°	Auriga 135°	Monoceros 185°	Field II 249°	S.A. 193 261°	Sagittarius 332°	Van Rhijn Standard
−0.5	8.67	8.45	8.30	8.26	8.25	8.18	8.00	.....
0.0	8.88	8.64	8.67	8.56	8.59	8.52	8.23	8.38
+0.5	9.08	8.97	8.79	8.85	8.89	8.82	8.43	.....
+1.0	9.25	9.17	8.96	9.04	9.10	9.03	8.65	9.04
+1.5	9.40	9.35	9.13	9.17	9.26	9.18	8.84	.....
+2.0	9.49	9.48	9.26	9.26	9.36	9.28	8.95	9.47
+2.5	9.56	9.42	9.32	9.30	9.43	9.32	9.00	.....
+3.0	9.57	9.43	9.40	9.30	9.47	9.36	9.04	9.56
+3.5	9.60	9.58	9.49	9.34	9.50	9.40	9.11	.....

The most disturbing result of Table 16 is that the general luminosity function apparently undergoes considerable variations in its shape over comparatively small distances in the galactic plane. The existence of such variations has been suggested previously. Maxwell[17] gave evidence for variations in the shape of the general luminosity function for the direction of the Cygnus cloud. Later, Seares[18] gave evidence for an excess of highly luminous stars in the vicinity of the sun, and the possible effects of such changes were discussed by Bok.[19] More recently, Miller and Hanna[20] have computed the variations for the Cygnus cloud, for which they find an excess of A and K stars and a deficiency of B and F stars, as compared to the standard function.

Luyten[21] and Schilt[22] have given some results that show that our knowledge of the

[13] *Op. cit.*

[14] *Ap. J.*, **97**, 277, 1943.

[15] *Groningen Pub.*, No. 47, Table 6, 1936.

[16] *Uppsala Medd.*, No. 61, 1935.

[17] *Lick Obs. Bull.*, No. 390, 1927.

[18] *Ap. J.*, **74**, 312, 1931; *Mt. W. Contr.*, No. 437.

[19] *Harvard Circ.*, No. 371, 1931.

[20] *A.J.*, No. 1139, 1942; *Swasey Obs. Reprints*, No. 8.

[21] *Ann. N.Y. Acad. Sci.*, **42**, 201, 1941.

[22] *Ann. N.Y. Acad. Sci.*, **42**, 259, 1941.

general luminosity function for absolutely faint stars is yet far from complete. The frequencies of stars with $M \geqq +6$, however, do not concern us especially in the analysis of the stellar distribution for fields in low galactic latitudes.

Our results in Table 17 indicate that the variations are quite erratic and large, even for absolute magnitudes $M = 0$ to $+4$, for which interval it had generally been supposed that the variations would be mild. We shall apparently have to be very careful in interpreting the densities derived from general star counts. These densities are at best representative for the most "effective" absolute magnitude. It is well to remember that this "effective" magnitude becomes fainter as we pass to fainter apparent magnitudes. The observed variations in the general luminosity function render it all the more necessary that we should supplement our star-count analyses with studies based on spectral distributions.

In a way, the most striking result of Table 17 is represented by the column for the Sagittarius cloud. We are likely to think of the direction to the center of galaxy as one of very high star density; and instead we find that at 200 parsecs from the sun the values of log $\varphi'(M)$ for $l = 332°$ are smaller than those for any other galactic longitude, including the anticenter directions. The average density at 200 parsecs for $l = 332°$ is just about equal to one-quarter of that at the same distance for $l = 40°$. The distance of 200 parsecs to which the results of Table 17 apply is so small that it is unlikely that uncertainties in the absorption characteristics to that distance might account for the deficiencies at $l = 332°$. We note, moreover, that the result is confirmed in a general way by the data for the Scutum cloud.

Apparently, there is no escaping the conclusion that for the direction of the Scutum and Sagittarius clouds the star densities drop at first and recover again at larger distances. This result has already been foreshadowed by an earlier investigation, based on the analysis of general star counts[19,23]. Studies based on spectra and colors of faint stars for the bright patches in the central directions of the Milky Way not only should yield important information on the stellar distribution in the more populated distant central regions of our galaxy but should further contribute important data bearing on local structure.

VI. Results and Conclusions

The investigation deals with the stellar distribution in two southern fields: one at $l = 261°$, $b = +1°$ (S.A. 193); the other at $l = 249°$, $b = +1°$ (Field II). In each case the area covered is 6 square degrees; the basic data are given in Tables 1 and 2. The main results of the analysis are the following:

1. Selected Area 193 is apparently free from obscuration to a distance of 1600 parsecs; beyond that the absorption is represented by $A_{pg} = 0.5$ mag/kpc to $r = 3000$ parsecs.

2. In Field II a value $A_{pg} = 0.5$ mag/kpc to $r = 1200$ parsecs accounts for the observed color excesses; there is no information for greater distances.

3. The density distribution for S.A. 193 (see Table 8) are similar to those of the Monoceros field. We add the comments:

a) The excess density for the B8–A0 stars persists to $r = 500$ parsecs; there is no marked decrease between $r = 500$ and $r = 1000$ parsecs;

b) The densities for the A1–A7 stars drop to 35 per cent of the value for the vicinity of the sun at $r = 500$ parsecs;

c) The F0–F2 and F5–F8 stars show the same steep negative gradients as were observed for the Monoceros field;

d) The gG0–gM stars yield slowly decreasing star densities.

[23] *The Distribution of the Stars in Space*, pp. 120 and 123, Chicago: University of Chicago Press, 1937.

4. The density distributions in Field II (see Table 13) are characterized by—

a) High densities for the B8–A0 stars, with the density at $r = 800$ parsecs equal to that near the sun;

b) A slight negative gradient for the A1–A7 stars;

c) Steep negative gradients for the F stars;

d) Slowly decreasing densities for the red giants.

5. For the fields in Monoceros and for Field II the predicted numbers of B0–B5 stars (computed from the observed averages for $m = 5.0$ along the galactic belt on the assumption of constant average space density) fall far above the numbers actually observed. This suggests a rapid decrease in star densities for the early B stars in the directions $l = 185°$ and $l = 249°$. For S.A. 193 (as for the neighboring region near η Carinae) we find, in contrast, fairly high and constant average densities for the early B stars. It is of interest to compare these results with those obtained for other sections. The behavior for the Monoceros field and Field II appear to be characteristic for the whole region between $l = 70°$ and $l = 252°$. In Cygnus the densities behave not unlike those for the Carina-Crux-Centaurus region. In Sagittarius and Scutum we have apparently an initial steep decrease, followed by a rapid rise in star density at greater distances.

6. Tables 15 and 16 show that for Field II and S.A. 193 the dependence of the shape of the general luminosity function on distance is again quite pronounced. Table 17 shows that large variations exist for almost all directions of the Milky Way. The behavior of the Sagittarius region is especially noteworthy.

AN INVESTIGATION ON DIFFERENTIAL GALACTIC ROTATION

PARIS PIŞMIŞ AND AGUSTÍN PRIETO
National Astrophysical Observatory, Tonanzintla, Mexico
Received January 18, 1945

ABSTRACT

Solutions for $\bar{r}A$ and K have been carried out, using Oort's equation and the radial velocities of 707 stars of spectral types O–B9, common to the catalogue of radial velocities of O- and B-type stars by Plaskett and Pearce and the catalogue of 1332 stars of Stebbins, Huffer, and Whitford. It appears that A does not show any variation with distance; its mean value is 0.011 ± 0.002 km/sec·pc, much smaller than the generally adopted value of 0.017 km/sec·pc.

Solutions carried out by dividing each distance group into two subgroups, one containing stars of spectral types O–B2 and c stars and the other, spectral types B3–B9, give $A = +0.016$ and $A = 0.009$ km/sec·pc, respectively. It is therefore concluded that the small value of A obtained from the general solution is due to an overestimation of the distances for the B3–B9 stars. This overestimation is caused, very probably, by the adoption (by Stebbins, Huffer, and Whitford) of too bright absolute magnitudes for those types.

The K-term practically vanishes in the nearest group. By dividing the spectral subgroups into quadrants in longitude it is shown that the disappearance of the K-term for the nearest stars is a real effect, whereas the large K-term obtained hitherto for the nearest early-type stars is probably due to the nonuniform distribution in longitude or to local irregularities.

Numerous investigations have been made to determine the coefficient A since the time when Oort first introduced the formulae for differential galactic rotation. A reliable value of this coefficient is desirable, since it is used quite often as a means for estimating distances.

Any determination of A requires a knowledge of the mean distances of the stars on which the determination is based; for, in the well-known formula for differential rotation,

$$r A \sin 2(l - l_0) \cos^2 b + K = V , \qquad (1)$$

where V denotes the radial velocity of a star after the solar-motion component is eliminated, A enters with a factor r, the distance of the star. In general, for a group of near-by stars for which reliable distances are available, the term $\bar{r}A$ will be indeterminate, and hence the value of A will not be reliable; while for stars far enough to give reliable values for A one is confronted with another difficulty, namely, the lack of reliable distances. The distances for the farther groups are, in general, photometric. Distances of this kind and, hence, A derived from them will be affected by the adopted value of the absorption coefficient.

Since the patchy distribution of the absorbing matter in the Galaxy is being emphasized more and more, the question arises as to how far a mean absorption coefficient represents the effect of the nonuniform distribution of the absorbing matter. R. E. Wilson has shown in a recent paper[1] that the nonuniformity of the absorbing matter will give rise to a spurious decrease of the coefficient A with increasing distance. If one were to force the derived values of A for different distance groups to agree by adjusting a mean coefficient of absorption, the result would be a value of A much higher than the true one.

The best value of A, therefore, can be obtained by using distances corrected for nonuniform absorption. In an earlier paper, one of the authors[2] made a solution of equation (1) with the aid of the radial velocities of O- and B-type stars determined by Plaskett and Pearce[3] and the distances given by Stebbins and Huffer.[4] Least-squares solutions were

[1] *Ap. J.*, **92**, 170, 1940.

[2] Paris Pişmiş, *Pub. Istanbul Univ. Obs.*, No. 10, 1938.

[3] *Pub. Dom. Ap. Obs.*, Vol. **5**, No. 3, 1933.

[4] *Pub. Washburn Obs.*, Vol. **15**, Part 5, 1934.

carried out for four distance groups. The material was, however, too scanty and not well distributed in galactic longitude.

At present the more extensive catalogue of Stebbins, Huffer, and Whitford offers us the possibility of extending the earlier investigation. The data for the present solution consist of stars common to the catalogue of 1010 stars of types O and B by Plaskett and Pearce[5] and the catalogue of 1332 stars by Stebbins, Huffer, and Whitford.[6]

The distances given in the latter catalogue are based on two assumptions: first, that of a constant ratio of general to selective absorption ($A/E = 7$) and, second, that of an average absolute magnitude for each subtype. The recent investigation on the six-color photometry of stars by Stebbins and Whitford[7] seems to support the high ratio of general to selective absorption; they further show that this ratio does not vary with the region of the sky considered. This implies that very probably no systematic errors depending on distance or direction will be introduced in the distances based on the assumption of the mentioned ratio.

The material consisting of 707 stars was divided into five distance groups. An equation of condition based on equation (1) was formed for each star. The solar motion was assumed to be 20 km/sec in the direction $\alpha = 271°$ and $\delta = 28°$, and its component was eliminated by the use of the graph by Pearce and Hill.[8] The longitude l_0 was assumed to be 325°. The equations were solved for $\bar{r}A$ and K in five distance groups by the method of least squares. The results with their probable errors appear in Table 1.

TABLE 1

SOLUTION FOR $\bar{r}A$ AND K USING 707 O- AND B-TYPE STARS

Group	Distance Limits (Pc)	Mean Distance	No. of Stars	$\bar{r}A$ (Km/Sec)	K (Km/Sec)	A (Km/Sec·Pc)
1.....	$r \leqslant 250$	182	128	+ 1.36±0.8	+0.36±0.3	+0.007±0.004
2.....	$250 < r \leqslant 500$	358	292	4.83±0.8	+0.81±0.5	.013± .002
3.....	$500 < r \leqslant 750$	589	177	5.62±1.2	+2.81±0.8	.009± .002
4.....	$750 < r \leqslant 1000$	855	57	10.40±2.7	−2.72±1.9	.012± .003
5.....	$1000 < r$	1443	53	+25.74±2.9	−7.95±2.3	+0.018±0.002

A does not show any variation with distance if we leave out the last group (this omission will be justified in the discussion to follow). The weighted mean over all groups gives $A = +0.011 \pm 0.001$ km/sec · pc. Excluding the first group, for which $\bar{r}A$ may be indeterminate, the weighted mean A is 0.012 ± 0.003. Both of these values are much smaller than the usually accepted one, 0.017 km/sec · pc.

The K-term is very small for the nearest two groups. This result was a real surprise, for solutions made hitherto had always yielded a K-term of the order of 4–5 km/sec for the nearest stars of types O and B. Moreover, as has been emphasized by one of the authors,[2] some earlier investigations indicate that the K-term decreases with distance. In general, there appears a decrease of the K-term in the farthest group, but the variation is by no means marked and smooth. The number of stars in the nearest three groups is sufficiently large (and the probable errors small enough) to make the determination of K and also of $\bar{r}A$ fairly reliable.

The material of the five groups is quite uniformly distributed between galactic longitudes 10° and 190°, whereas there exist large gaps at longitudes corresponding to southern declinations. Taking only the stars between $l = 10°$ and $l = 190°$, we have made a new solution of equation (1) for the five distance groups. (This interval covers a complete

[5] *Pub. Dom. Ap. Obs.*, Vol. **5**, No. 2, 1931.

[6] *Ap. J.*, **91**, 20, 1940.

[7] *Ap. J.*, **98**, 20, 1943.

[8] *Pub. Dom. Ap. Obs.*, Vol. **6**, No. 4, 1931.

wave of the differential rotation.) By this procedure one can avoid to some extent the effects of the nonuniform distribution of the velocities. The results obtained in this way should not differ essentially from those for the complete groups, provided there are no asymmetries (such as stream motion) in the groups considered. The results of the new solutions are given in Table 2. Again A shows no variation with distance. The weighted mean value of A is 0.013 ± 0.001, a value smaller than that found in previous investigations.

To give more weight to the determination of A, we have made a new solution, assuming $K = 0$. The results are given in Table 3. The weighted mean value of A is $+0.012 \pm 0.001$ km/sec · pc.

TABLE 2

SOLUTION USING STARS IN LONGITUDES 10°–190°

Group	Mean Distance (Pc)	No. of Stars	$\bar{r}A$ (Km/Sec)	K (Km/Sec)	A (Km/Sec·Pc)
1	177	105	+ 1.88	+ 0.50	+0.011
2	361	268	5.63	+ 0.92	.016
3	589	164	4.81	+ 1.30	.008
4	868	52	12.01	− 0.01	.014
5	1484	46	+21.22	−14.30	+0.014

TABLE 3

DETERMINATION OF A, ASSUMING $K=0$ (707 STARS)

Group	Mean Distance (Pc)	$\bar{r}A$ (Km/Sec)	A (Km/Sec·Pc)
1	182	+ 1.38	+0.007
2	358	5.17	.014
3	589	6.32	.011
4	855	10.56	.012
5	1443	+25.82	+0.018

It thus seems certain that the value of A obtained from the present material (spectral types O–B9 taken together) is approximately 0.012 km/sec · pc. Two possible explanations can be given for the small value which has been derived for A. Either it is real, which does not seem probable, or it is due to the circumstance that the distances given by Stebbins, Huffer, and Whitford are too large. The latter explanation may be the valid one for two reasons: The adopted ratio of general to selective absorption is too small and the mean absolute magnitudes adopted are too bright.

In the Washburn catalogue of 733 stars the assumed ratio of general to selective absorption was only 2. On the other hand, the absolute magnitudes adopted were too faint, compared with the recent catalogue of 1332 stars. In addition to this, the stars with c characteristics were not differentiated from the normal stars. Stebbins, Huffer, and Whitford assert that the increase of this ratio will be compensated by the increase of the absolute luminosities. To check on this we have made a comparison of the distances given by the two catalogues mentioned. A total of 643 stars is common to the two catalogues; they have average distances of 368 and 476 pc according to the early and later catalogues, respectively. It thus appears that the distances of the recent catalogue are, on the aver-

age, 26 per cent larger than those of the earlier one. Most of this difference is probably caused by the separation of the c stars, which are now assigned brighter absolute magnitudes. On the scale of the earlier distances the mean value of A, given in Table 1, would become 0.014 km/sec · pc, still too low compared to the generally adopted value.

To investigate the question further, as well as the peculiarity shown by the K-term, each of the distance groups was divided into two subdivisions, one (*a*) containing stars of types O–B2 and stars showing c characteristics and the other (*b*) containing stars of types B3–B9. This is essentially a subdivision with regard to absolute magnitude. The results of the least-squares solutions for $\bar{r}A$ and K and their probable errors are given in Table 4. All stars in distance group 5 are either types O–B2 or c stars; therefore its corresponding subgroup for B3–B9 types does not exist. The fourth subgroup for types B3–B9 will not be included in the discussion, for it has too few stars to yield reliable values for $\bar{r}A$ and K.

TABLE 4

SOLUTIONS OF SPECTRAL SUBGROUPS

GROUP	NO. OF STARS	MEAN DISTANCE (PC)	$\bar{r}A$ (KM/SEC)	K (KM/SEC)	A (KM/SEC · PC)
	Subdivision *a*: Types O–B2- and c Stars				
1	19	179	− 0.60± 1.6	+2.99±1.1	−0.003±0.009
2	53	371	+ 7.62± 2.1	+2.10±1.9	+ .020± .005
3	81	520	+ 9.53± 1.3	+3.72±0.8	+ .018± .003
4	48	894	+12.67± 2.8	+0.23±2.0	+ .013± .003
5	53	1443	+25.74± 2.9	−7.95±2.3	+0.018±0.002
	Subdivision *b*: Types B3–B9				
1	109	174	+ 1.67± 0.4	+0.0 ±0.3	+0.009±0.002
2	239	355	+ 4.21± 0.9	+0.4 ±0.2	+ .012± .003
3	96	580	+ 2.83± 1.9	+0.6 ±1.2	+ .005± .003
4	9	757	− 8.14±15.3	−1.2 ±8.9	−0.011±0.020
5	0	.....	.....	.....	.....

The coefficient A is systematically larger for subgroups *a* compared with that for subgroups *b*. We see, then, that the apparent increase of A in the last group of Table 1 is due to the fact that all stars are of types O–B2 or show c characteristics and hence yield a larger value of A than the average over all types. The weighted mean A for the five groups of subdivision *a* gives $A = 0.016 \pm 0.002$ km/sec · pc, omitting the first group, $A = 0.017 \pm 0.002$. These values are quite near to those obtained hitherto. The weighted mean over the first three groups for the B3–B9 stars is $A = 0.009 \pm 0.001$. We therefore conclude that the small value of A of the general solution is due to the later-type stars. It seems, therefore, that the assumed distances for the stars B3–B9 are too large, which results in a low value for A. The overestimation of the distances cannot be caused by an erroneous ratio of general to selective absorption, for the latter would affect all stars equally.[9] It is therefore highly probable that the adopted absolute magnitudes of B3–B9

[9] It seems unlikely that the normal colors of B3–B9 stars assumed by Stebbins, Huffer, and Whitford involve errors large enough to account for the overestimation of the derived distances.

stars are too bright. The correction to be applied to the mean absolute magnitudes for the average of B3–B9 stars adopted by Stebbins, Huffer, and Whitford[6] is of the order of 1.2 visual magnitude. This quantity was obtained by assuming that the mean A of the B3–B9 stars is of the order of 0.016 km/sec · pc. (The correction will amount to 1.4 visual magnitudes if we assume $A = 0.017$.)

The K-term of Table 1 presents an interesting aspect. It has been mentioned earlier that in solutions made hitherto the nearest early-type stars yielded a large positive K-term. In the present solution the K-term of the nearest group practically vanishes. The K-term for stars between longitudes 10° and 190° also shows the same peculiarity as that for the entire group. We shall discuss the different groups in some detail later.

It is worth while to call attention to the fact that in Table 4 the K-term for subdivision a is systematically larger than that for subdivision b by about +2.3 km/sec on the average for the first three groups. If significance could be attached to the K-term of all the

TABLE 5

AVERAGE RADIAL VELOCITIES, IN KM/SEC, CORRECTED FOR SOLAR MOTION FOR QUADRANTS IN GALACTIC LONGITUDE

Group	Subdivision *a*: Types O–B2 and c Stars				Subdivision *b*: Types B3–B9			
	Longitude Limits							
	325°–55°	55°–145°	145°–235°	235°–325°	325°–55°	55°–145°	145°–235°	235°–325°
1.....	− 0.1 (3)*	+ 2.0 (5)	+ 3.8 (5)	+ 4.1 (6)	+1.5 (30)	−1.1 (49)	+1.8 (26)	+3.8 (4)
2.....	+ 5.1 (6)	− 2.3 (22)	+ 7.8 (23)	8.5 (2)	2.7 (75)	1.2 (82)	+3.3 (82)	(0)
3.....	+ 9.2 (20)	− 1.5 (38)	+ 9.3 (22)	+19.0 (1)	4.0 (38)	0.4 (29)	+0.0 (29)	(0)
4.....	+ 8.9 (18)	+13.8 (23)	− 0.1 (7)	(0)	+3.5 (2)	−8.9 (2)	−0.0 (5)	(0)
5.....	+15.1 (12)	−33.5 (25)	+10.0 (16)	( )	.....	.....	.....	.....
Differential rotation according to Oort..	>0	<0	>0	<0	>0	<0	>0	<0

* Numbers in parentheses represent number of stars.

different subgroups, this difference of +2.3 km/sec could be interpreted as a physical red-shift, probably a gravitational red-shift which will be larger for the more luminous, hence the more massive, stars of subdivision a in comparison to the less luminous, and hence the less massive, stars of subdivision b.

In order to investigate the behavior of the K-term more closely and to account for the disappearance of this term for the nearest group of stars, we have made a study of the radial velocities in longitude quadrants. Each of the subgroups appearing in Table 4 was divided into four quadrants, which were chosen in such a way that at their limits the effect of the differential rotation on the radial velocities is zero (those limits are at 325°, 55°, 145°, and 235°, respectively). For each of the quadrants the mean radial velocity with the corresponding number of stars is given in Table 5. To compare the present results with a solution yielding a large K-term, we have given in Table 6 the mean radial velocities in four quadrants of the nearest group of Solution I in an earlier investigation mentioned before.[2] The reasons for this choice are, first, that the earlier groupings were also based on distances (Stebbins and Huffer) and, second, that the stars could easily be identified.

In the fourth quadrants of all groups in Tables 5 and 6 the radial velocities of the stars are either unknown or are too few to give reliable mean values. Our discussion, therefore,

will be based only on the three first quadrants. The first group of subdivision *a* and the last group (fourth) of subdivision *b* have too few stars to afford mean values reliable for discussion.

It is well known that the *K*-term represents the shift in radial velocity of the double wave of the differential rotation. The *K*-term has significance as a general effect only when this shift is systematic. This means that among the four quadrants considered in Table 5 the mean radial velocities in quadrants 1 and 3 should agree sensibly; a similar agreement should exist between quadrants 2 and 4. The mean radial velocity of two consecutive quadrants (or of all four quadrants) should give an estimate of the *K*-term. (Owing to the high concentration of the early-type stars to the galactic plane, we have assumed their mean galactic latitudes to be zero in discussing the quadrants.)

Among the subgroups of B3–B9 stars the one that comes nearest to satisfying the above condition is the nearest group, the group most essential for our discussion of the *K*-term. The double wave appears very clearly in the first three quadrants. It does not show any systematic shift. The mean value of the radial velocities in the first two quadrants practically vanishes, in agreement with the very small *K*-term obtained from the least-squares solution. There is no doubt, therefore, that the *K*-term of this group is a general effect and not due to irregularities in distribution.

TABLE 6

AVERAGE RADIAL VELOCITIES, IN KM/SEC, CORRECTED FOR SOLAR MOTION FOR QUADRANTS IN GALACTIC LONGITUDE
(47 Stars; Mean Distance, 189 Pc)

LONGITUDE LIMITS			
325°–55°	55°–145°	145°–235°	235°–325°
+3.7 (11)*	−2.8 (14)	+7.5 (21)	1.7 (1)

* Numbers in parentheses represent number of stars.

In Table 6 we see, on the other hand, that the large positive *K*-term which the least-squares solution of this group has yielded (+5.2 ± 1.6 km/sec; mean distance of group, 189 pc) is brought about by the excess of positive velocities in the third quadrant, which has the largest number of stars. If the number of stars in the other quadrants were comparable, one could decide whether the large *K*-term is due to a systematic shift or is caused by the streaming tendency of the stars in the third quadrant. But, as it stands now, the *K*-term in this group is a local effect. Out of the 47 stars of this group, 43 are included in the material of the present investigation. It is interesting to mention that these 43 stars are scattered over the three nearest groups of Table 1. Only 15 stars are of spectral types O–B2, and two others show c characteristics.

Of the remaining groups in Table 5, distance group 2 of B3–B9 stars indicates that probably its *K*-term is real—the mean velocities in the quadrants show a systematic positive shift. The third group shows asymmetry. Of the O–B2 and c-star groups, the second and the third distance groups indicate a systematic shift toward positive velocities. The fourth group shows an asymmetry and the fifth one a systematic shift toward negative velocities, pointing out that the *K*-term of this group is very probably a real effect.

In conclusion we may emphasize again that the *K*-term has significance as a general characteristic for a group only when the double wave of the velocities shows a systematic shift. It will not be safe to consider the *K*-term as a general effect unless the material on which it is based is well distributed in galactic longitude and is free of local effects, such as group motions.

ON THE RADIATIVE EQUILIBRIUM OF A STELLAR ATMOSPHERE. VI

C. U. Cesco, S. Chandrasekhar, and J. Sahade
Yerkes Observatory
Received February 14, 1945

ABSTRACT

In this paper the solutions to the problem of line formation in stellar atmospheres, in the third approximation, are tabulated for various values of the parameters which are involved and at close enough intervals to allow interpolation.

Numerical forms of the solution for the problem of the radiative equilibrium of a planetary nebula are also obtained.

This paper is of the nature of a supplement to two earlier papers[1] of this series and provides some further information relating to the problems of the formation of absorption lines in stellar atmospheres and the radiative equilibrium of a planetary nebula.

I. THE FORMATION OF ABSORPTION LINES; THE TABULATION OF THE SOLUTIONS IN THE THIRD APPROXIMATION

As we have seen in papers II (§ 7) and IV, the solution to the problem of line formation under certain "standard" circumstances and in the nth approximation depends on the roots k_α, $(\alpha = 1, \ldots, n)$, of the characteristic equation (II, eq. [91]) and on the solutions of the linear equations

$$\sum_{\alpha=1}^{n} \frac{L_\alpha}{1-\mu_i k_\alpha} = \mu_i - \frac{a_{\nu_0}}{b_\nu} \qquad (i = 1, \ldots, n), \quad (1)$$

which determine the constants of integration L_α, $(\alpha = 1, \ldots, n)$.

It is perhaps of some interest to note that the solution of the foregoing system of equations can be written down explicitly. Thus, in terms of the matrix

$$\boldsymbol{G} = (G_{ij}) = \left(\frac{1}{1-\mu_i k_j}\right) \quad (2)$$

and the vectors

$$\boldsymbol{L} = (L_\alpha) \qquad \text{and} \qquad \boldsymbol{M} = (M_i) = \left(\mu_i - \frac{a_{\nu_0}}{b_\nu}\right), \quad (3)$$

the system of equations which equation (1) represents is equivalent to

$$\boldsymbol{GL} = \boldsymbol{M}, \quad (4)$$

of which the formal solution is

$$\boldsymbol{L} = \boldsymbol{G}^{-1}\boldsymbol{M}. \quad (5)$$

That we can express the solution for $\boldsymbol{L}$ in this form in terms of the inverse of the matrix $\boldsymbol{G}$ is, of course, obvious. But what is noteworthy in our present context is that for the

[1] *Ap. J.*, **100**, 76, 355, 1944. These papers will be referred to as "II" and "IV," respectively.

particular matrix (2) it is possible to write the inverse quite simply. For, considering the determinant $|\boldsymbol{G}|$ of $\boldsymbol{G}$, it is evident that it vanishes when any two of the μ's are set equal; similarly, it also vanishes when any two of the k's are set equal. Accordingly, $|\boldsymbol{G}|$ cannot differ from

$$\frac{1}{\prod_{i,\,j}^{1,\,n}(1-\mu_i k_j)}\prod_{i\neq j}(\mu_i-\mu_j)\prod_{\alpha\neq\beta}(k_\alpha-k_\beta) \tag{6}$$

by more than a constant factor if we include in the two products in the numerator all distinct combinations $(\mu_i - \mu_j)$ and $(k_\alpha - k_\beta)$. (There are thus $n(n-1)/2$ terms in each of the two products in the numerator, while there are n^2 terms in the product in the denominator.) A simple inspection now shows that we have, in fact,

$$|\boldsymbol{G}| = \frac{1}{\prod_{i,\,j}^{1,\,n}(1-\mu_i k_j)}\prod_{i\neq j}(\mu_i-\mu_j)\prod_{\alpha\neq\beta}(k_\alpha-k_\beta) \tag{7}$$

if the cyclical order among the μ_i's and the k_α's is maintained.[2] And, since the matrix of every minor of $\boldsymbol{G}$ is also of the same form as $\boldsymbol{G}$ itself but with fewer rows and columns, it is apparent that the inverse of $\boldsymbol{G}$ can explicitly be written down. Thus, for the case $n = 3$, we clearly have

[2] For $n > 3$ the cyclical order has to be understood in the sense that if 1, ... , and n are regarded as the verticies of an inscribed polygon we enumerate the various sides $(i, i+1)$ and the diagonals $(i, i+2)$, $(i, i+3)$, etc., in their cyclical orders. Thus, for $n = 6$ the required order is maintained in the sequence (1, 2), (2, 3), (3, 4), (4, 5), (5, 6), (6, 1), (1, 3), (2, 4), (3, 5), (4, 6), (5,1), (6, 2), (1, 4), (2, 5), and (3, 6).

$$G^{-1}=\frac{\prod_{i,\,j}^{1,2,3}(1-\mu_i k_j)}{(\mu_1-\mu_2)(\mu_2-\mu_3)(\mu_3-\mu_1)(k_1-k_2)(k_2-k_3)(k_3-k_1)}$$

$$\times\begin{pmatrix}\dfrac{(\mu_2-\mu_3)(k_2-k_3)}{(1-\mu_2k_2)(1-\mu_2k_3)(1-\mu_3k_2)(1-\mu_3k_3)} & \dfrac{(\mu_3-\mu_1)(k_2-k_3)}{(1-\mu_1k_2)(1-\mu_1k_3)(1-\mu_3k_2)(1-\mu_3k_3)} & \dfrac{(\mu_1-\mu_2)(k_2-k_3)}{(1-\mu_1k_2)(1-\mu_1k_3)(1-\mu_2k_2)(1-\mu_2k_3)}\\ \dfrac{(\mu_2-\mu_3)(k_3-k_1)}{(1-\mu_2k_1)(1-\mu_2k_3)(1-\mu_3k_1)(1-\mu_3k_3)} & \dfrac{(\mu_3-\mu_1)(k_3-k_1)}{(1-\mu_1k_1)(1-\mu_1k_3)(1-\mu_3k_1)(1-\mu_3k_3)} & \dfrac{(\mu_1-\mu_2)(k_3-k_1)}{(1-\mu_1k_1)(1-\mu_1k_3)(1-\mu_2k_1)(1-\mu_2k_3)}\\ \dfrac{(\mu_2-\mu_3)(k_1-k_2)}{(1-\mu_2k_1)(1-\mu_2k_2)(1-\mu_3k_1)(1-\mu_3k_2)} & \dfrac{(\mu_3-\mu_1)(k_1-k_2)}{(1-\mu_1k_1)(1-\mu_1k_2)(1-\mu_3k_1)(1-\mu_3k_2)} & \dfrac{(\mu_1-\mu_2)(k_1-k_2)}{(1-\mu_1k_1)(1-\mu_1k_2)(1-\mu_2k_1)(1-\mu_2k_2)}\end{pmatrix}. \tag{8}$$

For $n > 3$ we have similar representations.

With G^{-1} as given by equation (8), the constants L_1, L_2, and L_3 of the third approximation can be found according to equation (5) and are

$$\left.\begin{aligned} L_1 &= \frac{(1-\mu_1 k_1)(1-\mu_2 k_1)(1-\mu_3 k_1)}{(k_1-k_2)(k_3-k_1)}\left[(k_2+k_3)-k_2k_3(\mu_1+\mu_2+\mu_3)+\frac{a_{\nu_0}}{b_\nu}k_2k_3\right], \\ L_2 &= \frac{(1-\mu_1 k_2)(1-\mu_2 k_2)(1-\mu_3 k_2)}{(k_2-k_3)(k_1-k_2)}\left[(k_3+k_1)-k_3k_1(\mu_1+\mu_2+\mu_3)+\frac{a_{\nu_0}}{b_\nu}k_3k_1\right], \\ L_3 &= \frac{(1-\mu_1 k_3)(1-\mu_2 k_3)(1-\mu_3 k_3)}{(k_3-k_1)(k_2-k_3)}\left[(k_1+k_2)-k_1k_2(\mu_1+\mu_2+\mu_3)+\frac{a_{\nu_0}}{b_\nu}k_1k_2\right]. \end{aligned}\right\} \quad (9)$$

Substituting the foregoing expressions for the L's in the equation for the emergent flux (IV, eq. [9]), we find that

$$\left.\begin{aligned} F_\nu(0) = \tfrac{4}{3}b_\nu\Bigg[1-\frac{3\lambda}{1-\lambda}\Bigg\{&\frac{k_1k_2+k_2k_3+k_3k_1}{k_1k_2k_3}(\mu_1+\mu_2+\mu_3)-\frac{k_1+k_2+k_3}{k_1k_2k_3} \\ &-(\mu_1+\mu_2+\mu_3)^2+(\mu_1\mu_2+\mu_2\mu_3+\mu_3\mu_1)+\frac{a_{\nu_0}}{b_\nu}\Bigg(\mu_1+\mu_2+\mu_3 \\ &-\frac{k_1k_2+k_2k_3+k_3k_1}{k_1k_2k_3}\Bigg)\Bigg\}\Bigg]. \end{aligned}\right\} \quad (10)$$

The roots k_1, k_2, and k_3 for various values of λ have already been tabulated in IV (Table 1). With these values for the k's, the constants L_1, L_2, and L_3 were determined for various values of λ and x (IV, eq. [18]). The results of the calculations are given in Table 1. In Table 2 the computed residual intensities are given.

It may finally be noted that in the second approximation the results analogous to equations (9) and (10) are

$$\left.\begin{aligned} L_1 &= \frac{(1-\mu_1 k_1)(1-\mu_2 k_1)}{k_1-k_2}\left[1-k_2(\mu_1+\mu_2)+\frac{a_{\nu_0}}{b_\nu}k_2\right], \\ L_2 &= \frac{(1-\mu_2 k_2)(1-\mu_1 k_2)}{k_2-k_1}\left[1-k_1(\mu_1+\mu_2)+\frac{a_{\nu_0}}{b_\nu}k_1\right], \end{aligned}\right\} \quad (11)$$

and

$$\left.\begin{aligned} F_\nu(0) = \tfrac{4}{3}b_\nu\Bigg[1-\frac{3\lambda}{1-\lambda}\Bigg\{&\frac{k_1+k_2}{k_1k_2}(\mu_1+\mu_2)-\frac{1}{k_1k_2}-(\mu_1+\mu_2)^2+\mu_1\mu_2 \\ &+\frac{a_{\nu_0}}{b_\nu}\left(\mu_1+\mu_2-\frac{k_1+k_2}{k_1k_2}\right)\Bigg\}\Bigg]. \end{aligned}\right\} \quad (12)$$

II. THE FIELD OF THE ULTRAVIOLET RADIATION IN A PLANETARY NEBULA

The equation of transfer for the ultraviolet radiation beyond the head of the Lyman series consistent with Zanstra's theory of the hydrogen-line emission in planetary nebulae has been considered in II, and the solution found in the form (II, eq. [83])

$$\left.\begin{aligned} I_i = S\sum_{a=1}^{n}\left\{\frac{L_a e^{-k_a\tau}}{1+\mu_i k_a}+\frac{L_{-a}e^{+k_a\tau}}{1-\mu_i k_a}\right\} \\ +pSe^{-(\tau_1-\tau)}\frac{1}{4(1-\mu_i)\left(1-p\sum_{j=1}^{n}\frac{a_j}{1-\mu_j^2}\right)} \quad (i=\pm 1,\ldots,\pm n), \end{aligned}\right\} \quad (13)$$

TABLE 1

VALUES OF L_α IN THE THIRD APPROXIMATION

λ	$x=0.1$			$x=0.125$			$x=0.15$			$x=1/6$			$x=0.175$		
	L_1	L_2	L_3	L_1	L_2	L_3	L_1	L_2	L_3	L_1	L_2	L_3	L_1	L_2	L_3
0.05	−0.014701	−0.16635	−0.0045033	−0.017522	−0.21435	−0.0054351	−0.020344	−0.26236	−0.0063669	−0.022224	−0.29436	−0.0069881	−0.023165	−0.31037	−0.0072987
.10	− .021170	− .11674	− .0071086	− .025153	− .15679	− .0086670	− .029136	− .19683	− .010225	− .031792	− .22352	− .011264	− .033119	− .23687	− .011784
.20	− .027302	− .050707	− .010099	− .032650	− .079414	− .012897	− .037998	− .10812	− .015694	− .041563	− .12726	− .017559	− .043346	− .13683	− .018492
.30	− .027914	− .010976	− .0097769	− .033877	− .031208	− .013733	− .039840	− .051441	− .017690	− .043816	− .064929	− .020327	− .045803	− .071674	− .021646
.40	− .025144	+ .010466	− .0060659	− .031186	− .0032326	− .010829	− .037227	− .016931	− .015592	− .041255	− .026063	− .018767	− .043269	− .030629	− .020355
.50	− .020449	+ .019086	− .00031817	− .026146	+ .010223	− .0052845	− .031843	+ .0013602	− .010251	− .035641	− .0045484	− .013562	− .037540	− .0075027	− .015217
.60	− .014957	+ .019835	+ .0051726	− .019968	+ .014353	+ .00063841	− .024978	+ .0088707	− .0038958	− .028318	+ .0052157	− .0069186	− .029988	+ .0033883	− .0084300
.70	− .0095545	+ .016514	+ .0084948	− .013602	+ .013305	+ .0048624	− .017649	+ .010095	+ .0012299	− .020347	+ .0079552	− .0011917	− .021696	+ .0068853	− .0024025
.80	− .0049302	+ .011430	+ .0087436	− .0077926	+ .0097291	+ .0062681	− .010655	+ .0080290	+ .0037925	− .012563	+ .0068955	+ .0021421	− .013517	+ .0063288	+ .0013169
.90	− .0016131	+ .0057508	+ .0058139	− .0031139	+ .0050618	+ .0045830	− .0046148	+ .0043721	+ .0033524	− .0056153	+ .0039123	+ .0025320	− .0061156	+ .0036824	+ .0021218
0.95	−0.00057312	+0.0028670	+0.0032419	−0.0013389	+0.0025546	+0.0026324	−0.0021046	+0.0022415	+0.0020232	−0.0026152	+0.0020328	+0.0016170	−0.0028704	+0.0019284	+0.0014139

λ	$x=0.20$			$x=0.225$			$x=0.25$			$x=0.275$			$x=0.3$		
	L_1	L_2	L_3	L_1	L_2	L_3	L_1	L_2	L_3	L_1	L_2	L_3	L_1	L_2	L_3
0.05	−0.025986	−0.35837	−0.0082305	−0.028808	−0.40638	−0.0091623	−0.031629	−0.45439	−0.010094	−0.034450	−0.50239	−0.011026	−0.037271	−0.55040	−0.011958
.10	− .037102	− .27692	− .013342	− .041085	− .31696	− .014901	− .045068	− .35700	− .016459	− .049051	− .39705	− .018018	− .053034	− .43709	− .019576
.20	− .048694	− .16553	− .021289	− .054042	− .19424	− .024087	− .059391	− .22295	− .026885	− .064739	− .25165	− .029682	− .070087	− .28036	− .032480
.30	− .051766	− .091906	− .025602	− .057729	− .11214	− .029559	− .063692	− .13237	− .033515	− .069655	− .15260	− .037471	− .075618	− .17284	− .041428
.40	− .049311	− .044327	− .025118	− .055352	− .058026	− .029881	− .061394	− .071724	− .034644	− .067435	− .085422	− .039407	− .073477	− .099121	− .044170
.50	− .043237	− .016366	− .020183	− .048934	− .025229	− .025150	− .054631	− .034092	− .030116	− .060328	− .042955	− .035082	− .066025	− .051818	− .040049
.60	− .034999	− .0020942	− .012964	− .040009	− .0075766	− .017498	− .045019	− .013059	− .022033	− .050029	− .018541	− .026567	− .055040	− .024024	− .031101
.70	− .025744	+ .0036758	− .0060349	− .029791	+ .00046618	− .0096674	− .033838	− .0027434	− .013300	− .037886	− .0059530	− .016932	− .041933	− .0091626	− .020565
.80	− .016380	+ .0046286	− .0011587	− .019242	+ .0029285	− .0036343	− .022105	+ .0012284	− .0061098	− .024967	− .00047182	− .0085855	− .027830	− .0021720	− .011061
.90	− .0076164	+ .0029927	+ .00089124	− .0091173	+ .0023030	− .00033935	− .010618	+ .0016131	− .0015700	− .012119	+ .00092360	− .0028006	− .013620	+ .00023391	− .0040311
0.95	−0.0036362	+0.0016153	+0.00080470	−0.0044019	+0.0013023	+0.00019547	−0.0051677	+0.00098897	−0.00041378	−0.0059334	+0.00067612	−0.0010230	−0.0066992	+0.00036305	−0.0016322

λ	$x=0.325$			$x=1/3$			$x=0.35$		
	L_1	L_2	L_3	L_1	L_2	L_3	L_1	L_2	L_3
0.05....	−0.040093	−0.59840	−0.012889	−0.041033	−0.61441	−0.013200	−0.042914	−0.64641	−0.013821
.10....	− .057017	− .47713	− .021134	− .058345	− .49048	− .021654	− .061000	− .51718	− .022693
.20....	− .075435	− .30907	− .035278	− .077218	− .31864	− .036210	− .080783	− .33777	− .038075
.30....	− .081581	− .19307	− .045384	− .083568	− .19981	− .046703	− .087544	− .21330	− .049341
.40....	− .079519	− .11282	− .048933	− .081533	− .11739	− .050521	− .085560	− .12652	− .053696
.50....	− .071722	− .060681	− .045015	− .073621	− .063635	− .046670	− .077419	− .069544	− .049981
.60....	− .060050	− .029506	− .035635	− .061720	− .031334	− .037146	− .065060	− .034988	− .040169
.70....	− .045980	− .012372	− .024197	− .047329	− .013442	− .025408	− .050028	− .015582	− .027830
.80....	− .030692	− .0038721	− .013537	− .031646	− .0044388	− .014362	− .033554	− .0055725	− .016012
.90....	− .015121	− .00045579	− .0052617	− .015621	− .00068569	− .0056719	− .016621	− .0011454	− .0064926
0.95....	−0.0074650	+0.000049971	−0.0022415	−0.0077202	−0.000054387	−0.0024445	−0.0082307	−0.00026305	−0.0028509

where $L_{\pm a}$, $(a = 1, \ldots, n)$, are $2n$ constants of integration, where k_a, $(a = 1, \ldots, n)$, are the n positive roots of the equation,

$$1 = p \sum_{j=1}^{n} \frac{a_j}{1 - \mu_j^2 k^2}, \tag{14}$$

and where the rest of the symbols have the same meanings as in paper II.

The boundary conditions which determine the constants of integrations are (cf. II, eqs. [84] and [85]).

$$I_i = I_{-i} \text{ at } \tau = \tau_1 \text{ for } i = 1, \ldots, n \tag{15}$$

and

$$I_{-i} = 0 \quad \text{at } \tau = 0 \text{ for } i = 1, \ldots, n. \tag{16}$$

TABLE 2

VALUES OF THE RESIDUAL INTENSITY GIVEN BY THE THIRD APPROXIMATION

λ	x												
	0.1	0.125	0.15	1/6	0.175	0.20	0.225	0.25	0.275	0.3	0.325	1/3	0.35
0.05	0.1722	0.1876	0.2012	0.2093	0.2132	0.2238	0.2333	0.2419	0.2496	0.2567	0.2631	0.2651	0.2690
0.10	0.2544	0.2724	0.2882	0.2977	0.3021	0.3145	0.3255	0.3355	0.3445	0.3526	0.3601	0.3625	0.3670
0.20	0.3794	0.3983	0.4148	0.4248	0.4294	0.4424	0.4540	0.4645	0.4739	0.4825	0.4904	0.4928	0.4976
0.30	0.4815	0.4995	0.5152	0.5246	0.5290	0.5413	0.5523	0.5622	0.5712	0.5794	0.5868	0.5891	0.5936
0.40	0.5717	0.5879	0.6021	0.6106	0.6146	0.6257	0.6356	0.6446	0.6526	0.6600	0.6667	0.6688	0.6729
0.50	0.6542	0.6683	0.6805	0.6879	0.6914	0.7010	0.7096	0.7174	0.7244	0.7307	0.7366	0.7384	0.7419
0.60	0.7313	0.7429	0.7531	0.7592	0.7621	0.7701	0.7772	0.7836	0.7894	0.7947	0.7996	0.8011	0.8040
0.70	0.8042	0.8133	0.8213	0.8260	0.8283	0.8345	0.8401	0.8451	0.8496	0.8538	0.8575	0.8587	0.8610
0.80	0.8739	0.8803	0.8860	0.8893	0.8909	0.8953	0.8993	0.9028	0.9060	0.9090	0.9116	0.9125	0.9141
0.90	0.9409	0.9446	0.9479	0.9498	0.9507	0.9533	0.9556	0.9576	0.9595	0.9611	0.9627	0.9632	0.9641
0.95	0.9736	0.9759	0.9779	0.9791	0.9797	0.9813	0.9828	0.9841	0.9852	0.9863	0.9872	0.9876	0.9881
1.00	1.0057	1.0066	1.0075	1.0080	1.0082	1.0088	1.0094	1.0100	1.0104	1.0109	1.0112	1.0114	1.0116

With the solution for the I_i's given by equation (13), these conditions require that

$$\sum_{a=1}^{n} \frac{k_a}{1 - \mu_i^2 k_a^2} (L_a e^{-k_a \tau_1} - L_{-a} e^{+k_a \tau_1}) = \frac{p}{4(1 - \mu_i^2)\left(1 - p \sum_{j=1}^{n} \frac{a_j}{1 - \mu_j^2}\right)} \quad (i = 1, \ldots, n) \tag{17}$$

and

$$\sum_{a=1}^{n} \left(\frac{L_a}{1 - \mu_i k_a} + \frac{L_{-a}}{1 + \mu_i k_a} \right) = -\frac{p e^{-\tau_1}}{4(1 + \mu_i)\left(1 - p \sum_{j=1}^{n} \frac{a_j}{1 - \mu_j^2}\right)} \quad (i = 1, \ldots, n). \tag{18}$$

The field of the diffuse ultraviolet radiation in the planetary nebula is best described in terms of its net flux, proportional to F, and its density, proportional to J. In our present scheme of approximation

$$F = 2\Sigma a_i \mu_i I_i \quad \text{and} \quad J = \tfrac{1}{2}\Sigma a_i I_i. \tag{19}$$

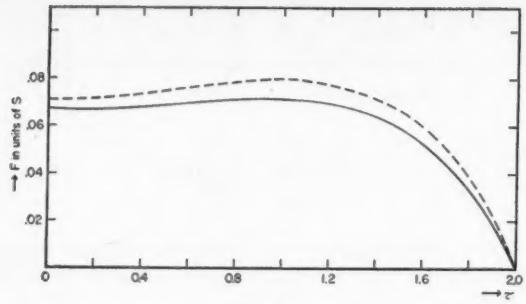

FIG. 1

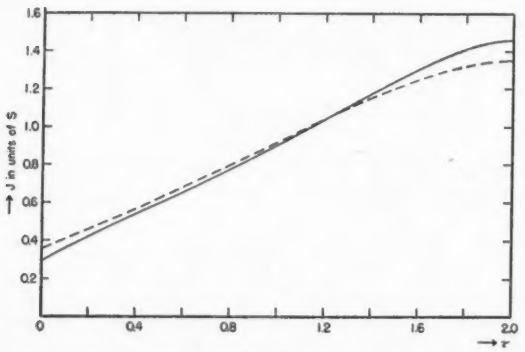

FIG. 2

TABLE 3

THE FIELD OF THE DIFFUSE ULTRAVIOLET RADIATION IN A PLANETARY NEBULA ($p=0.5$ AND $\tau_1=1$)

τ	F/S	J/S	τ	F/S	J/S
0	0.1122	0.0533	0.625	0.0621	0.1156
0.125	.1031	.0692	0.750	.0463	.1236
0.250	.0944	.0829	0.875	.0261	.1293
0.375	.0852	.0951	1.000	0.0000	0.1315
0.500	0.0747	0.1060			

TABLE 4

THE FIELD OF THE DIFFUSE ULTRAVIOLET RADIATION IN A PLANETARY NEBULA ($p=0.5$ AND $\tau_1=2$)

τ	F/S	J/S	τ	F/S	J/S
0	0.0677	0.0295	1.000	0.0713	0.0905
0.125	.0671	.0377	1.250	.0684	.1072
0.250	.0673	.0452	1.500	.0592	.1241
0.375	.0679	.0525	1.750	.0389	.1388
0.500	.0689	.0598	1.875	.0225	.1436
0.750	0.0707	0.0746	2.000	0.0000	0.1459

or, substituting for I_i according to equation (13), we find, after some minor reductions, that

$$F = 4S\frac{1-p}{p}\sum_{a=1}^{n}\frac{1}{k_a}(-L_a e^{-k_a\tau}+L_{-a}e^{+k_a\tau}) - pSe^{-(\tau_1-\tau)}\frac{1-\sum_{j=1}^{n}\frac{a_j}{1-\mu_j^2}}{1-p\sum_{j=1}^{n}\frac{a_j}{1-\mu_j^2}} \tag{20}$$

and

$$J = S\frac{1}{p}\sum_{a=1}^{n}(L_a e^{-k_a\tau}+L_{-a}e^{+k_a\tau}) + \tfrac{1}{4}pSe^{-(\tau_1-\tau)}\frac{\sum_{j=1}^{n}\frac{a_j}{1-\mu_j^2}}{1-p\sum_{j=1}^{n}\frac{a_j}{1-\mu_j^2}}. \tag{21}$$

As an illustration of the foregoing solutions, we shall consider the case $p = \frac{1}{2}$ and assume for τ_1 the values 1 and 2. For $p = \frac{1}{2}$ the characteristic roots are (cf. IV, Table 1, the entry for $\lambda = \frac{1}{2}$)

$$k_1 = 3.69160\,, \qquad k_2 = 0.964672\,, \qquad \text{and} \qquad k_3 = 1.34962\,. \tag{22}$$

For $\tau_1 = 1$, respectively 2, it was found that

$$\left.\begin{array}{ll} \tau_1 = 1\,; & \tau_1 = 2\,, \\ L_1 = -0.0071701\,; & L_1 = -0.0030984\,, \\ L_2 = -0.0072975\,; & L_2 = -0.0031239\,, \\ L_3 = -0.0047223\,; & L_3 = -0.0020265\,, \\ L_{-1} = -0.00025276\,; & L_{-1} = -0.00000619\,, \\ L_{-2} = +0.310465\,; & L_{-2} = +0.118659\,, \\ L_{-3} = -0.014003\,; & L_{-3} = -0.0035584\,. \end{array}\right\} \tag{23}$$

With these values for the constants, F and J were computed according to equations (20) and (21) for various values of τ ($\leq \tau_1$). The results of the calculations are summarized in Tables 3 and 4, and the solutions for the case $\tau_1 = 2$ are illustrated in Figures 1 and 2. In these figures we have further compared our present solutions on the third approximation (full-line curves) with those given earlier by Chandrasekhar[3] on the Milne-Eddington type of approximation (dashed-line curves).

[3] *Zs. f. Ap.*, **9**, 266, 1935.

ON THE RADIATIVE EQUILIBRIUM OF A STELLAR ATMOSPHERE. VII

S. CHANDRASEKHAR
Yerkes Observatory
Received March 9, 1945

ABSTRACT

In this paper the problem of the radiative equilibrium of a stellar atmosphere in local thermodynamic equilibrium is reconsidered with a view to examining in detail the effects of a continuous absorption coefficient, κ_ν, dependent on frequency. It is shown that when the material departs from grayness the corrections which have to be made to the temperature distribution are of two kinds: first, because the integrated Planck intensity B is not, in general, equal to the average integrated intensity J $(= \int\int I_\nu d\omega d\nu/4\pi)$ and, second, because the energy density of the radiation does not have the gray atmospheric value. To evaluate the corrections arising from these two sources, a systematic method of approximation has been developed in which the first approximation is assumed to be given by the solution for a gray atmosphere with a κ_ν equal to a certain appropriately chosen mean absorption coefficient $\bar{\kappa}$. It is found that the best way of choosing $\bar{\kappa}$ is to define it as a straight mean of κ_ν, weighted according to the net monochromatic flux $F_\nu^{(1)}$ (τ) of radiation of frequency ν in a gray atmosphere:

$$\bar{\kappa} = \int_0^\infty \kappa_\nu \frac{F_\nu^{(1)}}{F}\, d\nu \qquad (F = \text{integrated flux}).$$

Moreover, in a second approximation,

$$B^{(2)} = J^{(2)} + \tfrac{1}{4}\int_0^\infty \left(\frac{\kappa_\nu}{\bar{\kappa}} - 1\right)\frac{dF_\nu^{(1)}}{d\tau}\, d\nu,$$

where $J^{(2)}$ is the solution appropriate for J in this approximation. The solution for $J^{(2)}$ has, in turn, been obtained in an nth approximation.

To facilitate the use of the solutions in the higher approximations obtained in this paper, the monochromatic fluxes $F_\nu^{(1)}(\tau)$ and their derivatives $dF_\nu^{(1)}/d\tau$ have been evaluated for a range of values of τ and $\alpha = h\nu/kT_e$ (T_e denoting the effective temperature).

1. *Introduction.*—The solution to the problem of radiative transfer in an atmosphere in local thermodynamic equilibrium is fundamental to all investigations which are in any way related to the continuous spectrum of the stars. More particularly, the basic problem is one of solving the equation of transfer

$$\mu \frac{dI_\nu}{\rho dx} = -\kappa_\nu I_\nu + \kappa_\nu B_\nu, \tag{1}$$

under conditions of a constant net flux of radiation

$$\pi F = \pi \int_0^\infty F_\nu d\nu = 2\pi \int_0^\infty \int_{-1}^{+1} I_\nu \mu\, d\mu\, d\nu, \tag{1'}$$

in all the frequencies and where $B_\nu(T)$ is the Planck function for the temperature T at x. The complete solution to this problem depends only on the distribution of temperature in the atmosphere; for, once this is known, the source function $B_\nu(T)$ for the radiation of frequency ν is known at all points in the atmosphere and the determination of the intensity I_ν at any point and in any given direction is immediate (see eq. [25] below). However, when the continuous absorption coefficient κ_ν is allowed to be an arbitrary function of ν and x, the determination of the temperature distribution in the atmosphere is by no means a simple matter. Indeed, there exists at the present time no satisfactory attempt to solve the basic problem with any degree of generality. And what is already known in this connection[1] can be summarized quite simply.

[1] Cf., for what follows, A. Unsöld, *Physik der Sternatmosphären*, pp. 113–116, Berlin: Springer, 1938.

From the equation of transfer (1) we readily obtain

$$\frac{dK_\nu}{\rho dx} = -\tfrac{1}{4}\kappa_\nu F_\nu , \tag{2}$$

where, as usual, we have written

$$K_\nu = \frac{1}{2}\int_{-1}^{+1} I_\nu \mu^2 d\mu . \tag{3}$$

Defining the mean absorption coefficient $\bar{\kappa}$ by means of the relation

$$\frac{1}{\bar{\kappa}}\int_0^\infty \frac{dK_\nu}{\rho dx}\, d\nu = \int_0^\infty \frac{1}{\kappa_\nu}\frac{dK_\nu}{\rho dx}\, d\nu , \tag{4}$$

we can re-write equation (2) as an equation for integrated radiation in the form

$$\frac{dK}{d\tau} = \tfrac{1}{4}F , \tag{5}$$

where τ denotes the optical depth in the mean absorption coefficient $\bar{\kappa}$, measured from the boundary of the atmosphere normally inward. Remembering the constancy of the net integrated flux, we can integrate equation (5) to give

$$K = \tfrac{1}{4}F\tau + \text{constant} . \tag{6}$$

Using the conventional Milne-Eddington type of approximations, we readily derive from equation (6) the formula

$$J = \int_0^\infty J_\nu d\nu = \frac{1}{2}\int_0^\infty \int_{-1}^{+1} I_\nu d\mu d\nu = \tfrac{1}{2}F(1 + \tfrac{3}{2}\tau) . \tag{7}$$

But we *cannot*, in general, pass directly from this equation for J to an equation for the integrated Planck intensity B $(= \sigma T^4/\pi)$. For, according to the equation of transfer (1), the constancy of the net integrated flux implies only that

$$\int_0^\infty \kappa_\nu J_\nu d\nu = \int_0^\infty \kappa_\nu B_\nu d\nu ; \tag{8}$$

and we cannot infer (except when the material is "gray") that $J = B$. In other words, the formula for the temperature distribution which is in common use, namely,

$$T^4 = \tfrac{1}{2}T_e^4(1 + \tfrac{3}{2}\tau) . \tag{9}$$

where τ is the optical depth measured in the "Rosseland mean"[2] absorption coefficient,

[2] In practice this is defined by

$$\frac{1}{\bar{\kappa}}\int_0^\infty \frac{dB_\nu}{dT}\, d\nu = \int_0^\infty \frac{1}{\kappa_\nu}\frac{dB_\nu}{dT}\, d\nu .$$

But this is not the same as the mean absorption coefficient defined by equation (4). It would therefore seem that the use of the conventional Rosseland mean absorption coefficient in the theory of stellar atmospheres is of questionable value. On the other hand, an alternative form of equation (4), namely,

$$\bar{\kappa} = \frac{1}{F}\int_0^\infty \kappa_\nu F_\nu d\nu ,$$

would appear to provide a more satisfactory way of defining κ, as it has the further advantages of being a straight mean. Further remarks relating to this matter are made in § 5.

cannot, strictly speaking, be regarded as the solution of the fundamental equations in any well-defined scheme of approximation. Thus, while the use of equation (9) cannot be strictly defended, there does seem to be some evidence for the belief that the temperature distribution derived on the gray-body assumption provides a "first approximation" to the true distribution in some sense or another. For example, it is well known from the studies of Milne and Lindblad that the law of darkening in the different wave lengths over the solar disk and the intensity distribution in the continuous spectrum of the sun agree quite well with what can be predicted on the gray-body assumption. But attempts to improve on this agreement by allowing for a variation of κ_ν with ν on a "second approximation" generally indicate that the departures from grayness of the material is quite large.[3] It would, accordingly, appear that the solution for the temperature distribution on the gray-body assumption does provide a good first approximation even for substantial variations of κ_ν with ν. But, as to in what sense it is a first approximation can be understood only when we develop a systematic well-defined scheme of approximation and explicitly work out a second approximation. It is the object of this paper to provide such a scheme and to estimate the errors which are involved in the use of the solution (9).

2. *An iteration method for solving the equation of transfer for an atmosphere in local thermodynamic equilibrium and with a continuous absorption coefficient depending on the wave length.*—According to our remarks in the preceding section, it would appear that the temperature distribution in the atmosphere derived on the assumption of grayness of the material provides a first approximation. Assuming that this is the case, let κ be a certain mean absorption coefficient (undefined for the present) such that with $\kappa_\nu = \kappa =$ constant we obtain a first approximation. Let τ denote the optical depth measured in terms of this absorption coefficient. Further, let

$$\delta_\nu = \frac{\kappa_\nu}{\kappa} - 1 , \tag{10}$$

so that δ_ν is a measure of the departure from grayness of the material. With these definitions the equation of transfer (1) takes the form

$$\mu \frac{dI_\nu}{d\tau} = I_\nu - B_\nu + \delta_\nu (I_\nu - B_\nu) . \tag{11}$$

We suppose that this equation can be solved in two steps. First, we find the solution of the equation

$$\mu \frac{dI_\nu^{(1)}}{d\tau} = I_\nu^{(1)} - B_\nu^{(1)} \qquad [B_\nu^{(1)} = B_\nu (T^{(1)})] . \tag{12}$$

appropriate to the problem on hand, and use this solution in the term which occurs as the factor of δ_ν in equation (11). Thus, the second approximation will be given by the solution of

$$\mu \frac{dI_\nu^{(2)}}{d\tau} = I_\nu^{(2)} - B_\nu^{(2)} + \delta_\nu \mu \frac{dI_\nu^{(1)}}{d\tau} . \tag{13}$$

Formally, there is, of course, no difficulty in extending this method of iteration to obtain solutions to as high an approximation as may be needed. Thus, in the nth approximation we shall have

$$\mu \frac{dI_\nu^{(n)}}{d\tau} = I_\nu^{(n)} - B_\nu^{(n)} + \delta_\nu [I_\nu^{(n-1)} - B_\nu^{(n-1)}] . \tag{14}$$

[3] Cf. Unsöld, *op. cit.*, pp. 107–109 (see particularly Tables 24 and 26).

This method of iteration will obviously converge if δ_ν is sufficiently small. But the point to which attention may be drawn at this stage is that in practice the success of this method is not impaired even when δ_ν takes moderately large values of the order of 2 or 3 (see § 5 below).

In this paper we shall consider only the first two approximations.

In their integrated forms, equations (12) and (13) are

$$\mu \frac{dI^{(1)}}{d\tau} = I^{(1)} - B^{(1)} \tag{15}$$

and

$$\mu \frac{dI^{(2)}}{d\tau} = I^{(2)} - B^{(2)} + \mu \int_0^\infty \delta_\nu \frac{dI_\nu^{(1)}}{d\tau}\, d\nu . \tag{16}$$

The foregoing equations have, of course, to be solved under the conditions of a constant net integrated flux. In the first two approximations this condition requires, respectively, that

$$B^{(1)} = J^{(1)} \tag{17}$$

and

$$B^{(2)} = J^{(2)} + \frac{1}{2}\int_0^\infty \int_{-1}^{+1} \delta_\nu \frac{dI_\nu^{(1)}}{d\tau}\, \mu d\mu d\nu . \tag{18}$$

Equation (18) can be re-written in the form

$$B^{(2)} = J^{(2)} + \frac{1}{4}\int_0^\infty \delta_\nu \frac{dF_\nu^{(1)}}{d\tau}\, d\nu . \tag{19}$$

In other words, in the second approximation the integrated Planck intensity B differs from J by an amount which depends on the *nonconstancy* of the monochromatic fluxes F_ν. From general considerations we may expect (and this is confirmed by the calculations to be presented in § 5) that, unless δ_ν varies too widely over the relevant ranges of ν, the departures from constancy of the monochromatic fluxes F_ν will be of the second order of smallness. It is precisely on this account that the temperature distribution derived on the assumption of grayness of the material is as satisfactory as it has been found to be in practice.

We now proceed to the solutions of equations (15) and (16).

3. *The solution in the* (1, n) *approximation.*—Equations (15) and (17) together reduce to an equation of transfer of a standard type which has been treated in sufficient detail in earlier papers of this series.[4] Adopting in particular the scheme of approximation developed in paper II we can, in the nth approximation, write (II, eqs. [19] and [26])

$$I_i^{(1)} = \tfrac{3}{4}F \left\{ \sum_{a=1}^{n-1} \frac{L_a^{(1)}}{1+\mu_i k_a}\, e^{-k_a\tau} + \mu_i + Q^{(1)} + \tau \right\} \quad (i = \pm 1, \ldots, \pm n) , \tag{20}$$

where the n constants $L_a^{(1)}$, $(a = 1, \ldots, n-1)$, and $Q^{(1)}$ are determined by the equations (II, eq. [21])

$$\sum_{a=1}^{n-1} \frac{L_a^{(1)}}{1-\mu_i k_a} + Q^{(1)} - \mu_i = 0 \qquad (i = 1, \ldots, n) \tag{21}$$

[4] *Ap. J.*, **99**, 180, 1944, and **100**, 76, 1944. These papers will be referred to as "I" and "II," respectively.

and the k_a's are the $n-1$ distinct nonzero positive roots of the characteristic equation (II, eq. [10])

$$2 = \sum_{i=-n}^{+n} \frac{a_i}{1+\mu_i k_a}. \tag{22}$$ [5]

On this approximation the solution for $J^{(1)}$ is (II, eq. [29])

$$J^{(1)} = B^{(1)} = \tfrac{3}{4}F(\tau + q[\tau]) = \tfrac{3}{4}F\left(\tau + Q^{(1)} + \sum_{a=1}^{n-1} L_a^{(1)} e^{-k_a\tau}\right). \tag{23}$$

The corresponding formula giving the temperature distribution is

$$(T^{(1)})^4 = \tfrac{3}{4}T_e^4\left(\tau + Q^{(1)} + \sum_{a=1}^{n-1} L_a^{(1)} e^{-k_a\tau}\right). \tag{24}$$

Corresponding to the distribution of temperature (24), there is a determinate distribution of the intensities at various frequencies and at various levels. Thus, the intensity of the radiation of frequency ν at an optical depth τ and in a direction making an angle ϑ with the positive normal is given by

$$\left.\begin{aligned} I_\nu^{(1)}(\tau,\vartheta) &= \int_\tau^\infty e^{-(t-\tau)\sec\vartheta} B_\nu(T_t^{(1)}) \sec\vartheta\, dt \quad (0<\vartheta<\pi/2) \\ &= -\int_0^\tau e^{-(t-\tau)\sec\vartheta} B_\nu(T_t^{(1)}) \sec\vartheta\, dt \quad (\pi/2<\vartheta<\pi). \end{aligned}\right\} \tag{25}$$

In terms of this solution for $I_\nu^{(1)}(\tau,\vartheta)$ we can readily derive explicit formulae for quantities such as J_ν, F_ν, etc. In fact, it can be shown quite generally that

$$\left.\begin{aligned} \int_{-1}^{+1} I_\nu^{(1)}(\tau,\mu)\,\mu^j d\mu &= \int_\tau^\infty B_\nu(T_t^{(1)})\, E_{j+1}(t-\tau)\, dt \\ &\quad + (-1)^j \int_0^\tau B_\nu(T_t^{(1)})\, E_{j+1}(\tau-t)\, dt. \end{aligned}\right\} \tag{26}$$

where $E_{j+1}(x)$ stands for the exponential integral

$$E_{j+1}(x) = \int_1^\infty \frac{e^{-xw}}{w^{j+1}}\, dw. \tag{27}$$

In our further work we shall find that we also need expressions for the quantities

$$\int_{-1}^{+1} \frac{dI_\nu^{(1)}}{d\tau}\,\mu^j d\mu. \tag{28}$$

From the equation of transfer (15) we find that

$$\int_{-1}^{+1} \frac{dI_\nu^{(1)}}{d\tau}\,\mu^j d\mu = \int_{-1}^{+1} I_\nu^{(1)}(\tau,\mu)\,\mu^{j-1} d\mu - \frac{2}{j}\,\epsilon_{j,\,\mathrm{odd}} B_\nu(T_\tau^{(1)}), \tag{29}$$

where

$$\left.\begin{aligned} \epsilon_{j,\,\mathrm{odd}} &= 1 \quad \text{if } j \text{ is odd} \\ &= 0 \quad \text{otherwise.} \end{aligned}\right\} \tag{30}$$

[5] In the summation on the right-hand side of this equation there is no term with $i = 0$.

Using equation (26), we can re-write equation (29) as

$$\left.\begin{aligned}\int_{-1}^{+1}\frac{dI_\nu^{(1)}}{d\tau}\,\mu^i d\mu = &\int_\tau^\infty B_\nu(T_t^{(1)})\,E_j(t-\tau)\,dt\\ &+(-1)^{i-1}\int_0^t B_\nu(T_t^{(1)})\,E_j(\tau-t)\,dt-\frac{2}{j}\,\epsilon_{j,\ \mathrm{odd}}B_\nu(T_\tau^{(1)})\,.\end{aligned}\right\}\quad(31)$$

Equations (24), (25), (26), and (31) may be said to represent the solution to our problem in the (1, n) approximation referring to the fact that the equations of the first approximation have in turn been solved in an nth approximation.

4. *The solution of the equations in the* (2, n) *approximation.*—Turning next to the solution of the equations (16) and (18), we have to consider the equation

$$\mu\frac{dI^{(2)}}{d\tau}=I^{(2)}-\frac{1}{2}\int_{-1}^{+1}I^{(2)}d\mu+\mu\int_0^\infty\delta_\nu\frac{dI_\nu^{(1)}}{d\tau}\,d\nu-\frac{1}{2}\int_0^\infty\int_{-1}^{+1}\delta_\nu\mu\frac{dI_\nu^{(1)}}{d\tau}\,d\mu d\nu.\quad(32)$$

In solving this integrodifferential equation we shall follow the methods developed in the earlier papers of this series and replace the integrals which occur on the right-hand side of this equation by sums according to Gauss's formula for numerical quadratures. Thus, in the nth approximation, the equivalent systems of linear equations are

$$\left.\begin{aligned}\mu_i\frac{dI_i^{(2)}}{d\tau}=I_i^{(2)}-\tfrac{1}{2}\Sigma a_jI_j^{(2)}+\mu_i\int_0^\infty\delta_\nu\frac{dI_{\nu,\,i}^{(1)}}{d\tau}\,d\nu\\ -\frac{1}{2}\int_0^\infty\delta_\nu\Sigma a_j\mu_j\frac{dI_{\nu,\,j}^{(1)}}{d\tau}\,d\nu\quad(i=\pm1,\ldots,\pm n)\,,\end{aligned}\right\}\quad(33)$$

where we have used $I_j^{(2)}$ and $I_{\nu,j}^{(1)}$ to denote, respectively, $I^{(2)}(\tau,\mu_j)$ and $I_\nu^{(1)}(\tau,\mu_j)$ and the rest of the symbols have the same meanings as in paper II.

The system of equations represented by (33) is most conveniently solved by the method of the variation of the parameters. Thus, since the homogeneous part of the system of equations (33) is of the same form as that considered in II, equation (6), we seek a solution of our present system of the form (cf. II, eqs. [18] and [26])

$$\left.\begin{aligned}I_i^{(2)}=\tfrac{3}{4}F\Bigg\{&\sum_{a=1}^{n-1}\frac{e^{-k_a\tau}}{1+\mu_ik_a}L_a^{(2)}(\tau)\\ &+\sum_{a=1}^{n-1}\frac{e^{+k_a\tau}}{1-\mu_ik_a}L_{-a}^{(2)}(\tau)+\mu_i+Q^{(2)}(\tau)+\tau\Bigg\}\quad(i=\pm1,\ldots.+n)\,,\end{aligned}\right\}\quad(34)$$

where, as we have indicated, $L_a^{(2)}$, $L_{-a}^{(2)}$, ($a=1,\ldots.,n-1$), and $Q^{(2)}$ are all to be considered as functions of τ. It will be noticed that in writing the solution in this form we have treated as variable only $(2n-1)$ of the $2n$ constants of integration which the general solution of the homogeneous system associated with equation (33) involves. This is, however, permissible in view of the fact that equation (33) admits the flux integral

$$\Sigma a_i\mu_iI_i^{(2)}=\text{constant}\,,\quad(35)$$

and we can arrange that this constant of integration has the same value as in the (1, n) approximation corresponding to the circumstance of a *given* constant net integrated flux.

Substituting for $I_i^{(2)}$ from equation (34) in equation (33), we obtain the variational equation

$$\left.\begin{aligned}\tfrac{3}{4}F\mu_i\left\{\sum_{a=1}^{n-1}\frac{e^{-k_a\tau}}{1+\mu_i k_a}\frac{dL_a^{(2)}}{d\tau}+\sum_{a=1}^{n-1}\frac{e^{+k_a\tau}}{1-\mu_i k_a}\frac{dL_{-a}^{(2)}}{d\tau}+\frac{dQ^{(2)}}{d\tau}\right\}\\ =\mu_i\int_0^\infty\delta_\nu\frac{dI_{\nu,\,i}^{(1)}}{d\tau}\,d\nu-\tfrac{1}{2}\int_0^\infty\delta_\nu\Sigma a_j\mu_j\frac{dI_{\nu,\,j}^{(1)}}{d\tau}\,d\nu\quad(i=\pm1,\ldots,\pm n)\,.\end{aligned}\right\}\tag{36}$$

Of the $2n$ equations represented in the foregoing equation, only $2n-1$ are linearly independent, since the equation derived from (36) by multiplying with a_i and summing over all i's is identically satisfied (cf. II, eq. [25]). The rank of the systems (36) is, accordingly, $(2n-1)$—in agreement with the fact that we have only $(2n-1)$ functions $L_a^{(2)}$, $L_{-a}^{(2)}$, $(a=1,\ldots,n-1)$, and $Q^{(2)}$ to determine.

The order of the system of equations (36) can be further reduced to $(2n-2)$ by a proper averaging of the continuous absorption coefficient κ_ν to yield a $\bar{\kappa}$ to be used in the first gray-body approximation. Thus, multiplying equation (36) by $a_i\mu_i$ and summing over all i's, we obtain

$$\tfrac{1}{2}F\frac{dQ^{(2)}}{d\tau}=\int_0^\infty\delta_\nu\Sigma a_i\mu_i^2\frac{dI_{\nu,\,i}^{(1)}}{d\tau}\,d\nu\,,\tag{37}$$

use having been made of the relations (II, eq. [24] and eq. [58] below)

$$\sum_i a_i\mu_i^2=\tfrac{2}{3}\qquad\text{and}\qquad\sum_i\frac{a_i\mu_i^2}{1+\mu_i k_a}=0\,.\tag{38}$$

Accordingly, if we arrange that

$$\int_0^\infty\delta_\nu\Sigma a_i\mu_i^2\frac{dI_{\nu,\,i}^{(1)}}{d\tau}\,d\nu=2\int_0^\infty\delta_\nu\frac{dK_\nu^{(1)}}{d\tau}\,d\nu=0\,,\tag{39}$$

we shall have the integral

$$Q^{(2)}=\text{constant}=Q^{(1)}+\Delta Q\qquad\text{(say)}\,.\tag{40}$$

But equation (39) implies that the mean absorption coefficient $\bar{\kappa}$ has to be defined according to

$$\bar{\kappa}\int_0^\infty\frac{dK_\nu^{(1)}}{d\tau}\,d\nu=\int_0^\infty\kappa_\nu\frac{dK_\nu^{(1)}}{d\tau}\,d\nu\,,\tag{41}$$

or, alternatively (cf. eqs. [2] and [5]),

$$\bar{\kappa}=\frac{1}{F}\int_0^\infty\kappa_\nu F_\nu^{(1)}d\nu\,;\tag{42}$$

for with this choice of $\bar{\kappa}$ the departures of κ_ν from $\bar{\kappa}$, when similarly averaged, will be zero:

$$\int_0^\infty\delta_\nu\frac{dK_\nu^{(1)}}{d\tau}\,d\nu=\frac{1}{4}\int_0^\infty\delta_\nu F_\nu^{(1)}d\nu=0\,.\tag{43}$$

Attention may be drawn here to a consequence of the foregoing method of averaging κ_ν for the important special case when δ_ν is independent of τ, i.e., when $\kappa_\nu/\bar{\kappa}$ is independent of depth. In this case we can re-write equation (19) in the form

$$B^{(2)}=J^{(2)}+\frac{1}{4}\frac{d}{d\tau}\int_0^\infty\delta_\nu F_\nu^{(1)}d\nu\,,\tag{44}$$

and equation (43) now implies that

$$B^{(2)} = J^{(2)} \qquad (\kappa_\nu/\bar{\kappa} \text{ independent of } \tau)\,. \quad (45)$$

With $\bar{\kappa}$ defined as in equation (42), the variational equations become

$$\left.\begin{aligned} &\tfrac{3}{4}F\mu_i\left\{\sum_{a=1}^{n-1}\frac{e^{-k_a\tau}}{1+\mu_i k_a}\frac{dL_a^{(2)}}{d\tau}+\sum_{a=1}^{n-1}\frac{e^{+k_a\tau}}{1-\mu_i k_a}\frac{dL_{-a}^{(2)}}{d\tau}\right\}\\ &\quad=\mu_i\int_0^\infty \delta_\nu\frac{dI_{\nu,\,i}^{(1)}}{d\tau}\,d\nu-\frac{1}{2}\int_0^\infty \delta_\nu\Sigma a_j\mu_j\frac{dI_{\nu,\,j}^{(1)}}{d\tau}\,d\nu \quad (i=\pm1,\ldots,\pm n)\,. \end{aligned}\right\} \quad (46)$$

Though $2n$ equations are represented in the foregoing equation, only $2n-2$ of these are linearly independent, corresponding to the $(2n-2)$ functions $L_a^{(2)}$ and $L_{-a}^{(2)}$, $(a=1,\ldots,n-1)$, which are to be determined.

In view of that fact that the rank of the system (46) is less than the number of equations, it appears that the most symmetrical way of treating the variational equations is the following:

Multiply equation (46) by $a_i\mu_i^{m-1}$, $(m=1,\ldots,2n)$, and sum over all i's. We obtain

$$\left.\begin{aligned} &\tfrac{3}{4}F\left\{\sum_{a=1}^{n-1}D_{m,\,a}e^{-k_a\tau}\frac{dL_a^{(2)}}{d\tau}+(-1)^m\sum_{a=1}^{n-1}D_{m,\,a}e^{+k_a\tau}\frac{dL_{-a}^{(2)}}{d\tau}\right\}\\ &\quad=\bar{\delta}_m-\frac{\epsilon_{m,\,\text{odd}}}{m}\bar{\delta}_1 \quad (m=1,\ldots,2n)\,, \end{aligned}\right\} \quad (47)$$

where we have written

$$D_{m,\,a}=\sum_i\frac{a_i\mu_i^m}{1+\mu_i k_a}=(-1)^m\sum_i\frac{a_i\mu_i^m}{1-\mu_i k_a} \quad (48)$$

and

$$\bar{\delta}_m=\int_0^\infty\delta_\nu\sum_i a_i\mu_i^m\frac{dI_{\nu,\,i}^{(1)}}{d\tau}\,d\nu \quad (49)$$

and where $\epsilon_{m,\,\text{odd}}$ has the same meaning as in equation (30). It may be noted that in deriving equation (47) use has been made of the relation

$$\sum_i a_i\mu_i^{m-1}=\frac{2}{m}\epsilon_{m,\,\text{odd}} \qquad (m=1,\ldots,4n)\,. \quad (50)$$

There is a simple recursion formula which $D_{m,\,a}$ satisfies and which enables a direct evaluation of this quantity. We have

$$D_{m,\,a}=\frac{1}{k_a}\sum_i a_i\mu_i^{m-1}\left(1-\frac{1}{1+\mu_i k_a}\right), \quad (51)$$

or, using equation (50),

$$D_{m,\,a}=\frac{1}{k_a}\left(\frac{2}{m}\epsilon_{m,\,\text{odd}}-D_{m-1,\,a}\right) \qquad (m=1,\ldots,4n)\,, \quad (52)$$

which is the required recursion formula. For odd, respectively even, values of m, the formula takes the forms

$$D_{2j-1,\,a}=\frac{1}{k_a}\left(\frac{2}{2j-1}-D_{2j-2,\,a}\right) \quad (53)$$

and

$$D_{2j,\,a} = -\frac{1}{k_a} D_{2j-1,\,a}\,. \tag{54}$$

Combining the relations (53) and (54), we have

$$D_{2j-1,\,a} = \frac{1}{k_a}\left(\frac{2}{2j-1} + \frac{1}{k_a} D_{2j-3,\,a}\right) \tag{55}$$

and

$$D_{2j,\,a} = -\frac{1}{k_a^2}\left(\frac{2}{2j-1} - D_{2j-2,\,a}\right). \tag{56}$$

On the other hand, in our present notation the equation for the characteristic roots k_a can be written as (cf. eq. [22])

$$D_{0,\,a} = 2 \qquad (a = 1, \ldots, n-1)\,. \tag{57}$$

From the recursion formula (52) we now conclude that

$$D_{2,\,a} = -\frac{1}{k_a} D_{1,\,a} = -\frac{1}{k_a^2}(2 - D_{0,\,a}) = 0 \tag{58}$$

and

$$D_{3,\,a} = \frac{2}{3k_a} \quad \text{and} \quad D_{4,\,a} = -\frac{2}{3k_a^2}\,. \tag{59}$$

The formula (55) will now enable us to determine $D_{m,\,a}$ successively for all odd values of m greater than 3; similarly, the expressions for the even values of m follow from equation (56). In this manner we find that

$$D_{2j-1,\,a} = \frac{2}{(2j-1)\,k_a} + \frac{2}{(2j-3)\,k_a^3} + \ldots + \frac{2}{3k_a^{2j-3}} \qquad (j = 2, \ldots, n) \tag{60}$$

and

$$D_{2j,\,a} = -\frac{2}{(2j-1)\,k_a^2} - \frac{2}{(2j-3)\,k_a^4} - \ldots - \frac{2}{3k_a^{2j-2}} \qquad (j = 2, \ldots, n)\,. \tag{61}$$[6]

[6] In terms of these $D_{2j,a}$'s it is possible to write down an alternative form of the characteristic equation which, in contrast to equation (22), does not require an explicit knowledge of the Gaussian weights and divisions. For, if p_{2j}, $(j = 0, \ldots, n)$, are the coefficients of the polynomial $P_{2n}(\mu)$, so that

$$P_{2n}(\mu) = \sum_{j=0}^{n} p_{2j}\mu^{2j}\,,$$

it is evident that

$$\sum_{j=0}^{n} p_{2j} D_{2j,\,a} = \sum_i \frac{a_i}{1 + \mu_i k_a}\left(\sum_{j=0}^{n} p_{2j}\mu_i^{2j}\right) \equiv 0 \qquad (a = 1, \ldots, n-1)\,,$$

since the μ_i's are, by definition, the zeros of $P_{2n}(\mu)$. Hence, with the definitions

$$-D_{2j} = \frac{2}{(2j-1)k^2} + \frac{2}{(2j-3)k^4} + \ldots + \frac{2}{3k^{2j-2}} \qquad (j = 2, \ldots, n)$$

and

$$D_0 = 2 \quad \text{and} \quad D_2 = 0\,,$$

the equation for the characteristic roots takes the form

$$\sum_{j=0}^{n} p_{2j} D_{2j} = 0\,.$$

Returning to equation (47), we first observe that, since D_1, D_2, and $\bar{\delta}_2$ are all zero (cf. eqs. [39] and [49]), then, of the $2n$ equations represented by equation (47), those for $m = 1$ and 2 are identically satisfied. Accordingly, we need consider equation (47) only for values of $m = 3, \ldots, 2n$. For odd, respectively even, values of m, equation (47) takes the forms

$$\tfrac{3}{4}F\sum_{a=1}^{n-1} D_{2j-1,\,a}\left(e^{-k_a\tau}\frac{dL_a^{(2)}}{d\tau}-e^{+k_a\tau}\frac{dL_{-a}^{(2)}}{d\tau}\right)=\bar{\delta}_{2j-1}-\frac{1}{2j-1}\,\bar{\delta}_1 \quad (j=2,\ldots,n) \qquad (62)$$

and

$$\tfrac{3}{4}F\sum_{a=1}^{n-1} D_{2j,\,a}\left(e^{-k_a\tau}\frac{dL_a^{(2)}}{d\tau}+e^{+k_a\tau}\frac{dL_{-a}^{(2)}}{d\tau}\right)=\bar{\delta}_{2j} \qquad (j=2,\ldots,n)\,; \qquad (63)$$

or, substituting for $D_{2j-1,\,a}$ and $D_{2j,\,a}$ according to equations (60) and (61), we have

$$\left.\begin{aligned}&\frac{3}{2}\sum_{a=1}^{n-1}\left\{\frac{1}{3k_a^{2j-3}}+\frac{1}{5k_a^{2j-5}}+\ldots+\frac{1}{(2j-1)\,k_a}\right\}X_a=\bar{\delta}_{2j-1}-\frac{1}{2j-1}\,\bar{\delta}_1\\ &\qquad\qquad (j=2,\ldots,n)\end{aligned}\right\} \qquad (64)$$

and

$$\frac{3}{2}\sum_{a=1}^{n-1}\left\{\frac{1}{3k_a^{2j-2}}+\frac{1}{5k_a^{2j-4}}+\ldots+\frac{1}{(2j-1)\,k_a^2}\right\}Y_a=-\bar{\delta}_{2j} \quad (j=2,\ldots,n)\,, \qquad (65)$$

where, for the sake of brevity, we have written

$$\left.\begin{aligned}X_a&=F\left(e^{-k_a\tau}\frac{dL_a^{(2)}}{d\tau}-e^{+k_a\tau}\frac{dL_{-a}^{(2)}}{d\tau}\right),\\ Y_a&=F\left(e^{-k_a\tau}\frac{dL_a^{(2)}}{d\tau}+e^{+k_a\tau}\frac{dL_{-a}^{(2)}}{d\tau}\right).\end{aligned}\right\} \qquad (66)$$

The linear systems represented by equations (64) and (65) can be brought to forms more convenient for their solutions by the following procedure.

Considering, for example, equation (64), we find that the system of equations which this represents is

$$\left.\begin{aligned}\frac{3}{2}\sum_{a=1}^{n-1}\frac{1}{3k_a}\,X_a&=\bar{\delta}_3-\tfrac{1}{3}\,\bar{\delta}_1\,,\\ \frac{3}{2}\sum_{a=1}^{n-1}\left(\frac{1}{3k_a^3}+\frac{1}{5k_a}\right)X_a&=\bar{\delta}_5-\tfrac{1}{5}\,\bar{\delta}_1\,,\\ \frac{3}{2}\sum_{a=1}^{n-1}\left(\frac{1}{3k_a^5}+\frac{1}{5k_a^3}+\frac{1}{7k_a}\right)X_a&=\bar{\delta}_7-\tfrac{1}{7}\,\bar{\delta}_1\,,\\ \ldots\ldots\ldots\ldots&\ldots\ldots,\\ \frac{3}{2}\sum_{a=1}^{n-1}\left(\frac{1}{3k_a^{2n-3}}+\frac{1}{5k_a^{2n-5}}+\ldots+\frac{1}{2n-1}\,\frac{1}{k_a}\right)X_a&=\bar{\delta}_{2n-1}-\frac{1}{2n-1}\,\bar{\delta}_1\,.\end{aligned}\right\} \qquad (67)$$

The form of these equations suggests that we construct the following simpler system of equations:

$$
\left.
\begin{aligned}
&\frac{1}{2}\sum_{a=1}^{n-1}\frac{1}{k_a} X_a = \bar{\delta}_3 - \tfrac{1}{3}\bar{\delta}_1 = U_1 ,\\
&\frac{1}{2}\sum_{a=1}^{n-1}\frac{1}{k_a^3} X_a = \bar{\delta}_5 - \tfrac{1}{5}\bar{\delta}_1 - \tfrac{3}{5}U_1 = U_2 ,\\
&\frac{1}{2}\sum_{a=1}^{n-1}\frac{1}{k_a^5} X_a = \bar{\delta}_7 - \tfrac{1}{7}\bar{\delta}_1 - \tfrac{3}{5}U_2 - \tfrac{3}{7}U_1 = U_3 ,\\
&\quad \cdots\cdots\cdots\cdots\\
&\frac{1}{2}\sum_{a=1}^{n-1}\frac{1}{k_a^{2j-3}} X_a = \bar{\delta}_{2j-1} - \frac{1}{2j-1}\bar{\delta}_1 - \tfrac{3}{5}U_{j-2} - \tfrac{3}{7}U_{j-3} - \cdots - \frac{3}{2j-1}U_1 \\
&\qquad = U_{j-1}\\
&\quad \cdots\cdots\cdots\cdots ,\\
&\frac{1}{2}\sum_{a=1}^{n-1}\frac{1}{k_a^{2n-3}} X_a = \bar{\delta}_{2n-1} - \frac{1}{2n-1}\bar{\delta}_1 - \tfrac{3}{5}U_{n-2} - \tfrac{3}{7}U_{n-3} - \cdots - \frac{3}{2n-1}U_1 \\
&\qquad = U_{n-1} .
\end{aligned}
\right\} \qquad (68)
$$

In other words, we can reduce the systems of equations (67) to the simpler one

$$\sum_{a=1}^{n-1}\frac{1}{k_a^{2j-1}} X_a = 2U_j \qquad (j = 1, \ldots, n-1) , \qquad (69)$$

where the U_j's are defined as in equation (68).

Similarly, starting from equation (65), we can construct the simpler system

$$\sum_{a=1}^{n-1}\frac{1}{k_a^{2j}} Y_a = -2V_j \qquad (j = 1, \ldots, n-1) , \qquad (70)$$

where the quantities V_j $(j = 1, \ldots, n-1)$ are defined by the recurrence relation

$$V_{j-1} = \bar{\delta}_{2j} - \tfrac{3}{5}V_{j-2} - \tfrac{3}{7}V_{j-3} - \cdots - \frac{3}{2j-1}V_1 \quad (j = 3, \ldots, n) \qquad (71)$$

and

$$V_1 = \bar{\delta}_4 . \qquad (72)$$

We shall now show how it is possible to write down the solution of the equations (69) and (70) quite generally.

Considering first equation (69), we find that the system of equations which this represents can be written down as a single vector equation

$$\boldsymbol{KX} = 2\boldsymbol{U} , \qquad (73)$$

where $\boldsymbol{X}$ and $\boldsymbol{U}$ stand for the vectors

$$\boldsymbol{X} = (X_1, X_2, \ldots, X_{n-1}) \quad \text{and} \quad \boldsymbol{U} = (U_1, \ldots, U_{n-1}) \qquad (74)$$

and $\boldsymbol{K}$ for the matrix:

$$\boldsymbol{K} = \begin{pmatrix} \frac{1}{k_1} & \frac{1}{k_2} & \cdots & \frac{1}{k_{n-1}} \\ \frac{1}{k_1^3} & \frac{1}{k_2^3} & \cdots & \frac{1}{k_{n-1}^3} \\ \cdot & \cdot & \cdots & \cdot \\ \frac{1}{k_1^{2n-3}} & \frac{1}{k_2^{2n-3}} & \cdots & \frac{1}{k_{n-1}^{2n-3}} \end{pmatrix}. \tag{75}$$

Equation (73) expresses a relation between $\boldsymbol{U}$ and a linear transform of $\boldsymbol{X}$. This relation can be inverted into a relation between $\boldsymbol{X}$ and the linear transform of $\boldsymbol{U}$ obtained with the inverse of the matrix $\boldsymbol{K}$.[7] Thus

$$\boldsymbol{X} = 2\boldsymbol{K}^{-1}\boldsymbol{U}\,, \tag{76}$$

where $\boldsymbol{K}^{-1}$ denotes the inverse of $\boldsymbol{K}$. For the particular matrix $\boldsymbol{K}$ the inverse can be explicitly written down. But before we do this, it is first necessary to introduce certain definitions.

Consider the expansion of the product

$$\prod_{j\neq r}^{1,\,n-1} (x^2-k_j^2) = (x^2-k_1^2)\,(x^2-k_2^2)\ldots.(x^2-k_{r-1}^2)\,(x^2-k_{r+1}^2)\ldots.(x^2-k_{n-1}^2) \tag{77}$$

in descending powers of x^2. We have

$$\left.\begin{aligned} \prod_{j\neq r}^{1,\,n-1} (x^2-k_j^2) &= x^{2n-4} - x^{2n-6}\left(\sum_{\mu_1\neq r}^{1,\,n-1} k_{\mu_1}^2\right) + x^{2n-8}\left(\sum_{\mu_1\neq\mu_2\neq r}^{1,\,n-1} k_{\mu_1}^2 k_{\mu_2}^2\right) \\ &\quad - x^{2n-10}\left(\sum_{\mu_1\neq\mu_2\neq\mu_3\neq r}^{1,\,n-1} k_{\mu_1}^2 k_{\mu_2}^2 k_{\mu_3}^2\right) + \ldots. + (-1)^{n-2}\prod_{\mu\neq r}^{1,\,n-1} k_\mu^2\,; \end{aligned}\right\} \tag{78}$$

or, introducing the $(n-1)$ independent symmetric functions in the $(n-2)$ variables k_μ^2, $(\mu = 1, \ldots, r-1, r+1, \ldots n-1)$,

$$\left.\begin{aligned} S_{0,\,r} &= 1\,, \\ S_{1,\,r} &= -\sum_{\mu_1\neq r}^{1,\,n-1} k_{\mu_1}^2\,, \\ S_{2,\,r} &= +\sum_{\mu_1\neq\mu_2\neq r}^{1,\,n-1} k_{\mu_1}^2 k_{\mu_2}^2\,, \\ &\cdots\cdots\cdots\cdots \\ S_{j,\,r} &= (-1)^j \sum_{\mu_1\neq\mu_2\neq\ldots.\neq\mu_j\neq r}^{1,\,n-1} k_{\mu_1}^2 k_{\mu_2}^2 \ldots. k_{\mu_j}^2\,, \\ &\cdots\cdots\cdots\cdots\cdots\cdots\cdots\cdots\cdots\,, \\ S_{n-2,\,r} &= (-1)^{n-2} k_1^2 k_2^2 \ldots. k_{r-1}^2 k_{r+1}^2 \ldots. k_{n-1}^2\,, \end{aligned}\right\} \tag{79}$$

[7] The existence of the inverse can be inferred from the linear independence of the equations (67), or more directly from the nonvanishing of the determinant of $\boldsymbol{K}$. The determinant of $\boldsymbol{K}$ can be written

we can re-write the expansion on the right-hand side of equation (78) in the form

$$\prod_{j\neq r}^{1\ldots n-1}(x^2-k_j^2)=\sum_{\lambda=0}^{n-2}x^{2n-2\lambda-4}S_{\lambda,\,r}\,. \tag{80}$$

In terms of the functions $S_{\lambda,r}$, ($\lambda=0,1,\ldots,n-2$, and $r=1,\ldots,n-1$), defined in this manner, the inverse of the matrix $\boldsymbol{K}$ can be written down. We have

$$\boldsymbol{K}^{-1}=\begin{pmatrix}
\dfrac{k_1^{2n-3}S_{0,\,1}}{\prod_{j\neq1}(k_1^2-k_j^2)} & \dfrac{k_1^{2n-3}S_{1,\,1}}{\prod_{j\neq1}(k_1^2-k_j^2)} & \cdots & \dfrac{k_1^{2n-3}S_{\lambda,\,1}}{\prod_{j\neq1}(k_1^2-k_j^2)} & \cdots & \dfrac{k_1^{2n-3}S_{n-2,\,1}}{\prod_{j\neq1}(k_1^2-k_j^2)} \\
\dfrac{k_2^{2n-3}S_{0,\,2}}{\prod_{j\neq2}(k_2^2-k_j^2)} & \dfrac{k_2^{2n-3}S_{1,\,2}}{\prod_{j\neq2}(k_2^2-k_j^2)} & \cdots & \dfrac{k_2^{2n-3}S_{\lambda,\,2}}{\prod_{j\neq2}(k_2^2-k_j^2)} & \cdots & \dfrac{k_2^{2n-3}S_{n-2,\,2}}{\prod_{j\neq2}(k_2^2-k_j^2)} \\
\cdots & \cdots & \cdots & \cdots & \cdots & \cdots \\
\dfrac{k_a^{2n-3}S_{0,\,a}}{\prod_{j\neq a}(k_a^2-k_j^2)} & \dfrac{k_a^{2n-3}S_{1,\,a}}{\prod_{j\neq a}(k_a^2-k_j^2)} & \cdots & \dfrac{k_a^{2n-3}S_{\lambda,\,a}}{\prod_{j\neq a}(k_a^2-k_j^2)} & \cdots & \dfrac{k_a^{2n-3}S_{n-2,\,a}}{\prod_{j\neq a}(k_a^2-k_j^2)} \\
\cdots & \cdots & \cdots & \cdots & \cdots & \cdots \\
\dfrac{k_{n-1}^{2n-3}S_{0,\,n-1}}{\prod_{j\neq n-1}(k_{n-1}^2-k_j^2)} & \dfrac{k_{n-1}^{2n-3}S_{1,\,n-1}}{\prod_{j\neq n-1}(k_{n-1}^2-k_j^2)} & \cdots & \dfrac{k_{n-1}^{2n-3}S_{\lambda,\,n-1}}{\prod_{j\neq n-1}(k_{n-1}^2-k_j^2)} & \cdots & \dfrac{k_{n-1}^{2n-3}S_{n-2,\,n-1}}{\prod_{j\neq n-1}(k_{n-1}^2-k_j^2)}
\end{pmatrix}. \tag{81}$$

That the foregoing matrix does, in fact, define the inverse of the matrix $\boldsymbol{K}$ can be verified directly. Thus,

$$\left.\begin{aligned}(\boldsymbol{K}^{-1}\boldsymbol{K})_{l,\,m}&=\sum_{\lambda=0}^{n-2}\frac{k_l^{2n-3}S_{\lambda,\,l}}{\prod_{j\neq l}(k_l^2-k_j^2)}\frac{1}{k_m^{2\lambda+1}}\\&=\left(\frac{k_l}{k_m}\right)^{2n-3}\frac{1}{\prod_{j\neq l}(k_l^2-k_j^2)}\sum_{\lambda=0}^{n-2}k_m^{2n-2\lambda-4}S_{\lambda,\,l}\,,\end{aligned}\right\} \tag{82}$$

or, according to equation (80),

$$(\boldsymbol{K}^{-1}\boldsymbol{K})_{l,\,m}=\left(\frac{k_l}{k_m}\right)^{2n-3}\frac{1}{\prod_{j\neq l}(k_l^2-k_j^2)}\prod_{j\neq l}(k_m^2-k_j^2)\,. \tag{83}$$

---

down as it is related to the well-known Vandermonde determinant (cf. O. Perron, *Algebra*, Vol. 1, § 22, pp. 92–94, Leipzig: Gruyter, 1932). We have

$$|K|=\frac{1}{k_1k_2\ldots k_{n-1}}\prod_{i>j}^{1,\,n-1}\left(\frac{1}{k_i^2}-\frac{1}{k_j^2}\right). \tag{75'}$$

If $l \neq m$, the product which occurs in the numerator of the right-hand side of equation (83) includes the term $j = m$ and consequently vanishes. On the other hand, if $l = m$, the right-hand side of equation (83) clearly reduces to 1. Hence,

$$(\boldsymbol{K}^{-1}\boldsymbol{K})_{l,\,m} = 1 \text{ if } l = m \text{ and zero otherwise}, \tag{84}$$

proving the inverse relationship between the matrices (75) and (81).

Hence, with $\boldsymbol{K}^{-1}$ as defined in equation (81), equation (76) determines $\boldsymbol{X}$. In terms of the components X_a of $\boldsymbol{X}$ this equation becomes

$$\left.\begin{aligned} X_a = F\left(e^{-k_a\tau}\frac{dL_a^{(2)}}{d\tau} - e^{+k_a\tau}\frac{dL_{-a}^{(2)}}{d\tau}\right) = +\frac{2k_a^{2n-3}}{\prod_{j\neq a}(k_a^2 - k_j^2)}\sum_{\lambda=0}^{n-2} S_{\lambda,\,a}U_{\lambda+1}(\tau) \\ (a = 1, \ldots, n-1). \end{aligned}\right\} \tag{85}$$

Similarly, the solution of equation (70) is found to be

$$\left.\begin{aligned} Y_a = F\left(e^{-k_a\tau}\frac{dL_a^{(2)}}{d\tau} + e^{+k_a\tau}\frac{dL_{-a}^{(2)}}{d\tau}\right) = -\frac{2k_a^{2n-2}}{\prod_{j\neq a}(k_a^2 - k_j^2)}\sum_{\lambda=0}^{n-2} S_{\lambda,\,a}V_{\lambda+1}(\tau) \\ (a = 1, \ldots, n-1). \end{aligned}\right\} \tag{86}$$

From equations (85) and (86) we obtain

$$F\frac{dL_a^{(2)}}{d\tau} = +\frac{k_a^{2n-3}}{\prod_{j\neq a}(k_a^2 - k_j^2)}\sum_{\lambda=0}^{n-2} S_{\lambda,\,a}\left[U_{\lambda+1}(\tau) - k_aV_{\lambda+1}(\tau)\right]e^{+k_a\tau} \tag{87}$$

and

$$F\frac{dL_{-a}^{(2)}}{d\tau} = -\frac{k_a^{2n-3}}{\prod_{j\neq a}(k_a^2 - k_j^2)}\sum_{\lambda=0}^{n-2} S_{\lambda,\,a}\left[U_{\lambda+1}(\tau) + k_aV_{\lambda+1}(\tau)\right]e^{-k_a\tau}. \tag{88}$$

In their integrated forms the foregoing equations are

$$\left.\begin{aligned} FL_a^{(2)}(\tau) = \frac{k_a^{2n-3}}{\prod_{j\neq a}(k_a^2 - k_j^2)}\sum_{\lambda=0}^{n-2} S_{\lambda,\,a}\int_0^\tau e^{+k_a\tau}\left[U_{\lambda+1}(\tau) - k_aV_{\lambda+1}(\tau)\right]d\tau \\ + F(L_a^{(1)} + \Delta L_a) \quad (a = 1, \ldots, n-1) \end{aligned}\right\} \tag{89}$$

and

$$\left.\begin{aligned} FL_{-a}^{(2)}(\tau) = \frac{k_a^{2n-3}}{\prod_{j\neq a}(k_a^2 - k_j^2)}\sum_{\lambda=0}^{n-2} S_{\lambda,\,a}\int_\tau^\infty e^{-k_a\tau}\left[U_{\lambda+1}(\tau) + k_aV_{\lambda+1}(\tau)\right]d\tau \\ (a = 1, \ldots, n-1), \end{aligned}\right\} \tag{90}$$

where in equation (89) ΔL_a, $(a = 1, \ldots, n-1)$, are $(n-1)$ constants of integration. However, it will be noticed that in integrating equation (88) in the form (90) we have made a particular choice of the constants of integrations so as to be compatible with the requirement that none of the quantities tend to infinity exponentially as $\tau \to \infty$ (cf. eq. [34]).

Finally, the constants of integration ΔL_a, $(a = 1, \ldots, n-1)$, and ΔQ (cf. eq. [40]) which occur in the solution of the variational equations are to be determined from the boundary conditions

$$I_{-i} = 0 \text{ at } \tau = 0 \text{ for } i = 1, \ldots, n . \tag{91}$$

Explicitly, these conditions reduce to (cf. II, eq. [21])

$$\sum_{a=1}^{n-1} \frac{L_a^{(1)} + \Delta L_a}{1 - \mu_i k_a} + Q^{(1)} + \Delta Q = \mu_i - \sum_{a=1}^{n-1} \frac{L_{-a}^{(2)}(0)}{1 + \mu_i k_a} \quad (i = 1, \ldots, n) ; \tag{92}$$

or, since the $L_a^{(1)}$'s and $Q^{(1)}$ satisfy the relation

$$\sum_{a=1}^{n-1} \frac{L_a^{(1)}}{1 - \mu_i k_a} + Q^{(1)} = \mu_i \qquad (i = 1, \ldots, n) , \tag{93}$$

the equations which determine ΔL_a and ΔQ are

$$\sum_{a=1}^{n-1} \frac{\Delta L_a}{1 - \mu_i k_a} + \Delta Q = - \sum_{a=1}^{n-1} \frac{L_{-a}^{(2)}(0)}{1 + \mu_i k_a} \quad (i = 1, \ldots, n) . \tag{94}$$[8]

This completes the formal solution to the problem in the $(2, n)$ approximation.

5. *The solution in the* $(2, 1)$ *approximation.*—The discussion of this case is of particular interest, as in this approximation

$$J^{(2)} = J^{(1)} , \tag{95}$$

and equation (19) becomes

$$B^{(2)} = J^{(1)} + \frac{1}{4} \int_0^\infty \delta_\nu \frac{dF_\nu^{(1)}}{d\tau} \, d\nu . \tag{96}$$

Substituting for $J^{(1)}$ its solution in the first approximation (II, eqs. [30] and [35]), we have

$$B^{(2)} = \tfrac{3}{4} F \left(\tau + \frac{1}{\sqrt{3}} + \frac{1}{3F} \int_0^\infty \delta_\nu \frac{dF_\nu^{(1)}}{d\tau} \, d\nu \right) . \tag{97}$$

It may be recalled that in the foregoing equations the optical depth τ is evaluated in terms of the mean absorption coefficient $\bar{\kappa}$ defined by (cf. eq. [42])

$$\bar{\kappa} = \int_0^\infty \kappa_\nu \left(\frac{F_\nu^{(1)}}{F} \right) d\nu . \tag{98}$$

From equations (97) and (98) it is apparent that, when δ_ν is independent of depth,

$$B^{(2)} = B^{(1)} = \tfrac{3}{4} F \left(\tau + \frac{1}{\sqrt{3}} \right) \quad (\delta_\nu \text{ independent of } \tau) . \tag{99}$$

[8] It is possible to write down explicitly the inverse of the linear transformation which appears on the left-hand side of this system (cf. *Ap. J.*, **101**, 320, 1945, eq. [8]). But, as the practical use to which these solutions can be put is limited, we shall not develop further these formalities here.

In other words, we have shown that *in a Milne-Eddington type of approximation the temperature distribution obtained on the gray-body assumption continues to be valid in a second approximation if the mean absorption coefficient* κ *(in terms of which* τ *has to be defined) is a straight average of* κ_ν*, weighted according to the net monochromatic flux of radiation of frequency* ν *in a gray atmosphere, and if, further,* $\kappa_\nu/\bar{\kappa}$ *is independent of depth.* This answers the question that we asked at the outset (§ 1), namely, as to the conditions under which an equation for the temperature distribution of the form (9) may be expected to hold even when the material departs from perfect grayness. We may draw particular attention to the fact that our answer has not provided any justification for averaging κ_ν according to the conventional method of Rosseland. Indeed, the Rosseland mean, as customarily defined by

$$\frac{1}{\bar{\kappa}}\int_0^\infty \frac{dB_\nu}{dT}\,d\nu = \int_0^\infty \frac{1}{\kappa_\nu}\frac{dB_\nu}{dT}\,d\nu\,, \tag{100}$$

weights κ_ν falsely and overemphasizes the violet region of the spectrum. On the other hand, our present discussion would rather suggest that in all preliminary considerations it would be preferable (and simpler) to average κ_ν directly, weighting with the Planck function corresponding to the effective temperature of the star. One further remark concerning the requirement of the constancy of $\kappa_\nu/\bar{\kappa}$ with depth may be made. With the negative ion of hydrogen firmly established as the principal source of absorption in stellar atmospheres of the solar and neighboring types, the requirement of the constancy of κ_ν/κ with depth is likely to be met fairly satisfactorily.

Returning to equations (97) and (98), we see that a practical use of these equations will require a knowledge of the monochromatic fluxes $F_\nu^{(1)}$ at various depths in a gray atmosphere.

Now, according to equation (26), we can write

$$F_\nu^{(1)}(\tau) = 2\int_\tau^\infty B_\nu(T_t^{(1)})\,E_2(t-\tau)\,dt - 2\int_0^\tau B_\nu(T_t^{(1)})\,E_2(\tau-t)\,dt\,, \tag{101}$$

where

$$T_t^{(1)} = T_e\left[\tfrac{3}{4}(t+q[t])\right]^{1/4}. \tag{102}$$

Writing

$$a = \frac{h\nu}{kT_e}\,, \tag{103}$$

we can express equation (101) in the form

$$\frac{F_a^{(1)}(\tau)}{F} = \frac{30}{\pi^4}\,\frac{a^3}{e^{1.23275a}-1}\,f_a(\tau)\,, \tag{104}$$

where

$$f_a(\tau) = (e^{1.23275a}-1)\left\{\int_\tau^\infty \frac{E_2(t-\tau)\,dt}{e^{a/[3/4(t+q)]^{1/4}}-1} - \int_0^\tau \frac{E_2(\tau-t)\,dt}{e^{a/[3/4(t+q)]^{1/4}}-1}\right\} \tag{105}$$

and

$$1.23275\ldots. = \left(\frac{4}{\sqrt{3}}\right)^{1/4}. \tag{106}$$

Using for $q(\tau)$ the solution on the fourth approximation given in II, equation (54), Miss Frances Herman and the writer have numerically evaluated the function $f_a(\tau)$ defined as in equation (105) for various values of a and τ. The results of the numerical integrations are summarized in Tables 1 and 2. In Table 1 we give the values of $f_a(\tau)$,

and in Table 2 these are converted according to equation (104) to give the monochromatic fluxes directly. And finally, in Table 3, we give values of $dF_a^{(1)}/d\tau$ obtained by direct numerical differentiation of the fluxes tabulated in Table 2.

TABLE 1

THE FUNCTION $f_a(\tau)$

τ	a								
	0	1	2	3	4	6	8	10	12
0	0.601	0.682	0.803	0.982	1.236	2.10	3.82	7.42	15.2
0.1	.529	.619	.757	.960	1.249	2.23	4.20	8.32	17.3
0.2	.472	.568	.717	.938	1.257	2.35	4.58	9.24	19.4
0.3	.424	.524	.680	.915	1.259	2.46	4.94	10.19	21.7
0.4	.384	.485	.647	.893	1.257	2.56	5.29	11.15	24.1
0.5	.348	.450	.615	.869	1.251	2.64	5.62	12.11	26.6
0.6	.318	.420	.586	.847	1.244	2.72	5.95	13.08	29.1
0.7	.292	.393	.561	.826	1.236	2.79	6.26	14.06	31.8
0.8	.267	.368	.535	.804	1.224	2.85	6.56	15.03	34.6
0.9	.247	.346	.513	.784	1.214	2.90	6.84	16.00	37.4
1.0	.229	.326	.493	.765	1.203	2.95	7.12	16.96	40.3
1.2	.198	.292	.455	.729	1.177	3.04	7.64	18.85	46.2
1.4	.173	.264	.423	.696	1.152	3.10	8.11	20.70	52.2
1.6	.153	.241	.396	.666	1.126	3.16	8.54	22.49	58.4
1.8	.137	.221	.372	.639	1.101	3.20	8.94	24.23	64.5
2.0	0.124	0.204	0.351	0.613	1.076	3.23	9.30	25.90	70.7

TABLE 2

THE MONOCHROMATIC FLUXES $F_a^{(1)}(\tau)$ IN UNITS OF F

τ	a							
	1	2	3	4	6	8	10	12
0	0.0864	0.1837	0.2074	0.1772	0.0856	0.0314	0.01013	0.00305
0.1	.0784	.1732	.2027	.1791	.0911	.0346	.01135	.00345
0.2	.0719	.1640	.1981	.1801	.0961	.0376	.01261	.00388
0.3	.0663	.1556	.1933	.1804	.1005	.0406	.01390	.00434
0.4	.0615	.1480	.1886	.1802	.1044	.0435	.01521	.00482
0.5	.0571	.1407	.1835	.1793	.1078	.0462	.01652	.00532
0.6	.0532	.1342	.1789	.1783	.1110	.0489	.01785	.00584
0.7	.0498	.1282	.1745	.1772	.1138	.0515	.01918	.00638
0.8	.0466	.1225	.1699	.1755	.1163	.0539	.02050	.00693
0.9	.0439	.1174	.1656	.1740	.1186	.0563	.02182	.00749
1.0	.0413	.1128	.1616	.1724	.1207	.0586	.02314	.00807
1.2	.0370	.1042	.1540	.1688	.1240	.0628	.02572	.00925
1.4	.0335	.0968	.1470	.1651	.1268	.0667	.02824	.01046
1.6	.0305	.0906	.1406	.1614	.1289	.0702	.03069	.01169
1.8	.0280	.0850	.1349	.1578	.1306	.0735	.03306	.01293
2.0	0.0259	0.0803	0.1295	0.1543	0.1319	0.0764	0.03534	0.01417

In Figure 1 we have illustrated the distribution in frequency of the net flux of radiation at various depths. It is of particular interest to observe how the redistribution in the frequencies takes place as we descend into the atmosphere.

With the data given in Tables 2 and 3 we should be able to use the solution (97) to determine the temperature distribution under a wide range of practical conditions. We shall return to such applications in later papers.

TABLE 3

THE DERIVATIVES OF THE MONOCHROMATIC FLUXES: $dF_\nu^{(1)}/d\tau$ IN UNITS OF F

τ	a							
	1	2	3	4	6	8	10	12
0.	−0.086	−0.11	−0.044	+0.024	+0.0585	+0.0323	+0.0120	+0.0039
0.1	.072	.098	.046	+ .015	.0523	.0311	.0124	.0044
0.2	.060	.088	.047	+ .007	.0467	.0302	.0128	.0048
0.3	.052	.080	.048	+ .001	.0417	.0293	.0130	.00465
0.4	.046	.074	.0485	− .005	.0367	.0281	.0131	.00490
0.5	.041	.068	.048	− .008	.0327	.0270	.0132	.00510
0.6	.036	.063	.046	− .010	.0295	.0260	.0133	.00530
0.7	.033	.058	.045	− .013	.0264	.0250	.0133	.00544
0.8	.030	.054	.043	− .015	.0240	.0242	.0132	.00558
0.9	.027	.050	.041	− .016	.0215	.0233	.0132	.00573
1.0	.024	.046	.040	− .017	.0193	.0222	.0131	.00583
1.2	.020	.040	.036	− .018	.0152	.0202	.0128	.00598
1.4	.016	.034	.033	− .0185	.0121	.0186	.0124	.00610
1.6	.014	.029	.030	− .0185	.0095	.0170	.0120	.00617
1.8	.011	.026	.028	− .018	.0075	.0156	.0116	.0062
2.0	−0.010	−0.022	−0.025	−0.017	+0.0060	+0.0142	+0.0112	+0.0062

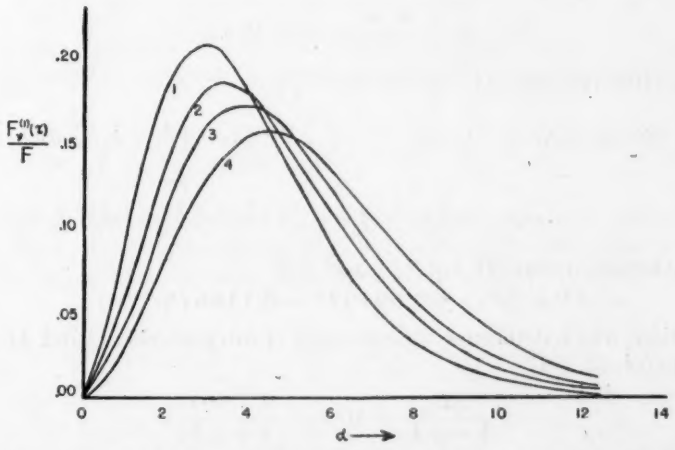

FIG. 1.—The frequency distribution of the net flux of radiation at various depths in a gray atmosphere. The abscissa measures the frequency (in units of kT_e/h), and the ordinate measures the flux (in units of the constant net integrated flux F). The curves *1*, *2*, *3*, and *4* refer to the depths $\tau=0$, 0.5, 1, and 2, respectively.

6. *The solutions for the temperature distribution in higher approximations.*—Turning next to solutions in higher approximations, we have (cf. eq. 34 and II, eqs. [28] and [29])

$$J^{(2)} = \tfrac{3}{4}F\left\{\tau + Q^{(2)} + \sum_{a=1}^{n-1} L_a^{(2)}(\tau)\, e^{-k_a\tau} + \sum_{a=1}^{n-1} L_{-a}^{(2)}(\tau)\, e^{+k_a\tau}\right\}; \qquad (107)$$

or, substituting for $Q^{(2)}$, $L_a^{(2)}$ and $L_{-a}^{(2)}$ according to equations (40), (89), and (90), we have

$$\left.\begin{aligned} J^{(2)} = J^{(1)} + \tfrac{3}{4}F\left(\Delta Q + \sum_{a=1}^{n-1}\Delta L_a e^{-k_a\tau}\right) \\ + \frac{3}{4}\sum_{a=1}^{n-1}\frac{k_a^{2n-3}}{\prod_{j\neq a}(k_a^2-k_j^2)}\sum_{\lambda=0}^{n-2}S_{\lambda,\,a}\Big\{e^{-k_a\tau}\int_0^\tau e^{+k_a\tau}\left[U_{\lambda+1}(\tau) - k_a V_{\lambda+1}(\tau)\right]d\tau \\ + e^{+k_a\tau}\int_\tau^\infty e^{-k_a\tau}\left[U_{\lambda+1}(\tau) + k_a V_{\lambda+1}(\tau)\right]d\tau\Big\}, \end{aligned}\right\} \quad (108)$$

where it may be recalled that the constants of integration ΔQ and ΔL_a, ($a = 1, \ldots, n-1$), are to be determined according to equation (94). Corresponding to the foregoing solution for $J^{(2)}$, there is the temperature distribution

$$\frac{\sigma}{\pi}(T^{(2)})^4 = B^{(2)} = J^{(2)} + \frac{1}{4}\int_0^\infty \delta_\nu(\tau)\frac{dF_\nu^{(1)}}{d\tau}\,d\nu. \quad (109)$$

Equations (108) and (109) show that, when the material departs from being gray, the corrections which have to be made to the temperature distribution are of two kinds: first, because B is not, in general, equal to J, and, second, because the energy density of the radiation does not have the gray-atmosphere value. It is only under very special conditions (which we have already discussed in § 5) that these corrections vanish in a second approximation.

The solution (108) simplifies considerably for the case $n = 2$. For, in this (2, 2) approximation there is only one characteristic root (II, eq. [40]):

$$k_1 = \frac{\sqrt{35}}{3} = 1.97203; \quad (110)$$

and equation (108) becomes (cf. eqs. [68] and [72])

$$\left.\begin{aligned} J^{(2)} = J^{(1)} + \tfrac{3}{4}F(\Delta Q + \Delta L_1 e^{-k_1\tau}) + \tfrac{3}{4}e^{-k_1\tau}\int_0^\tau e^{+k_1\tau}(\bar{\delta}_3 - \tfrac{1}{3}\bar{\delta}_1 - k_1\bar{\delta}_4)\,d(k_1\tau) \\ + \tfrac{3}{4}e^{+k_1\tau}\int_\tau^\infty e^{-k_1\tau}(\bar{\delta}_3 - \tfrac{1}{3}\bar{\delta}_1 + k_1\bar{\delta}_4)\,d(k_1\tau), \end{aligned}\right\} \quad (111)$$

where it may be noted that (II, eqs. [30] and [42])

$$J^{(1)} = \tfrac{3}{4}F(\tau + 0.694025 - 0.116675e^{-k_1\tau}). \quad (112)$$

The equations which determine the constants of integrations ΔQ and ΔL_1 in the solution (111) are (cf. eq. [94])

$$\frac{\Delta L_1}{1-\mu_1 k_1} + \Delta Q = -\frac{L_{-1}^{(2)}(0)}{1+\mu_1 k_1} \quad (113)$$

and

$$\frac{\Delta L_1}{1-\mu_2 k_1} + \Delta Q = -\frac{L_{-1}^{(2)}(0)}{1+\mu_2 \kappa_1}. \quad (114)$$

From these equations we find that

$$\Delta L_1 = \frac{(1-\mu_1 k_1)(1-\mu_2 k_1)}{(1+\mu_1 k_1)(1+\mu_2 k_1)}L_{-1}^{(2)}(0) \quad (115)$$

and

$$\Delta Q = -\frac{2}{(1+\mu_1 k_1)(1+\mu_2 k_1)}L_{-1}^{(2)}(0). \quad (116)$$

Substituting these values for ΔL_1 and ΔQ in equation (111), we obtain

$$\left.\begin{aligned} J^{(2)} &= J^{(1)} \\ &+ \frac{3\,[\,(1-\mu_1 k_1)\,(1-\mu_2 k_1)\,e^{-k_1\tau}-2\,]}{4\,(1+\mu_1 k_1)\,(1+\mu_2 k_1)} \int_0^\infty e^{-k_1\tau}\,(\bar{\delta}_3 - \tfrac{1}{3}\bar{\delta}_1 + k_1\bar{\delta}_4)\,d\,(k_1\tau) \\ &+ \tfrac{3}{4}\,e^{-k_1\tau}\int_0^\tau e^{+k_1\tau}\,(\bar{\delta}_3 - \tfrac{1}{3}\bar{\delta}_1 - k_1\bar{\delta}_4)\,d\,(k_1\tau) \\ &+ \tfrac{3}{4}\,e^{+k_1\tau}\int_\tau^\infty e^{-k_1\tau}\,(\bar{\delta}_3 - \tfrac{1}{3}\bar{\delta}_1 + k_1\bar{\delta}_4)\,d\,(k_1\tau)\,. \end{aligned}\right\} \quad (117)$$

From equation (117) we find that for $\tau = 0$ (cf. II, eq. [71]),

$$\left.\begin{aligned} J^{(2)}(0) &= \frac{\sqrt{3}}{4}F + \frac{\sqrt{3}}{2}\,\frac{k_1}{(1+\mu_1 k_1)\,(1+\mu_2 k_1)} \\ &\qquad \times \int_0^\infty e^{-k_1\tau}\,(\bar{\delta}_3 - \tfrac{1}{3}\bar{\delta}_1 + k_1\bar{\delta}_4)\,d\,(k_1\tau)\,. \end{aligned}\right\} \quad (118)$$

The boundary temperature in the second approximation is therefore given by

$$\left.\begin{aligned} \frac{\sigma}{\pi}\,(T_0^{(2)})^4 &= \frac{\sigma}{\pi}\,(T_0^{(1)})^4 + \frac{1}{4}\int_0^\infty \left(\delta_\nu \frac{dF_\nu^{(1)}}{d\tau}\right)_{\tau=0} d\nu \\ &+ \frac{\sqrt{3}}{2}\,\frac{k_1}{(1+\mu_1 k_1)\,(1+\mu_2 k_1)}\int_0^\infty e^{-k_1\tau}\,(\bar{\delta}_3 - \tfrac{1}{3}\bar{\delta}_1 + k_1\bar{\delta}_4)\,d\,(k_1\tau)\,. \end{aligned}\right\} \quad (119)$$

It is seen that a practical use of the foregoing solutions in the (2, 2) approximation will require, in addition to the monochromatic fluxes $F_\nu^{(1)}$, a knowledge also of the quantities

$$M_\nu^{(1)}(\tau) = \frac{1}{2}\int_{-1}^{+1} \frac{dI_\nu^{(1)}}{d\tau}\,\mu^3 d\mu \qquad \text{and} \qquad N_\nu^{(1)}(\tau) = \frac{1}{2}\int_{-1}^{+1} \frac{dI_\nu^{(1)}}{d\tau}\,\mu^4 d\mu\,, \quad (120)$$

as these will be needed in the evaluation of $\bar{\delta}_3$ and $\bar{\delta}_4$. However, since the first approximation refers only to a gray atmosphere, $M_\nu^{(1)}$ and $N_\nu^{(1)}$ can be expressed in terms of $F_\nu^{(1)}$. For, from the equation of transfer appropriate to this case (eq. [12]), we can readily show that

$$\frac{dK_\nu^{(1)}}{d\tau} = \tfrac{1}{4}F_\nu^{(1)}; \qquad \frac{dM_\nu^{(1)}}{d\tau} = K_\nu^{(1)}(\tau) - \tfrac{1}{3}B_\nu^{(1)}(\tau)\,, \quad (121)$$

and

$$\frac{dN_\nu^{(1)}}{d\tau} = M_\nu^{(1)}(\tau)\,; \quad (122)$$

and, accordingly, $M_\nu^{(1)}(\tau)$ and $N_\nu^{(1)}(\tau)$ can be obtained successively by quadratures involving at each stage only known functions. Numerical work relating to these quantities with applications to practical problems will be given in later papers.

In conclusion, I wish to record my indebtedness to Miss Frances Herman for assistance with the very laborious numerical work which was involved in the preparation of Tables 1, 2, and 3.

ON THE RADIATIVE EQUILIBRIUM OF A STELLAR ATMOSPHERE. VIII

S. CHANDRASEKHAR
Yerkes Observatory
Received February 14, 1945

ABSTRACT

In this paper the methods which have been developed in the earlier papers of this series have been applied to the solution of the equation of transfer

$$\mu \frac{dI}{d\tau} = I(\tau, \mu) - B(\tau) ; \quad B = \frac{1}{2}\int_{-1}^{+1} I d\mu + \tfrac{1}{4}Fe^{-\tau \sec \beta},$$

representing the radiative equilibrium of an atmosphere exposed to a parallel beam of radiation of flux πF per unit area normal to itself and incident at an angle β normal to the boundary of the atmosphere.

General solutions in the *nth* approximation have been found; and it is shown that, on the method of solution adopted, it is true in every approximation that

$$\frac{B(0)}{B(\infty)} = \frac{\sec \beta}{\sqrt{3}}.$$

It is further shown that the angular distribution of the "reflected" radiation for the problem on hand is related, in a simple way, with the law of darkening in an atmosphere characterized by a constant net flux and with no incident radiation. Thus, elementary and simple proofs have been obtained for the results first established by E. Hopf, using a special theory involving integral equations.

1. *Introduction.*—A problem in the theory of radiative transfer which has considerable practical interest is the one relating to the reflection effect in eclipsing binaries. This problem was first considered by A. S. Eddington[1] and later in greater detail by E. A. Milne.[2] As was shown particularly by Milne, the problem basic to the consideration of this effect is that of the radiative equilibrium of a semi-infinite atmosphere exposed to a parallel beam of radiation of flux πF per unit area normal to itself and incident at an angle β normal to the boundary of the atmosphere (see Fig. 1). In other words, we require to solve the equation of transfer (cf. Milne, *op. cit.*)

$$\mu \frac{dI}{d\tau} = I - \frac{1}{2}\int_{-1}^{+1} I d\mu - \tfrac{1}{4}Fe^{-\tau \sec \beta}, \tag{1}$$

where I denotes the specific intensity of the integrated radiation derived from the material. The solution of the equation of transfer (1) was obtained by Milne in an approximation equivalent to that of Schwarzschild's and applied to the reflection problem. Later, certain exact results relating to the solution of equation (1) were proved by E. Hopf.[3] But apparently there has been no attempt to obtain solutions explicitly in approximations higher than those of Milne's. In this paper we propose to apply to the solution of equation (1) the methods which have been developed in the earlier papers of this series.[4] And, as we shall see, the application of these methods to the solution of equation (1) leads also to simple and elementary proofs of the exact results of Hopf.

[1] *M.N.*, **86**, 320, 1926.

[2] *M.N.*, **87**, 43, 1926; also *Handb. d. Ap.*, **3**, No. 1, 134–141, 1930.

[3] *Mathematical Problems of Radiative Equilibrium* (Cambridge Mathematical Tract No. 31), pp. 55–59, Cambridge, England, 1934.

[4] See particularly *Ap. J.*, **100**, 76, 1944. This paper will be referred to as "II." Familiarity with the methods and results of this paper will be assumed in the present investigation.

2. *The solution of equation (1) in the nth approximation.*—As in paper II, we replace the integral on the right-hand side of equation (1) by a sum according to Gauss's formula for numerical quadratures and obtain an equivalent system of linear equations which in the nth approximation is

$$\mu_i \frac{dI_i}{d\tau} = I_i - \tfrac{1}{2}\Sigma a_j I_j - \tfrac{1}{4}Fe^{-\tau \sec\beta} \quad (i = \pm 1, \ldots, \pm n). \quad (2)$$

where the various symbols have the same meaning as in II.

It is seen that the homogeneous system associated with equation (2) is the same as that considered in II, §§ 2-6. Accordingly, the complementary function for the solution of equation (2) is the same as the general solution (II, eq. [18]) of the homogeneous sys-

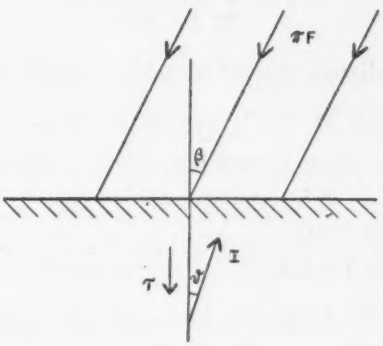

FIG. 1

tem. To complete the solution we need only find a particular integral. This can be found in the following manner.

Setting

$$I_i = \tfrac{1}{4}Fh_i e^{-\tau \sec\beta} \qquad (i = \pm 1, \ldots, \pm n). \quad (3)$$

in equation (2) (the h_i's are certain constants unspecified for the present) we verify that we must have

$$h_i(1 + \mu_i \sec\beta) = \tfrac{1}{2}\Sigma a_j h_j + 1 \quad (i = \pm 1, \ldots, \pm n). \quad (4)$$

Equation (4) implies that the constants h_i must be expressible in the form

$$h_i = \frac{\gamma}{1 + \mu_i \sec\beta} \qquad (i = \pm 1, \ldots, \pm n). \quad (5)$$

where the constant γ has to be determined by the condition (cf. eq. [4])

$$\gamma = \tfrac{1}{2}\gamma\Sigma \frac{a_i}{1 + \mu_i \sec\beta} + 1. \quad (6)$$

In other words,

$$I_i = \tfrac{1}{4}F \frac{\gamma}{1 + \mu_i \sec\beta} e^{-\tau \sec\beta} \quad (i = \pm 1, \ldots, \pm n) \quad (7)$$

with

$$\gamma = \frac{1}{1 - \sum_{j=1}^{n} \frac{a_j}{1 - \mu_j^2 \sec^2\beta}} \quad (8)$$

represents a particular integral of the equation (2). Adding to this particular integral the general solution of the homogeneous system which is compatible with the boundedness of the solution for $\tau \to \infty$, we have

$$I_i = \tfrac{1}{4}F\left\{\sum_{a=1}^{n-1}\frac{M_a e^{-k_a\tau}}{1+\mu_i k_a} + X + \frac{\gamma e^{-\tau\sec\beta}}{1+\mu_i\sec\beta}\right\} \quad (i = \pm 1, \ldots, \pm n), \tag{9}$$

where M_a, $(a = 1, \ldots, n-1)$, and X are n constants of integration, to be determined by the boundary conditions at $\tau = 0$, and the k_a's $(a = 1, \ldots, n-1)$ are the $(n-1)$ distinct nonvanishing positive roots characteristic of the equation (cf. II, eq. [11])

$$1 = \sum_{j=1}^{n}\frac{a_j}{1-\mu_j^2 k^2}. \tag{10}$$

At $\tau = 0$ we have no radiation derived from the material. Accordingly, we should require that

$$I_{-i} = 0 \text{ at } \tau = 0 \text{ and for } i = 1, \ldots, n. \tag{11}$$

From equation (9) we now conclude that the equations which determine the M_a's and X are

$$\sum_{a=1}^{n-1}\frac{M_a}{1-\mu_i k_a} + X + \frac{\gamma}{1-\mu_i\sec\beta} = 0 \quad (i = 1, \ldots, n). \tag{12}$$

In terms of the solution (9) for the I_i's we can obtain a convenient formula for J, defined by

$$J = \frac{1}{2}\int_{-1}^{+1} I\,d\mu = \tfrac{1}{2}\Sigma a_j I_j \tag{13}$$

in our present scheme of approximation. We have

$$J = \tfrac{1}{8}F\left\{\sum_{a=1}^{n-1}M_a e^{-k_a\tau}\sum_i\frac{a_i}{1+\mu_i k_a} + X\sum_i a_i + \gamma e^{-\tau\sec\beta}\sum_i\frac{a_i}{1+\mu_i\sec\beta}\right\}. \tag{14}$$

Using equations (6) and (10), we can reduce the foregoing equation to the form

$$J = \frac{1}{4}F\left\{\sum_{a=1}^{n-1}M_a e^{-k_a\tau} + X + (\gamma-1)\,e^{-\tau\sec\beta}\right\}. \tag{15}$$

The temperature distribution in the atmosphere is given by (cf. eq. [1])

$$\frac{\sigma}{\pi}T^4 = B(\tau) = J + \tfrac{1}{4}Fe^{-\tau\sec\beta}. \tag{16}$$

Substituting for J from equation (15), we obtain

$$B(\tau) = \tfrac{1}{4}F\left(\sum_{a=1}^{n-1}M_a e^{-k_a\tau} + X + \gamma e^{-\tau\sec\beta}\right). \tag{17}$$

As $\tau \to 0$, respectively ∞, we have

$$B(0) = \tfrac{1}{4}F\left(\sum_{a=1}^{n-1}M_a + X + \gamma\right) \tag{18}$$

and

$$B(\infty) = \tfrac{1}{4}FX. \tag{19}$$

The law of darkening in the atmosphere corresponding to the temperature distribution (16) is readily found. We have

$$I(0,\mu) = \tfrac{1}{4}F\left\{\sum_{\alpha=1}^{n-1}\frac{M_\alpha}{1+k_\alpha\mu}+X+\frac{\gamma}{1+\mu\sec\beta}\right\}. \tag{20}$$

This completes the formal solution. In the following section we shall show how the explicit forms of the solutions in the various approximations can be written down directly in terms of the respective solutions of the associated homogeneous equation

$$\mu\frac{dI}{d\tau} = I - \frac{1}{2}\int_{-1}^{+1} I\,d\mu\,, \tag{21}$$

given in paper II.

3. *The relation of the solution of equation (1) with that of the associated homogeneous equation (21).*—In the preceding section we have obtained the solutions for the temperature distribution and for the law of darkening for an atmosphere exposed to an incident parallel beam of radiation. The explicit numerical forms which these solutions will take in any particular approximation will depend on the solution of the linear equations for the constants of integration M_α, ($\alpha = 1, \ldots, n-1$), and X (cf. eq. [12]). However, we shall now show how a straightforward solution of these equations can be avoided by expressing the constants M_α and X in terms of the solutions of the homogeneous equation (21) in the respective approximations. The analysis which follows is closely related to that of II, § 6.

Consider the function $G(\mu)$ defined by

$$G(\mu) = \sum_{\alpha=1}^{n-1}\frac{M_\alpha}{1-k_\alpha\mu}+X+\frac{\gamma}{1-\mu\sec\beta}. \tag{22}$$

According to the boundary conditions (12),

$$G(\mu_i) = 0 \qquad (i = 1, \ldots, n). \tag{23}$$

This fact enables us to determine $G(\mu)$ explicitly. For, by multiplying equation (22) by the function (cf. II, eq. [58])

$$(1-\mu\sec\beta)R(\mu) = (1-\mu\sec\beta)\prod_{\alpha=1}^{n-1}(1-k_\alpha\mu), \tag{24}$$

we obtain a polynomial of degree n in μ which vanishes for $\mu = \mu_i$, $i = 1, \ldots, n$. The function $G(\mu)\,R(\mu)\,(1-\mu\sec\beta)$ cannot, therefore, differ from the polynomial (cf. II, eq. [59])

$$P(\mu) = \prod_{j=1}^{n}(\mu-\mu_j) \tag{25}$$

by more than a constant factor, which can be determined by comparing the coefficients of the highest powers of μ in the two expressions. In the former the coefficient of μ^n is unity, while in the latter it is

$$(-1)^n k_1 k_2 \ldots k_{n-1} X \sec\beta\,. \tag{26}$$

Hence,

$$G(\mu) = (-1)^n k_1 k_2 \ldots k_{n-1} X\,\frac{\sec\beta}{1-\mu\sec\beta}\,\frac{P(\mu)}{R(\mu)}. \tag{27}$$

Comparing this with the function $S(\mu)$ introduced in II, equations (56) and (61), we see that

$$G(\mu) = X \frac{\sec \beta}{1 - \mu \sec \beta} S(\mu) . \tag{28}$$

Several consequences follow from equations (27) and (28).

First, we observe that, according to equation (28),

$$G(0) = X S(0) \sec \beta. \tag{29}$$

But it has been shown in II that (cf. II, eqs. [62] and [70])

$$S(0) = \frac{1}{\sqrt{3}}. \tag{30}$$

Hence (cf. eq. [22])

$$G(0) = \sum_{a=1}^{n-1} M_a + X + \gamma = X \frac{\sec \beta}{\sqrt{3}}. \tag{31}$$

From equations (18), (19), and (31) it therefore follows that

$$\frac{B(0)}{B(\infty)} = \frac{\sec \beta}{\sqrt{3}}. \tag{32}$$

This is an exact result, since it is valid in all approximations. Relation (32) has been proved earlier by Hopf (*op. cit.*) but by entirely different methods of more advanced character.

By turning next to the constants M_a, it is apparent from equation (22) that

$$M_a = \lim_{\mu \to k_a^{-1}} (1 - k_a \mu) G(\mu) \quad (a = 1, \ldots, n-1). \tag{33}$$

Using the explicit form of $G(\mu)$ (eq. [27]) in the foregoing equation, we find that

$$M_a = (-1)^n k_1 k_2 \ldots k_{n-1} X \frac{\sec \beta}{1 - (\sec \beta / k_a)} \frac{P(\mu = k_a^{-1})}{R_a(\mu = k_a^{-1})} \quad (a = 1, \ldots, n-1), \tag{34}$$

where we have written

$$R_a(\mu) = \prod_{i \neq a}^{1, n-1} (1 - k_i \mu) \quad (a = 1, \ldots, n-1). \tag{35}$$

On the other hand, the constants L_a in II, equation (19), are given by (cf. II, § 6)

$$L_a = (-1)^n k_1 k_2 \ldots k_{n-1} \frac{P(\mu = k_a^{-1})}{R_a(\mu = k_a^{-1})} \quad (a = 1 \ldots, n-1). \tag{36}$$

Hence,

$$M_a = X \frac{k_a}{k_a \cos \beta - 1} L_a \quad (a = 1, \ldots, n-1), \tag{37}$$

which relates the constants of integration for our present problem with those of the solution of the homogeneous equation (21) to which the L_a's refer.

Again, from equations (22) and (27) we infer that

$$\left.\begin{aligned}\gamma &= \lim_{\mu \to \cos\beta} (1 - \mu \sec\beta) G(\mu) \\ &= (-1)^n k_1 k_2 \ldots k_{n-1} X \sec\beta \frac{P(\cos\beta)}{R(\cos\beta)},\end{aligned}\right\} \tag{38}$$

or, more explicitly,

$$\gamma = (-1)^n k_1 k_2 \ldots k_{n-1} X \sec\beta \frac{\prod_{j=1}^{n} (\cos\beta - \mu_j)}{\prod_{a=1}^{n-1} (1 - k_a \cos\beta)}. \tag{39}$$

On the other hand, we know that (cf. eq. [8])

$$\gamma = \frac{1}{1 - \sum_{j=1}^{n} \frac{a_j}{1 - \mu_j^2 \sec^2\beta}}. \tag{40}$$

Equations (39) and (40) therefore determine X. However, the evaluation of X is effected more conveniently by expressing the right-hand side of equation (40) differently, as follows:

Consider the function

$$T(x) = 1 - \sum_{j=1}^{n} \frac{a_j}{1 - \mu_j^2 x}. \tag{41}$$

Multiplying this equation by

$$\prod_{j=1}^{n} (1 - \mu_j^2 x), \tag{42}$$

we obtain a polynomial of degree n in x, which clearly vanishes for

$$x = 0 \text{ and } x = k_a^2 \qquad (a = 1, \ldots, n-1). \tag{43}$$

Accordingly,

$$T(x) \prod_{j=1}^{n} (1 - \mu_j^2 x) \tag{44}$$

cannot differ from

$$x \prod_{a=1}^{n-1} (x - k_a^2) \tag{45}$$

by more than a constant factor. The constant of proportionality can be determined by comparing the coefficients of the highest powers. In this manner we find that

$$T(x) = (-1)^n \mu_1^2 \mu_2^2 \ldots \mu_n^2 \frac{x \prod_{a=1}^{n-1} (x - k_a^2)}{\prod_{j=1}^{n} (1 - \mu_j^2 x)}. \tag{46}$$

But (cf. eqs. [40] and [41])

$$\gamma = \frac{1}{T(\sec^2 \beta)} . \tag{47}$$

Hence,

$$\gamma = (-1)^n \frac{\cos^2 \beta}{\mu_1^2 \mu_2^2 \ldots . \mu_n^2} \frac{\prod_{j=1}^{n} (1 - \mu_j^2 \sec^2 \beta)}{\prod_{a=1}^{n-1} (\sec^2 \beta - k_a^2)} . \tag{48}$$

Comparing the two expressions for γ given by equations (39) and (48), we find that

$$X = \frac{\cos \beta}{\mu_1^2 \mu_2^2 \ldots . \mu_n^2 k_1 k_2 \ldots . k_{n-1}} \frac{\prod_{j=1}^{n} (\cos \beta + \mu_j)}{\prod_{a=1}^{n-1} (1 + k_a \cos \beta)} . \tag{49}$$

But (cf. II, eqs. [58], [59], and [61])

$$S(-\cos \beta) = k_1 k_2 \ldots . k_{n-1} \frac{\prod_{j=1}^{n} (\cos \beta + \mu_j)}{\prod_{a=1}^{n-1} (1 + k_a \cos \beta)} . \tag{50}$$

Hence, combining equations (49) and (50) and remembering that (II, eq. [68])

$$\mu_1^2 \mu_2^2 \ldots . \mu_n^2 k_1^2 k_2^2 \ldots . k_{n-1}^2 = \tfrac{1}{3} , \tag{51}$$

we obtain

$$X = 3 S(-\cos \beta) \cos \beta , \tag{52}$$

where it might be recalled that $S(\mu)$ determines the law of darkening for the standard problem considered in II (cf. II, eqs. [32] and [56]).

Substituting for X from equation (52) in equation (28), we have

$$G(\mu) = 3 \frac{\cos \beta}{\cos \beta - \mu} S(\mu) S(-\cos \beta) . \tag{53}$$

Now the law of darkening given by equation (20) can be expressed simply in terms of $G(\mu)$. We have (cf. eqs. [20] and [27])

$$I(0, \mu) = \tfrac{1}{4} F G(-\mu) . \tag{54}$$

Hence,

$$I(0, \mu) = \tfrac{3}{4} F \frac{\cos \beta}{\cos \beta + \mu} S(-\mu) S(-\cos \beta) , \tag{55}$$

which relates the angular distribution of the "reflected" radiation for the problem under consideration with the law of darkening in an atmosphere characterized by a constant

net flux and with no incident radiation. This relation between these two problems expressed by equation (55) is an exact one, inasmuch as it is true in all orders of approximations. Our present derivation of equation (55) thus provides an alternative elementary proof of a result first established by Hopf by means of the theory of integral equations. It is remarkable that our present method of solving the equation of transfer should retain in every approximation all the known exact features of the problem.[5]

Applications of the theory presented here to problems of the reflection effect in eclipsing binaries will be found in a later paper.

[5] This is not the case in the method of approximation used by Milne. His solution (*M.N.*, **87**, 48, eq. [14], 1926) is not, for example, strictly compatible with the result (eq. [55]).

THE WOLF-RAYET SPECTROSCOPIC BINARIES HD 186943, HD 193928, AND HD 211853*

W. A. HILTNER
McDonald and Yerkes Observatories
Received March 16, 1945

ABSTRACT

These three Wolf-Rayet stars have been investigated as spectroscopic binaries.

For HD 186943, spectral type WN5, hydrogen absorption lines were measured, as well as the emission bands *He* II 4686, *N* v 4603, and *N* v 4619. The absorption lines belong to the early B-type companion. The following elements have been derived: $P = 9.550$ days, $e = 0.0$ (assumed), K_{WR} (*He* II 4686) = 235 km/sec, $K_B = 65$ km/sec, $M_{WR} \sin^3 i = 5.8 \odot$, and $M_B \sin^3 i = 21.0 \odot$. There are pronounced differences in the gamma-velocities of the three emission bands, none agreeing with the gamma-velocity for the hydrogen absorption. The amplitude of the velocity-curve for *N* v 4603 and *N* v 4619 is smaller than that for *He* II 4686. Also, the *N* v velocity-curve shows a phase shift of 0.8 day with respect to *He* II 4686.

The spectral type of HD 193928 is about WN6. Only the Wolf-Rayet component of the system is observable. The following elements have been derived from 30 McDonald spectrograms: $P = 21.64$ days, $e = 0.0$ (assumed), $K = 130$ km/sec, γ (*He* II 4686) = +59 km/sec, γ (*N* v 4603) = −119 km/sec, and $f(m) = 4.94$. Absorption lines near λ 3873 and λ 4453 have been measured and identified as *He* I displaced to the violet by approximately 1200 km/sec. These lines were abnormally strong on July 14, 1944, and from observed displacements and changes in dilution we conclude that the *He* I atoms recede from the star with approximately uniform velocity. A similar conclusion was suggested from earlier observations of HD 214419.

The spectrum of HD 211853, spectral class WN6, has well-defined absorption lines as well as emission bands. For the emission bands alone, the following elements are obtained: $P = 6.6864$ days, $e = 0.0$ (assumed), $K = 245$ km/sec. The gamma-velocities of *He* II 4686 and *N* v 4603 are in good agreement, both bands being displaced to the red, with respect to *N* IV 4058, by 200 km/sec. None of the emission gamma-velocities agrees with that of the absorption lines. The measurements of the absorption lines give a strange velocity-curve. If one interprets the velocity-curve as that of the early B companion with $K = 95$ km/sec, we have the following minimum masses for the two components: $M_{WR} \sin^3 i = 7.6 \odot$ and $M_B \sin^3 i = 19.6 \odot$. The line *He* II 4686 undergoes variations in structure.

The available data on discrepant gamma-velocities are collected and briefly discussed.

In 1941 O. C. Wilson[1] announced the discovery of three spectroscopic binaries in which one component of each system was a Wolf-Rayet star. Up to that time only one other known spectroscopic binary possessed a Wolf-Rayet component, HD 193576,[2] and one visual double, HD 219460.[3] Since this announcement by Wilson, only two other Wolf-Rayet binaries have been discovered.[4] In 1940 Wilson[5] called attention to a number of Wolf-Rayet stars that have undisplaced absorption lines, which he suggested might belong to a second component. Stars HD 186943 and HD 211853 were in this list. To this list the author wishes to add HD 193077, which is probably a spetroscopic binary. The star HD 168206, on Wilson's list of Wolf-Rayet stars with absorption lines, has been found to be a spectroscopic binary from spectrograms taken on July 25, 1941, 6^h02^m U.T., and on June 16, 1944, 4^h56^m U.T. The relative displacement of carbon blend near λ 4635 on the two spectrograms is about 250 km/sec.

* *Contributions from the McDonald Observatory, University of Texas,* No. 108.

[1] *Pub. A.S.P.*, **53**, 295, 1941.

[2] Wilson, *Pub. A.S.P.*, **51**, 55, 1939.

[3] *Ibid.*, **52**, 404, 1940.

[4] HD 214419, Dean B. McLaughlin and W. A. Hiltner, *Pub. A.S.P.*, **53**, 328, 1941, and HD 152270, O. Struve, *Ap. J.*, **100**, 199, 1944.

[5] *Pub. A.S.P.*, **52**, 405, 1940.

PLATE XXXIII

SPECTRA OF WOLF-RAYET SPECTROSCOPIC BINARIES

(*a*) HD 211853, (*b*) HD 193928, (*c*) HD 186943

PLATE XXXIV

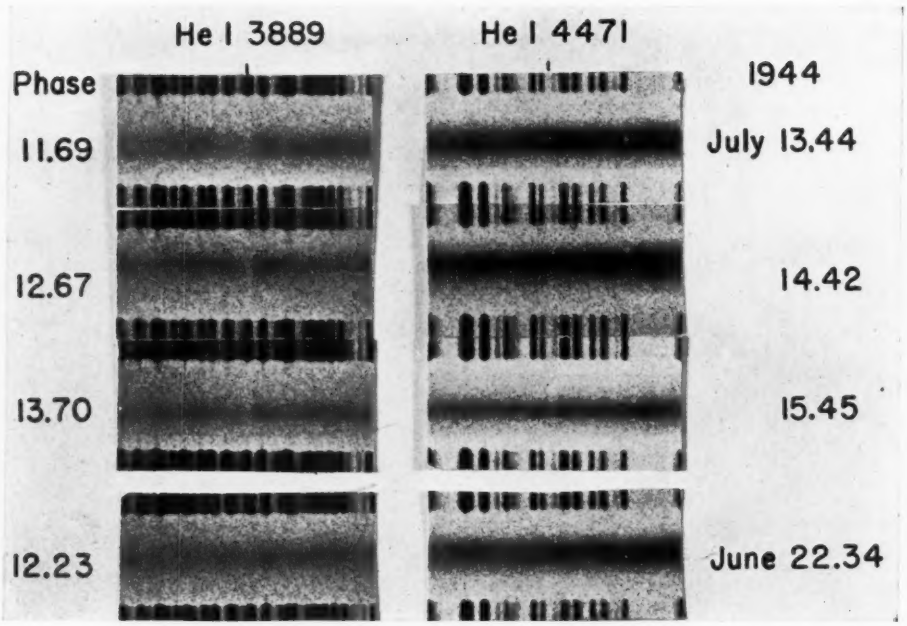

THE SPECTRUM OF HD 193928

Note that on July 13.44, *He* I 3889 is normal and that *He* I 4471 is present as a weak sharp line. On July 14.42, *He* I 3889 and *He* I 4471 are abnormally strong and sharp. On July 15.45, *He* I 3889 has not changed in intensity from the previous day, but *He* I 4471 is appreciably weaker. This phenomenon is apparently not periodic, as is shown by the spectrogram taken on June 22.34 at phase 12.23.

No detailed spectroscopic investigation of these three stars had been undertaken, and the binary nature of only the last one had been confirmed.[6] Consequently, the three stars were placed on the observing program of the 82-inch reflector of the McDonald Observatory in the summer of 1944. The Cassegrain spectrograph with two quartz prisms and 500-mm camera was used. The dispersion is 42 A/mm at λ 4000 and 70 A/mm at λ 4700. Eastman 103a-0 emulsion was employed throughout.

HD 186943[7]

The spectrum of this star is WN5. The predominating feature in the photographic region of the spectrum is *He* II 4686. Its width is approximately 56 A. The only other measurable emission features are *N* v 4603 and *N* v 4618. These bands are relatively narrow—only 17 A in width. There are weak diffuse emission features of *N* IV 4058 and *He* II of the Pickering series, but all are too indefinite to measure for radial velocity. The absorption features of the spectrum are extremely weak, characterized primarily by hydrogen. The line *He* I 4471 is observed only infrequently. Wilson suspected absorption features in this star and attributed them to the companion star.

The line *He* II 4686 was measured for radial velocity on 32 spectrograms. Settings were made only on the center of the band, and no attempt was made to measure the position of the edges in order to obtain an improved value of the displacement of this band. There is some indication that the band undergoes periodic variations in shape, but the evidence is not conclusive. This point merits careful photometric observations.

The period of 9.550 days was determined with the help of Wilson's published relative velocities. Spectrograms taken 0.2 day apart do not suggest a period of about 1 day.

Radial velocities as determined by *He* II 4686 are recorded in Table 1 and are plotted in Figure 1. The wave lengths employed in computing radial velocities for this star and the subsequent stars studied in this paper are recorded in Table 2. Phases were computed in days with the formula

$$\text{Phase zero} = \text{JD } 2431262.20 + 9.550\,E\,.$$

The measurements are well distributed in phase, and a solution with the eccentricity near zero is suggested. The following elements were obtained graphically, assuming that the eccentricity is zero:

$P = 9.550$ days	$K = 235$ km/sec
$e = 0.0$ (assumed)	$\gamma = +115$ km/sec

The only other emission features measured in HD 186943 are *N* v 4603 and *N* v 4619. When plotted separately, they give very similar velocity-curves except for a difference in the gamma-velocity. The means for the two lines are recorded in Table 1 and are plotted in Figure 2. For 31 spectrograms we find that

$$N\text{v}\,4603 - N\text{v}\,4619 = -150 \text{ km/sec}\,.$$

The velocity-curve for the Wolf-Rayet component of HD 186943 as determined by *N* v again suggests an eccentricity near zero but an amplitude smaller than that obtained for *He* II 4686. The difference is large (160 and 235 km/sec) and is certainly real. Another striking difference is brought out when the velocity-curves of *He* II and *N* v are shown together (see Fig. 2). A phase difference of about 0.8 day is strongly suggested. A phase difference of *N* IV and *He* II of the Pickering series was suggested by the radial-velocity measurements of HD 214419[8] but was not so striking as in HD 186943.

[6] McLaughlin and Hiltner, *op. cit.*, p. 330.

[7] $\alpha = 19^h42^m2$; $\delta = +28°01'$ (1900); sp., Oa; mag. ptm., 9.98.

[8] W. A. Hiltner, *Ap. J.*, **99**, 278, 1944.

Hydrogen absorption lines were measured on 28 spectrograms. At best, the lines were difficult to measure. A magnification of only seven times was employed during measurement. The lines $H\gamma$, $H\delta$, H 8, H 9, H 10, and H 11 were measured when possible, but the number of absorption lines measured per plate varied from one to six. The mean velocity for each plate is recorded in Table 2 and is plotted in Figure 3. The scatter of the measure-

TABLE 1

RADIAL VELOCITIES OF HD 186943

PLATE	DATE, U.T.	PHASE	VELOCITY (KM/SEC)		
			He II 4686	N V	H_{abs}
CQ 3263	1944 June 15.314	3.764	+180	+228	− 44
3272	16.260	4.710	+ 32	+229	.....
3295	18.285	6.735	−152	+ 9	+ 1
3304	19.241	7.691	− 49	− 4	.....
3315	20.256	8.706	− 18	− 69	+ 2
3327	21.241	0.141	+152	− 26	+133
3328	21.297	0.197	+ 76	+ 43	+ 13
3339	22.218	1.118	+273	+121	.....
3340	22.272	1.172	+304	+168	− 22
3349	27.246	6.146	− 69	+ 55	− 49
3350	27.303	6.203	− 78	+ 37	+ 37
3363	July 1.290	0.640	+221	+ 90	+ 19
3378	2.313	1.663	+355	+ 85	− 75
3399	4.327	3.677	+296	+230	−144
3412	5.371	4.721	+ 90	+217	+ 64
3421	6.311	5.661	− 14	+ 82	+ 36
3430	7.220	6.570	−122	+ 75	+ 70
3443	8.366	7.716	− 55	.....	+ 74
3446	11.244	1.044	+280	+111	− 11
3455	12.226	2.026	+307	+217	− 23
3457	12.350	2.150	+343	+217	− 6
3465	13.274	3.074	+356	+277	− 93
3466	13.329	3.129	+352	+246	− 32
3480	15.203	5.003	+118	+153	+ 19
3481	15.246	5.046	+ 42	+120	− 30
3490	16.184	5.984	− 26	+ 68	+ 4
3494	16.378	6.178	−191	+ 68	.....
3501	17.203	7.003	−151	− 38	+ 87
3503	17.357	7.157	−103	− 90	+ 90
3510	18.179	7.979	− 98	− 99	+123
3517	20.285	0.535	+174	+ 76	+ 7
4049	Dec. 7.117	6.667	−108	− 6	+ 18

ments is large. However, a variation in velocity in a phase opposite to the emission is strongly suggested. An approximate solution follows:

$$e = 0.0 \text{ (assumed)}$$
$$K = 65 \text{ km/sec}$$
$$\gamma = 10 \text{ km/sec}$$

Assuming that the absorption lines result from the companion star, which we classify only as an early B-type star, and accepting the *He* II 4686 velocity-curve as representative of the Wolf-Rayet star, the following minimum masses are derived:

$$M_W \sin^3 i = 5.8 \odot$$

$$M_B \sin^3 i = 21.0 \odot .$$

HD 193928[9]

The spectrum of this star has a type between WN5 and WN6. Its emission features, especially *He* II 4686, are stronger than in any of the five known Wolf-Rayet spectroscopic binaries of the nitrogen sequence. In the photographic region, in addition to *He* II 4686, there are emission bands of *He* II of the Pickering series, N III, *N* IV, and *N* V. Hydrogen emission must be weak. Only one absorption feature is normally present: a diffuse line at approximately λ 3873. Details of the absorption in this star will be given in a later paragraph.

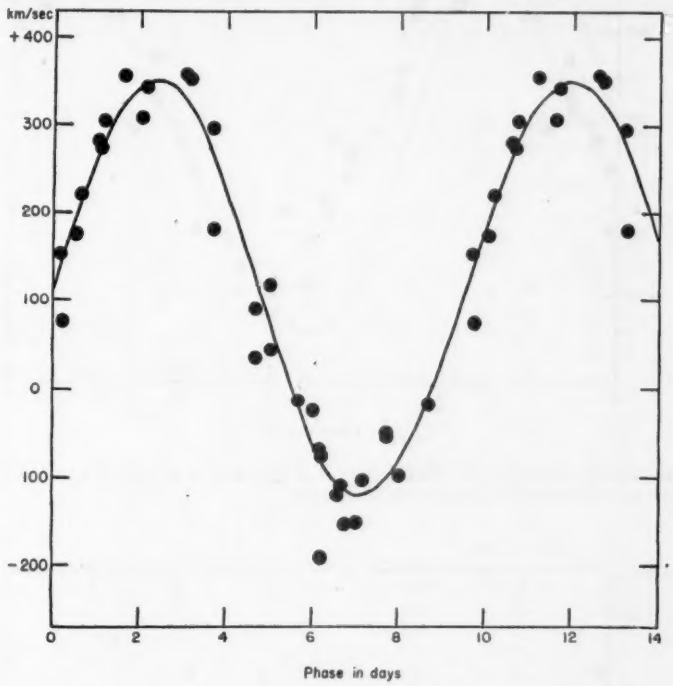

FIG. 1.—The velocity-curve of HD 186943 from *He* II 4686

TABLE 2

STELLAR WAVE LENGTHS FOR THE DETERMINATION OF RADIAL VELOCITIES

Line	Wave Length	Line	Wave Length
H 11	3770.63	*Hδ*	4101.74
H 10	3797.90	*Hγ*	4340.48
H 9	3835.39	*He* I	4471.48
He I	3888.65	*N* V	4603.2
H 8	3889.05	*N* V	4619.4
N IV	4057.80	*He* II	4685.81

In addition to the strong band *He* II 4686, *N* V 4603 and *N* IV 4058 were measured for radial velocity. Other emission bands were not measured, since they are fainter and are

[9] $\alpha = 20^h17^m.8$; $\delta = +36°36'$ (1900); sp., Oa; mag. ptm., 9.43.

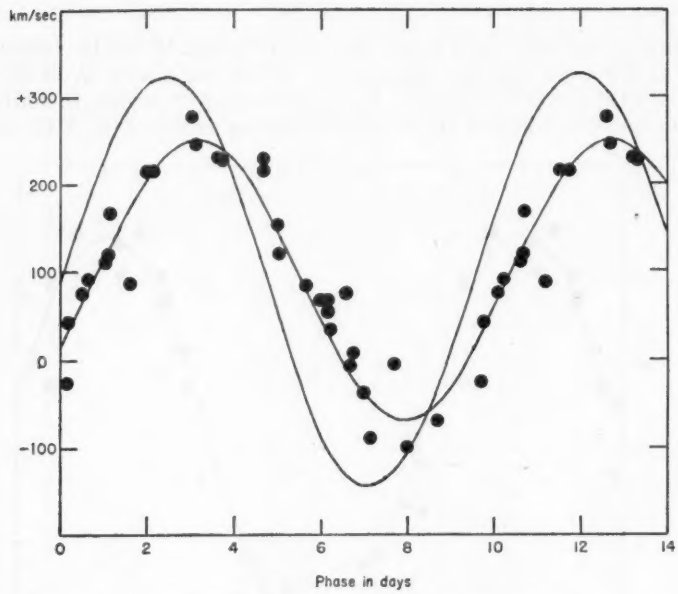

FIG. 2.—The velocity-curve of HD 186943 from *N* v 4603 and *N* v 4619. The curve for *He* II 4686 is drawn in to show the differences in amplitude and phase.

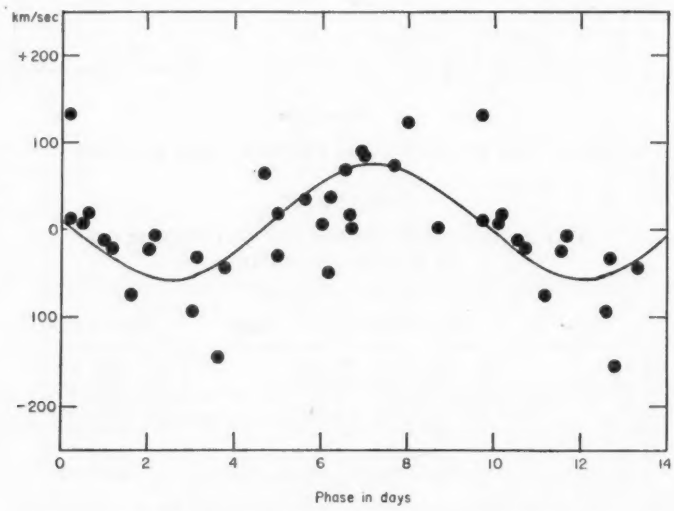

FIG. 3.—The velocity-curve of HD 186943 from hydrogen absorption

relatively difficult to measure on narrow spectrograms. Widened spectrograms were difficult to obtain, for the magnitude is 10.5 and the period was thought to be about 1 day after the first few spectrograms were obtained. The line *N* IV 4058 appears to vary appreciably in structure. Very frequently the band possessed a narrow band superimposed on the wide band and appeared near either the violet or the red side of the broad band, or both. The narrow band seems to appear more frequently on the violet edge, but the evidence is not conclusive. The velocity-curve for this band is distorted, and this distortion

TABLE 3

RADIAL VELOCITIES OF EMISSION FEATURES IN HD 193928

PLATE	DATE, U.T.	PHASE	VELOCITY (KM/SEC)		
			He II 4686	*N* V 4603	*N* IV 4058
CQ 3199	1944 May 9.456	10.626	+ 5	− 60	− 54
3264	June 15.369	5.259	+169	− 54	.....
3273	16.325	6.215	+200	+ 49	− 27
3296	18.367	8.257	+119	+ 44	+ 44
3329	21.350	11.240	+ 40	−152	−189
3341	22.342	12.232	+ 55	−206	−134
3351	27.361	17.251	− 25	−294	−187
3379	July 2.377	0.627	+125	−140	− 57
3422	6.369	4.619	+242	− 76	+ 11
3434	7.340	5.590	+185	+ 14	− 51
3456	12.285	10.535	+ 51	−124	− 46
3467	13.388	11.638	+ 10	−164	−171
3468	13.444	11.694	+ 6	−164	−220
3471	14.370	12.620	− 9	−103	−197
3472	14.423	12.673	− 16	−186	−184
3482	15.296	13.546	− 75	−181	−115
3483	15.348	13.598	− 16	−207	−132
3484	15.401	13.651	− 99	−155	−165
3485	15.452	13.702	− 60	−194	−145
3491	16.231	14.481	− 38	−194	−221
3492	16.280	14.531	− 10	−263	−237
3493	16.332	14.582	− 73	−237	−221
3502	17.256	15.506	− 80	−255	−221
3504	17.411	15.661	− 48	−251	−182
3505	17.458	15.708	− 54	−268	−201
3511	18.234	16.484	− 67	−256	−175
3512	18.292	16.542	− 69	−220	−162
3518	20.339	18.639	− 72	−256	−179
3521	20.434	18.684	− 45	−204	−179
4048	Dec. 7.072	6.842	+179	− 42	− 68

is probably related to the variation in structure of the band. The behavior of *N* IV 4058, as well as of the other bands, certainly deserves careful analysis in the future. A spectrophotometric analysis can be more profitably undertaken now than when the spectrograms for this investigation were taken, since the period and, consequently, the phases are now known. Photometric spectrograms would require an exposure of, say, 3 hours, in contrast to the present exposure time of $1\frac{1}{4}$ hours.

The radial-velocity measurements of the emission features are recorded in Table 3. The lines *He* II 4686 and *N* V 4603 gave almost identical velocity-curves except for a difference of gamma-velocity of

$$He\,\text{II}\ 4686 - N\,\text{V}\ 4603 = +178\ \text{km/sec}.$$

The mean velocities of these two lines are plotted in Figure 4. A period of 21.64 days was derived with the help of three relative radial velocities published by Wilson. A period of about 1 day has been eliminated by spectrograms obtained in one evening over a period of 0.2 day. The observations are not well distributed in phase, and consequently the elements are not well defined. However, the following elements are indicated:

$P = 21.64$ days	γ (λ 4686) $= +59$ km/sec
$e = 0.0$ (assumed)	γ (λ 4603) $= -119$ km/sec
$K = 130$ km/sec	$f(m) = 4.94\ \odot$

This large mass function is similar to that derived for HD 214419, which in this case is $f(m) = 4.38$.

The strongest absorption feature in HD 193928 is a diffuse line with an approximate wave length of 3873 A. This line was measured on 24 spectrograms (all that were suffi-

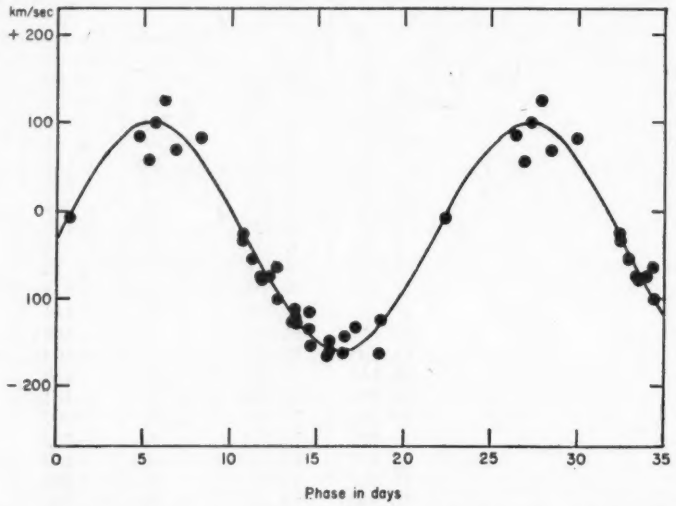

FIG. 4.—The velocity-curve of HD 193928 from *He* II 4686 and *N* V 4603

ciently well exposed in this region), and the measured wave lengths are recorded in Table 4. The measurements, when plotted (see Fig. 5), indicate that this line possesses a displacement similar to that obtained for the emission features of the spectrum. Infrequently a second line was measured at a wave length near λ 4453. The measurements are also recorded in Table 4. The behavior of this line with phase is uncertain because of scatter in the measurements. On July 13, phase 11.7 days, this line appeared unusually sharp but still faint (see Pl. XXXIV), but λ 3873 appeared normal on this date. On July 14 (phase 12.6 days) both lines were abnormally strong and sharp. On the following day, λ 4453 had weakened appreciably, but λ 3873 remained nearly as strong as during the previous night. On July 16, λ 4453 was no longer visible with certainty, and λ 3873 was only slightly stronger than normal. The behavior of these lines does not appear to be related with phase, since on June 22, phase 12.2 days, the line λ 4453 was very weak and diffuse and λ 3873 had a normal intensity. If λ 4453 is identified as *He* I 4471 and λ 3873 as *He* I 3889, we find that the resulting radial velocities are almost identical for

$$V(3889) - V\,4471 = 6\ \text{km/sec}\,.$$

Furthermore, it is observed that for the two spectograms obtained on July 14, when the two lines were sharp and consequently could be measured with greater precision, the

TABLE 4

RADIAL VELOCITIES OF *He* I ABSORPTION IN HD 193928

Date, U.T.	Phase	λ	Velocity *He* I 3889 (Km/Sec)	λ	Velocity *He* I 4471 (Km/Sec)
1944 May 9.456	10.626	3873.12	−1298	4453.52	−1204
June 21.350	11.240	3872.58	1240	4452.93	1245
22.342	12.232	3872.92	1214	4451.78	1322
27.361	17.251	3871.74	1305	.....	.....
July 6.369	4.619	3875.70	999	.....	.....
7.340	5.590	3874.22	1113	4454.67	1128
12.285	10.535	3873.59	1162	4452.62	1265
13.388	11.638	3873.51	1168	4451.47	1342
13.444	11.694	3872.71	1230	4453.51	1206
14.370	12.620	3873.16	1195	4453.69	1194
14.423	12.673	3873.16	1195	4453.69	1194
15.348	13.598	.....	.....	4454.94	1110
15.401	13.651	3873.00	1207	4453.02	1238
15.452	13.702	3873.13	1197	4453.79	1187
16.231	14.481	3872.33	1259	.....	.....
16.280	14.531	3872.85	1219	.....	.....
16.332	14.582	3872.29	1262	.....	.....
17.256	15.506	3871.80	1300	.....	.....
17.411	15.661	3871.83	1298	.....	.....
17.458	15.708	3872.61	1237	.....	.....
18.234	16.484	3872.64	1235	4453.02	1238
18.292	16.542	3871.91	1291	.....	.....
20.339	18.639	3871.82	1298	.....	.....
20.434	18.684	3871.62	1314	4452.58	−1268
Dec. 7.072	6.842	3873.96	−1132	.....	.....

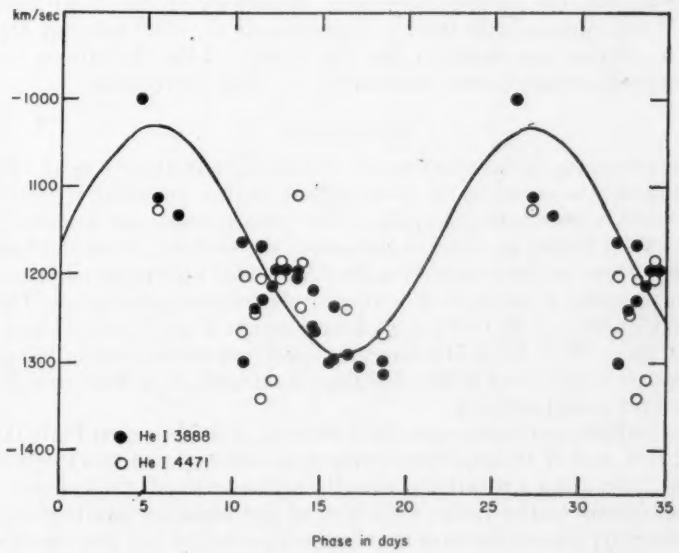

FIG. 5.—The radial velocity observations of *He* I 3888 and *He* I 4471

radial velocities agree within 1 km/sec. If the above identifications are correct, then we should expect to observe *He* I 4026. The behavior of this line is uncertain. On a widened spectrogram taken on July 14, when *He* I 4471 was at maximum intensity, there is certainly a line present at λ 4010; but a narrow spectrogram obtained the same evening gives no indication of a line at this wave length, although it shows λ 3873 and λ 4453 quite strongly. However, in spite of this peculiar behavior of *He* I 4026, it appears logical to conclude that we are observing *He* I absorption lines resulting from light from the central core of the Wolf-Rayet star passing through that part of the shell which is ejected toward the observer. This conclusion is supported by the total widths of the measurable bands. The total width of *He* II 4686 is 2400 km/sec. The average velocity of the *He* I absorption lines is 1200 km/sec. The variation in intensity must be interpreted in terms of abundance, and any variation in dilution that may have occurred while the lines were unusually strong can be interpreted by a variation in distance of the material from the central core of the Wolf-Rayet star.

The variation in intensity and the radial velocity measures of λ 3889 and λ 4471 may provide some information on the velocity variation of the ejected *He* I atoms with distance from the central core of the Wolf-Rayet star. On July 14 both *He* I 3889 and *He* I 4471 were strong. Their velocities were, respectively, 1195 and 1194 km/sec. The next night, July 15, four spectrograms were obtained, but only two were well exposed. Line *He* I 3889 was of approximately the same intensity as on the previous night; but *He* I 4471 was much weaker, indicating a change in dilution during the interval of twenty-four hours. The radial velocities of λ 3889 and λ 4471 are −1202 and −1178 km/sec. The velocity given by λ 3889 should be given greater weight. It is evident that in an interval of twenty-four hours, during which time a marked change in dilution occurred, the velocity of the ejected gas remained constant within the errors of the measurements. In this connection we should call attention to a similar phenomenon in HD 214419.[8] This star normally shows the Wolf-Rayet component of *He* I 4471, 4026, and 3889. However, a second component of these lines was observed on November 13, 1943, with a displacement of −800 km/sec. On the following night, November 14, only the displaced component of λ 3889 was present, still with a displacement of −800 km/sec. Here, again, a large change in dilution was observed, but the velocity of the *He* I atoms remained constant as the material receded from the core of the Wolf-Rayet star.

HD 211853[10]

The emission features in the spectrum of this star are relatively weak. The line *He* II 4686 predominates in intensity in the photographic region. Its width is 2500 km/sec, and it shows variation in structure with phase. The most pronounced asymmetry occurs at phase 3.3 (the Wolf-Rayet star on the far side of the system), when the band is shaded toward the red. There is some suggestion that *N* IV 4058 undergoes periodic variation in structure, but the band is too weak to make the observations conclusive. The other principal emission features are *He* II of the Pickering series, *N* III, *N* V 4603, and possibly *He* I, especially λ 4471. Plate XXXIII shows the spectrum of this star in the photographic region. Its spectral type is near WN6. The lines *He* II 4686, *N* IV 4058, and *N* V 4603 have been measured for radial velocity.

Absorption features in this star are quite evident, as is shown on Plate 000. The lines *Hγ*, *Hδ*, *H* 8, *H* 9, and *H* 10 are always present on well-exposed spectrograms. They are usually diffuse, indicating a rotational velocity of the order of 230 km/sec.

The measurements of the radial velocities of the emission bands give very similar velocity-curves except for differences in the gamma-velocity and have been combined to give the following elements:

[10] $\alpha = 22^h15^m.0$; $\delta = -55°36'$ (1900); sp., Ob; mag. ptm., 9.0.

$P = 6.6864$ days
$e = 0.0$ (assumed)
$K = 245$ km/sec

γ (4686) = +50 km/sec
γ (4603) = +62 km/sec
γ (4058) = −125 km/sec

The period was improved by referring to Wilson's published relative velocities. A period of about 1 day has been eliminated by obtaining as many as 5 spectrograms in the same evening over an interval of 0.14 day or less. The measured radial velocities are collected in Table 5, and the mean velocities for the emission features are plotted in Figure 6.

TABLE 5

RADIAL VELOCITIES OF HD 211853

PLATE	DATE, U.T.	PHASE (DAYS)	VELOCITY (KM/SEC)		
			Emission	H_{abs}	He I 4471
CQ 3175	1944 May 7.465	1.483	+312	−185	.....
3265	June 15.428	0.326	+ 76	−162	.....
3275	16.424	1.322	+246	− 50	.....
3284	17.433	2.331	+185	− 87	− 49
3297	18.437	3.335	+ 6	−140	−158
3305	19.321	4.219	−176	− 89	− 36
3306	19.383	4.281	−152	− 20	.....
3307	19.441	4.339	−166	− 56	− 81
3316	20.325	5.223	−208	+ 14	.....
3317	20.380	5.278	−213	+ 28	.....
3318	20.433	5.331	−202	+ 16	+ 57
3330	21.397	6.295	+ 13	− 42	− 61
3331	21.433	6.331	− 8	−107	− 61
3342	22.410	0.622	+187	−117	−182
3343	22.448	0.660	+188	−123	.....
3352	27.412	5.624	−179	+ 35	+ 78
3353	27.450	5.662	−137	+ 35	+ 24
3354	28.448	6.660	+ 25	−114	−121
3356	30.334	1.860	+296	−106	.....
3357	30.389	1.915	+275	− 36	.....
3358	30.435	1.961	+305	− 90	.....
3364	July 1.358	2.884	+ 92	− 32	− 44
3365	1.399	2.925	+130	− 66	.....
3366	1.435	2.961	+121	− 26	− 76
3380	2.433	3.959	− 28	− 54	−117
3381	2.462	3.988	− 56	− 98	.....
3386	3.322	4.848	−212	− 62	− 19
3387	3.358	4.884	−134	− 27	− 84
3388	3.392	4.918	−175	− 26	.....
3389	3.427	4.953	−148	− 24	+ 17
3390	3.458	4.984	−198	− 20	−100
3401	4.408	5.934	−115	+ 14	+ 50
3402	4.437	5.963	− 68	+ 12	+ 5
3413	5.428	0.268	+135	− 84	.....
3414	5.461	0.301	+ 85	−150	−142
3423	6.414	1.254	+295	−133	−117
3445	8.451	3.291	+ 59	− 67	.....
3451	11.381	6.221	− 63	+ 50	+ 5
3458	12.407	0.561	+212	−126	−146
3459	12.444	0.598	+198	−116	−190
3513	19.474	0.942	+292	−133	−207
4050	Dec. 7.157	1.219	+256	− 40	.....

Hydrogen absorption, consisting usually of $H\gamma$, $H8$, $H9$, $H10$, and $H11$, was measured on all spectrograms. The mean radial velocity for each spectrogram is recorded in Table 6 and plotted in Figure 7. The form of the velocity-curve is not well defined because of

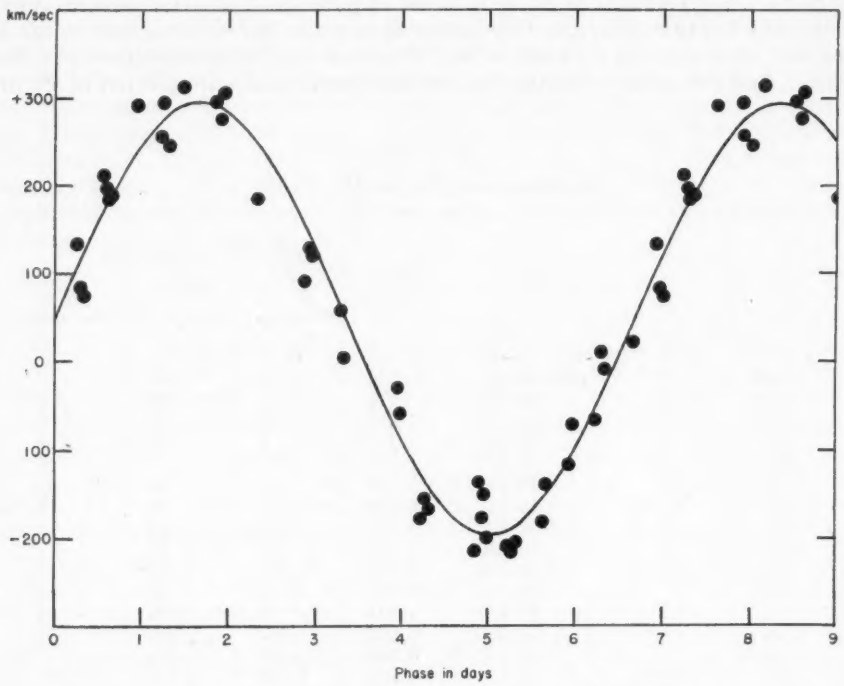

FIG. 6.—The velocity-curve of HD 211853 from *He* II 4686, *N* V 4603, and *N* IV 4058

TABLE 6

RADIAL VELOCITIES OF *He* I 3889 ABSORPTION IN HD 211853

Plate	Phase	λ	Velocity (Km/Sec)	Plate	Phase	λ	Velocity (Km/Sec)
CQ 3445.....	3.291	3873.5	−1160	CQ 3318.....	5.331	3872.9	−1210
3386.....	4.848	3872.3	1260	3352.....	5.624	3871.6	1310
3387.....	4.884	3872.9	1210	3353.....	5.662	3871.7	1300
3389.....	4.953	3872.3	1260	3451.....	6.221	3871.6	1310
3390.....	4.984	3871.8	1300	3330.....	6.295	3871.3	1330
3316.....	5.223	3872.5	1240	3331.....	6.331	3871.5	1320
3317.....	5.278	3872.7	−1230	3354.....	6.660	3870.7	−1380

the large scatter. However, the hydrogen-absorption velocity appears approximately constant at −65 km/sec from phase 1.6 days to 4.9 days, at which time there is a marked increase in velocity, reaching a maximum of +40 km/sec at phase 5.6 days. The velocity then decreases rapidly to −150 km/sec at phase 0.8 day. Although *He* I 4471 was measured less frequently than the hydrogen lines, it verifies the general form of the velocity-curve, especially the rapid decrease in velocity.

The interpretation of the absorption velocity-curve is not clear, and it certainly deserves further careful examination. From phase 1.6 days to phase 4.9 days, when the velocity of the absorption lines remains approximately constant, the B-type component of the system is between the observer and the Wolf-Rayet component. From phases 4.9 to 1.6 days, when the velocity of the absorption lines is changing rapidly, the B-type component is on the far side of the system. This suggests that the observed variation in velocity may be related to a rotation effect of the B-type component. This suggestion does not appear adequate, primarily because it is necessary to assume that the two stars are nearly in contact and that the resulting mass of the B-type component would become unreasonably large. If one wishes to interpret this velocity-curve as resulting from the second component, one is faced with an eccentricity of about 0.4, in contrast to an eccentricity near zero obtained for the emission lines. This discrepancy may possibly find

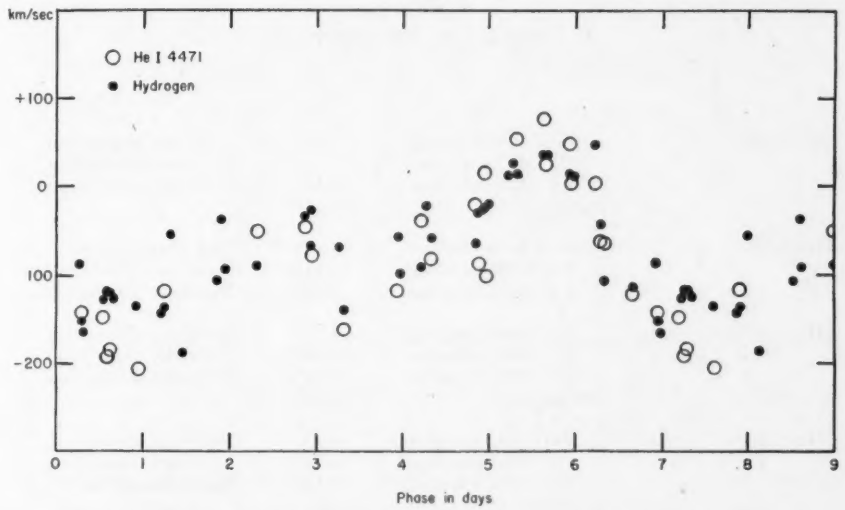

FIG. 7.—The radial velocity variations of hydrogen and *He* I 4471 absorption

its explanation in streams of gas which are known to distort velocity-curves of certain eclipsing variable stars. Pending further investigations of the form of the velocity-curve, we shall assume that we have a measure of the variation in velocity of the companion star, which we will classify only as early B, with $K = 95$ km/sec. This permits us to compute the following minimum masses:

$$M_{WR} \sin^3 i = 7.6 \odot ,$$

$$M_B \sin^3 i = 19.6 \odot .$$

In HD 193928 an absorption line near λ 3873 was observed, and evidence was presented indicating that this line should be identified with *He* I 3889. In HD 211853 a similar line was measured whenever detected on the spectograms. The results of the measurements are listed in Table 6. It is to be observed that the line was usually measured between phases 4.8 and 6.6 days (on 13 of 16 spectrograms), but only once between phase 0.0 and 4.8 days and then at phase 3.3 days. This indicates that the line may be variable with phase and is probably related to the general variations in the spectrum of the Wolf-Rayet star with phase. The average velocity of this line when identified as *He* I 3889 is −1260 km/sec.

DISCUSSION

In all the four Wolf-Rayet spectroscopic binaries thus far investigated by the author, the so-called "center of mass," or gamma-velocity, has shown considerable divergence, from one emission line to another. The data thus far available on this question are collected in Table 7. Wilson measured three emission bands (*He* II 4686, *N* V 4600, and *N* V 4619) in HD 193576 and, upon accepting Edlén's computed wave lengths for the two *N* V lines, as we have done in the present investigation, observed that

$$V\,(4603) = \overline{V\,(4603) - V\,(4686)} = +8 \text{ km/sec}$$

$$V\,(4619) = \overline{V\,(4619) - V\,(4686)} = -19 \text{ km/sec}\ .$$

TABLE 7

OBSERVED γ-VELOCITIES

Star	Line	γ (Km/Sec)	Remarks
HD 186943	*He* II 4686 emission	+115	No violet absorption
	N V 4603 emission	+ 15	No violet absorption
	N V 4619 emission	+165	No violet absorption
	H_{abs}	+ 10	
HD 193928	*He* II 4686 emission	+ 59	Violet absorption?
	N V 4603 emission	−119	Weak violet absorption
	N IV 4058 emission	−100	No violet absorption
HD 211853	*He* II 4686 emission	+ 50	No violet absorption
	N V 4603 emission	+ 62	No violet absorption
	N IV 4058 emission	−125	No violet absorption
	H_{abs}	− 55	
HD 214419	*He* II 4686 emission	+137	No violet absorption
	N IV 4058 emission	− 75	No violet absorption
	He II emission Pickering	+180	Violet absorption

He also observed that the gamma-velocity for the Wolf-Rayet star was more positive by 90 km/sec than the gamma-velocity of the absorption-line component. The conclusion was made that the emission bands were shifted to the red by 90 km/sec. Struve[11] concluded that in HD 151932, which is located in the cluster NGC 6231, *N* IV 4058 gave the velocity of the cluster and that *He* II 4686 possesses a red shift of 85 km/sec. The spectrum of this star is remarkably similar to HD 214419. The emission bands are of similar width, and each star shows violet absorption edges of certain bands which are variable in intensity. In HD 214419, *He* II 4686 is displaced to the red by 212 km/sec with respect to *N* IV 4058. In this connection attention should be drawn to HD 211853, in which *He* II 4686 is again displaced to the red with respect to *N* IV 4058; but neither band gives a velocity comparable to the absorption lines which probably belong to the B-type component.

The existence of different gamma-velocities for various emission bands is certainly real and cannot be explained in terms of inaccurate laboratory wave lengths. It is difficult to draw any general conclusions concerning the behavior of the various bands, other than that, thus far, *He* II 4686 is always displaced to the red with respect to *N* IV 4058.

[11] *Op. cit.*, p. 192.

Violet absorption edges do not, in general, appear adequate to explain all the displacements of emission bands with respect to each other. For example, in HD 186943, *He* II 4686, *N* v 4603, and *N* v 4619 do not show any visible violet absorption, although the observed gamma-velocities differ by as much as 150 km/sec. This phenomenon of discrepant gamma-velocities is probably associated with the observed variations in profiles of certain emission bands, for which a nonsymmetrical shell about the Wolf-Rayet type component offers, at present, the most plausible explanation.

In Figure 2 it is clearly shown that the velocity-curve as determined by the emission bands of *N* v differs, not only in amplitude, but also in phase from that of *He* II 4686 by approximately 0.8 day. These differences are certainly real, and an explanation must be sought. To explain the differences in phase, the "transit-time-effect," as developed by Wilson,[12] immediately suggests itself; but the assumption that the shell of the Wolf-Rayet star is not appreciably influenced by the more massive B-type companion does not appear to be justified.

TABLE 8

MASSES OF WR STARS

Star	Type	WR Star	Absorption Star	Ratio
HD 152270.....	WC6+	$M \sin^3 i = 1.9\ \odot$	$M \sin^3 i = 6.9\ \odot$	0.28
HD 186943.....	WN5	$M \sin^3 i = 5.8\ \odot$	$M \sin^3 i = 21.0\ \odot$	.28
HD 193576.....	WN5	$M = 12.4\ \odot$	$M = 31.8\ \odot$	.39
HD 211853.....	WN6+	$M \sin^3 i = 7.6\ \odot$	$M \sin^3 i = 19.6\ \odot$	0.39
HD 193928.....	WN6	$f(m) = 4.94\ \odot$	.....	.....
HD 214419.....	WN6−	$f(m) = 4.38\ \odot$	.....	.....

At the present time six Wolf-Rayet stars have been investigated as spectroscopic binaries. In four of the six stars, an absorption-line component is present; and in the other two, only the Wolf-Rayet component has been observed. This gives us some information concerning the masses of these peculiar objects. All the data known at present is summarized in Table 8.[13] The ratio of the mass of a Wolf-Rayet star to that of an early-type absorption star appears to be fairly well defined, with a value of $\frac{1}{3}$. Less can be said with certainty concerning the mass of a Wolf-Rayet star, but the evidence suggests that the mass of a Wolf-Rayet star is of the order of ten times that of the sun. With the completion by the author of a photometric investigation of the three spectroscopic binaries discussed in this paper, more information should become available concerning the mass of a Wolf-Rayet star.

The author wishes to express his thanks to Dr. O. Struve and Dr. S. Chandrasekhar for many helpful discussions.

[12] *Ap. J.*, **95**, 409, 1942.

[13] HD 152270, O. Struve, *Ap. J.*, **100**, 387, 1944; HD 193576, O. C. Wilson, *Ap. J.*, **95**, 406, 1942; and HD 214419, W. A. Hiltner, *Ap. J.*, **99**, 274, 1944.

THE SPECTROSCOPIC ORBIT OF RZ ERIDANI*

CARLOS U. CESCO AND JORGE SAHADE
Yerkes and McDonald Observatories
Received March 29, 1945

ABSTRACT

The orbital elements of RZ Eridani, derived from 52 spectrograms, are as follows: $P = 39.28074$ days (photometric); $K = 25.8$ km/sec; $\omega = 314.3°$; $e = 0.36$; T = phase 28.0 days after minimum of light; $\gamma = +32.0$ km/sec; $a \sin i = 13 \times 10^6$ km; $f(m) = 0.06\ \odot$. The system is found to consist of a "metallic-line" main-sequence star, whose spectrum, in the region λλ 4000–4300, matches that of ι Peg (F5 V), which at primary minimum is eclipsed by a subgiant G8 star surrounded by an envelope of calcium gas.

The star BD−10°993 (8.0 mag.; $\alpha = 4^h36^m9$, $\delta = -10°57'5$ [1855.0]) = HD 30050 (Sp. A5) = AG Cbr M. 1174 (8.1 mag.), an eclipsing binary of the Algol type, was discovered as such in 1916 by Miss J. C. Mackie[1] on Harvard plates. Its provisional designation was 45.1916.

TABLE 1

STAR LINES USED FOR THE DETERMINATION OF THE RADIAL VELOCITIES OF RZ ERIDANI

Ca II	3933.67	*Ca* I	4226.73
Fe I	3952.73	*Ti* II	4290.22
Fe I	4005.25	*Fe* I	4325.77
Fe I	4045.82	*Hγ*	4340.47
Sr II	4077.73	*Sc* II	4374.51
Hδ	4101.74	*Fe* I	4383.55
Fe I	4143.87	*Mg* II	4481.26

During the months of August, September, October, and December, 1944, the star was included in the program of the 82-inch reflecting telescope of the McDonald Observatory for the purpose of determining its spectroscopic orbit. Fifty-two spectrograms were secured in that period, all of them on Eastman 103 a-O emulsion and with a dispersion of 40 A/mm at λ 3933. Except at minimum light, the exposure time was of about 40 minutes in fair seeing.

The spectrograms taken in the phases corresponding to maximum light show only one component; but on three plates taken during eclipse, namely, at phases 0.274, 0.381, and 0.493 day, the spectrum is purely that of the secondary star. The determination of the spectral types of both components was very kindly made by Dr. W. W. Morgan, who examined the spectrograms CQ 3847 (phase 11.212 days) and CQ 4080 (phase 0.493 day) (see Pl. XXXV). Dr. Morgan's statement is as follows:

CQ 3847.—In the range λλ 4000–4300 the type is about F5; in this region the spectrum matches that of the main-sequence star ι Peg (F5 V) fairly closely. The K line, however, is weak for this class. The ratio H/K corresponds approximately to spectral type A5[2]. The spectrum probably belongs to the peculiar "metallic-line" group. The ratio λ 4045/λ 4077 indicates a higher luminosity than ι Peg ($M_{vis} = +3.4$). The classification given is uncertain because of unfamiliarity with plates of the dispersion used and the unavailability of suitable comparison stars.

* *Contributions from the McDonald Observatory, University of Texas*, No. 109.

[1] *Harvard Circ.*, No. 196, 1916; *A.N.*, 207, 215, 1918.

[2] Probably the classification of the HDC for this star was made by taking into account the *Ca* II K line.

PLATE XXXV

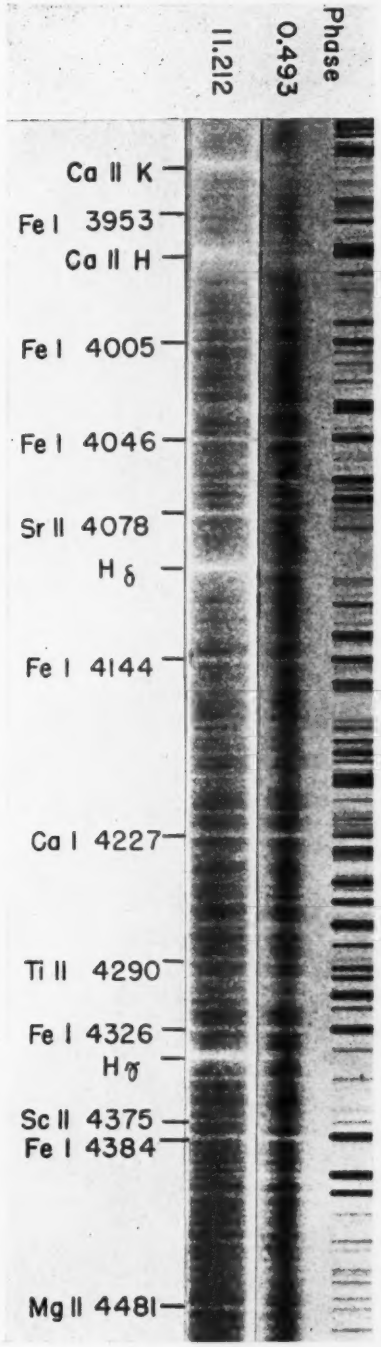

SPECTRA OF RZ ERIDANI

UNIV. OF MICH.

TABLE 2

RADIAL VELOCITIES OF RZ ERIDANI

Plate	Date 1944	U.T.	Phase (in Days)	Radial Velocity (in Km/Sec)
CQ 3792	Sept. 23	10:51	0.274	+44.9*
4078	Dec. 11	2:54	0.381	10.0*
4080	11†	5:36	0.493	23.9*
4086	12	9:44	1.666	27.5
4087	12	10:17	1.688	15.6
4092	13	5:07	2.473	29.1
4104	14	4:48	3.460	25.2
3797	Sept. 27	10:25	4.255	32.1
3803	28	9:33	5.219	32.6
3804	28	10:18	5.250	21.6
4140	Dec. 17	3:55	6.423	27.4
3815	Sept. 30	8:40	7.182	31.4
3816	30	9:18	7.209	26.1
3827	Oct. 1	8:40	8.168	25.1
3828	1	9:20	8.210	26.0
3832	2	10:40	9.266	30.0
4191	Dec. 20	2:52	9.379	16.0
3838	Oct. 3	9:50	10.231	15.7
3847	4	9:23	11.212	15.3
3654	Aug. 26	11:34	11.584	21.1
3861	Oct. 5	8:20	12.168	2.4
3862	5	8:58	12.195	27.3
3658	Aug. 27	11:33	12.583	29.8
3878	Oct. 6	8:35	13.179	13.1
3895	7	8:42	14.184	10.6
3897	7	10:49	14.272	12.1
3664	Aug. 30	11:16	15.571	1.4
3665	30	11:38	15.587	24.6
3675	31	11:37	16.586	14.0
3920	Oct. 10	8:22	17.170	19.0
3685	Sept. 1	10:44	17.549	15.1
3935	Oct. 11	8:54	18.192	12.7
3696	Sept. 2	10:43	18.548	17.6
3941	Oct. 12	10:44	19.268	9.3
3955	13	9:28	20.216	14.4
3969	14	10:10	21.245	24.0
3984	15	8:43	22.184	6.3
3995	16	9:09	23.202	21.2
4008	17	9:08	24.202	25.7
4025	18	9:42	25.225	37.9
3713	Sept. 10	11:02	26.562	45.3
3730	13	12:01	29.603	65.9
3743	14	11:59	30.601	62.4
3754	15	11:30	31.581	57.0
3763	17	11:56	33.599	56.6
3771	19	11:23	35.576	43.5
3772	19	11:58	35.601	56.0
3782	21	10:20	37.533	41.2
4073	Dec. 9	5:06	37.753	34.3
4074	9	6:05	37.794	42.1
3787	Sept. 22	9:10	38.484	31.1
3788	22	9:52	38.513	+44.7

* The velocity is that of the fainter component of RZ Eridani.

† The emission lines of *Ca* II give +30.2 km/sec.

CQ 4080.—The spectral type is probably a subgiant of class G8. The luminosity appears to be definitely fainter than that of a normal giant. The visual absolute magnitude is probably around +3. The same remarks apply to the accuracy of the classification.

The spectrum of the secondary component shows *Ca* II, H and K, emission lines.

In Table 1 are listed the lines measured for radial velocities, and in Table 2 the results of our measurements, which are plotted in Figure 1. In this figure the crosses represent the values derived for the secondary star. Of the three plates obtained during the eclipse, the best is CQ 4080; the other two plates are rather poor and do not go beyond λ 4000. The radial velocity derived from the emission lines on spectrogram CQ 4080 is almost the same as the one derived from the absorption lines. Therefore, we conclude that the G8 component is surrounded by an envelope of calcium gas.

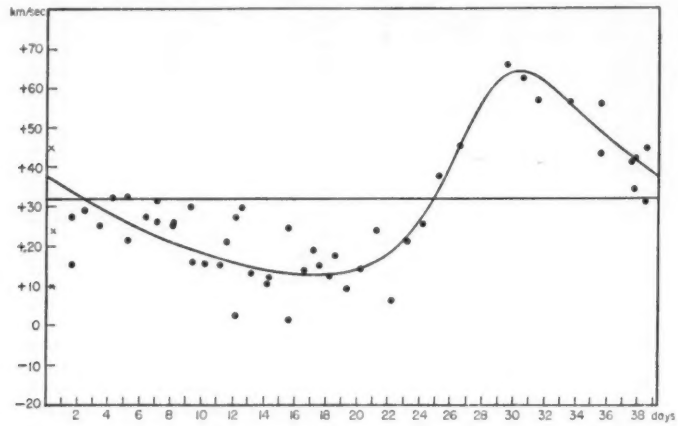

FIG. 1

In plotting the measurements we have adopted as the period the value given by Gadomski,[3] which was a mean between his results and those of Hertzsprung, namely, 39.28074 days. The phases were computed by considering as the time of minimum the date JD 2423854.057, given by Schneller in his *Katalog und Ephemeriden Veränderlicher Sterne für 1941.*

The orbital elements were derived by applying the method of Lehmann-Filhés, and the results are shown in Table 3. No attempt was made to perform a least-squares solu-

TABLE 3

ORBITAL ELEMENTS OF RZ ERIDANI

$P =$ 39.28074 days (assumed)	$\gamma =$ + 32.0 km/sec
$K =$ 25.8 km/sec	$a \sin i =$ 13×10^6 km
$\omega =$ 314.3°	$\frac{m_2^3 \sin^3 i}{(m_1 + m_2)^2} = 0.06 \odot$
$e =$ 0.36	
$T =$ phase 28.0 days	

tion because of the scattering of the measurements. Before this computation was made, we plotted, tentatively, the measurements derived only from the *H* lines and those derived from the metallic lines; but, since the trend of the curves was quite similar, we have considered the straight means of the velocities derived from all the lines, in the determination of the elements.

[3] *Circ. Obs. Cracovie*, No. 24, 1927.

The time of mid-eclipse, computed from the condition $v + \omega = 90°$, is phase 39.0 days, a value which is in good agreement with the photometric elements.

The only light-curve of RZ Eridani which has ever been published, so far as we know, is the one by Gadomski,[4] who found:

D	2.2 days	M	7.81 mag.
d	0.0 days	m	9.05 mag.

Gadomski's observations seem to indicate[5] the probable existence of a secondary minimum of amplitude 0.2 mag., which is advanced by 0.4 day.

The eccentricity of 0.36 which we have obtained seems to be real, as the spectrum of the primary star does not show any change in the different phases; hence, the possibility of a distortion of the velocity-curve was rejected. Furthermore, in a system with such a long period as that of RZ Eridani we would expect an eccentricity of the order which we have found. It is to be hoped that new photometric observations of this star will give more exact information about the secondary minimum and will provide a check of our spectroscopic observations.

We are indebted to Dr. C. Payne-Gaposchkin for suggesting the study of this star, to Dr. O. Struve for taking some of the spectrograms and for discussion of the material, and to Dr. W. W. Morgan for helping us in classifying the spectra.

[4] *Bull. Acad. polonaise d. Sci. et d. Lettres*, Ser. A, p. 303, 1926.

[5] *Ibid.*, p. 310.

NOTES

SERIES LINES OF MAGNESIUM IN THE SOLAR SPECTRUM

In an earlier note[1] our knowledge of two series of *Mg* lines ($3^1D - n^1F^o$ and $3^3D - n^3F^o$) previously recognized in the laboratory by Paschen[2] was extended and improved with the aid of solar data.

The purpose of the present note is to correct two errors which occurred in connection with $n = 5$, to which we formerly assigned solar lines λ 9257.01 and λ 10813.14 in the singlet and triplet series, respectively. Better solar spectrograms now fail to show λ 10813.14, which had been observed only on a plate on which other weak lines were subsequently found to be spurious. In place of these early assignments we now introduce for $n = 5$ two other solar lines, λ 9255.79 and λ 10811.14, of more appropriate intensity. We have also revised the solar wave lengths, intensities, term values, $n^{1,3}F^o$, Rydberg denominators, n^*, and series limits, as shown in Table 1.

Our erroneous assignments resulted from an attempt to fit the solar series to Paschen's laboratory wave lengths, λ 9257.9 and λ 10812.9; but experience now shows that his data for *Mg* require larger and more diverse corrections than we at first supposed. For this reason and since less than half of the lines in Table 1 have been found in the laboratory, we base our identifications on improved series relations.

The identity of the $^1F^o$ and $^3F^o$ terms is now established beyond question, and two new members are added to the singlet series.

The limits of the series, 3^1D and 3^3D, shown at the top of Table 1, have been derived by adding 1.5 cm^{-1} and 1.37 cm^{-1}, respectively, to Paschen's values. As we state the limits, their difference is equal to 1553.97, the weighted mean value of $\Delta\nu$. In obtaining the mean $\Delta\nu$ we have excluded the first and have given weight 1 to the next four, and weight $\frac{1}{3}$ to the last four, values.

Wave lengths of the two new singlet lines are predicted by assuming that $n - n^*$ converges to the value +0.0478, as indicated by the data for $n < 12$. With this assumption n^* takes the values 12.9522 and 13.9522; and the corresponding term values are computed from the relation $n^{1,3}F^o = R_\infty \div n^{*2}$, where R_∞ is the Rydberg constant for a nucleus of infinite mass. We take $R_\infty = 109737.303$ cm^{-1}, as given by Birge,[3] and find the terms to be 654.13 and 563.73, respectively; their combinations with the series limits give predicted wave lengths λ 6841.17 and λ 6799.10. Since the agreement of the observed lines shown in Table 1 is satisfactory, their terms and Rydberg denominators are derived and tabulated.

The best lines of these series are difficult to measure; the weakest are at the limit of visibility. It is, therefore, notable that between λ 6900 and λ 10,800 the accordance among the values of $\Delta\nu$ corresponds to errors in the measurements no greater than 0.02 or 0.03 A. Since the measured intervals, $\Delta\nu$, are independent and overlap in wave length, it is probable that throughout this region our scale of wave lengths is free of systematic errors large enough to affect the identification of solar lines.

Estimates of intensity for wide diffuse lines are generally difficult—the more so when, as for these *Mg* lines, a great range of wave length and of intensity is involved. Beyond

[1] Russell, Babcock, and Moore, *Phys. Rev.*, **46**, 826, 1934.

[2] *Sitz. d. Preuss. Akad. d. Wiss., Phys.-math. Kl.*, **32**, 709, 1931.

[3] *Reports on Progress in Physics* (London Physical Society), **8**, 129, 1941.

λ 9000, our estimates in Table 1 may be systematically too low; at shorter wave lengths an error of two units may readily occur. In spot spectra the Zeeman effect further increases the uncertainty. The data show, nevertheless, a tendency of these lines to weaken

TABLE 1

INFRARED SERIES OF *Mg* I IN THE SUN

n	$3^1D_2 = 15267.50$ (EP 5.73 VOLTS)			$3^3D_{3,2,1} = 13713.53$ (EP 5.92 VOLTS)			DERIVED RESULTS		
	$3^1D - n^1F^\circ$	Int.		$3^3D - n^3F^\circ$	Int.		$\Delta\nu$	$n^{1,3}F^\circ$	n^*
		Disk	Spot		Disk	Spot			
4	12083.79 8273.28	5N	.....	14877.1† 6719.9	.....	.....	(1553.4)	6994.22	3.9610
5	9255.79 10801.09	4N	3	10811.14‡ 9247.18	5N	4N	1553.91	4466.38	4.9568
6	8213.041 12172.42	4N	3N	9414.95 10618.49	5N	5N	1553.93	3095.06	5.9545
7	7691.569 12997.68	9N	9N	8736.040 11443.69	10N	5N	1553.99	2269.83	6.9531
8	7387.700 13532.29	5N	5N	8346.131 11978.31	6N	2	1553.98	1735.22	7.9524
9	7193.183 13898.23	1N	ob?¶	8098.746 12344.20	5N	5N	1554.03	1369.30	8.9522
10	7060.446§‖ 14159.52	4N	4	7930.819 12605.59	2N	2N	1553.93	1107.96	9.9521
11	6965.408‖ 14352.71	−1N	ob	7811.16 12798.68	1N	ob?	1554.03	914.82	10.9524
12	6894.89‖ 14499.50	−3N	.....	7722.64 12945.38	−1N	−2N	1554.12	768.07	11.9530
13	6841.19**‖ 14613.32	−3N	.....	masked	.....	.....	.....	654.18	12.9518
14	6799.05**‖ 14703.88	−3N	.....	masked	.....	.....	.....	563.62	13.9535

† Uncorrected laboratory value by Paschen.
‡ Not fully resolved from strong solar line λ 10810.89.
§ Blend with atmospheric line.
‖ Spot effects for five weakest singlets are confused by molecular absorption.
¶ ob = obliterated.
** Blend with weak solar line.

in spots. The apparent anomalies shown in the progression of intensity along these series are possibly analogous to the abnormal weakening noted by Fowler[4] in λ 6965 of *K* and λ 2722 of *Ca*.

[4] *Report on Series in Line Spectra*, pp. 102, 124, London, 1922.

The Photometric Atlas of the Solar Spectrum by Minnaert, Mulders, and Houtgast[5] shows that in the disk equivalent widths progress along the series, though none too smoothly. A calibration of estimated intensities for solar lines beyond λ 6600 in terms of equivalent width is in progress.

HAROLD D. BABCOCK
CHARLOTTE E. MOORE

MOUNT WILSON OBSERVATORY
PRINCETON UNIVERSITY OBSERVATORY
February 1945

NOTE ON THE FUTURE ORBIT OF COMET DELAVAN (1914V)

Following E. Strömgren's work[1] on the original orbit of near-parabolic comets, several investigators have carried perturbations backward in similar and more recent cases, always finding that, when such objects are followed far enough back from the time of perihelion, the hyperbolic excess of the eccentricity invariably becomes negative. The obvious deduction that comets are permanent members of the solar system has, however, been weakened by the case of an orbit which, though originally elliptic, was found to extend to nearly stellar distances at aphelion. A typical example is that of Comet Delavan 1914V, where the orbit was determined within narrow limits.[2]

Chandrasekhar[3] has called attention to the interest of such a case in connection with the question of the stability of binary systems and to the desirability of integrating the cometary motion *forward* so as to find whether the orbit reverts in the future to an eccentricity as nearly parabolic as when the comet approached the outskirts of the solar system. Starting from the slightly hyperbolic elements[2] deduced from the discussion of all the material available on this comet, I have computed the co-ordinates over a period of nearly twenty years, taking into account the perturbations due to the four major planets. From the values obtained for 1933, June 17 and November 14, separated by an interval of 160 days, I found, after reduction to the center of gravity of the solar system, the following dynamical elements:

$$e = 0.999861 \qquad \text{and} \qquad \frac{1}{a} = +0.000126.$$

The comet was at that time at a distance of 39 A.U. from the sun, and this circumstance reduces to a maximum of 8 per cent the further possible changes in the major axis. The elliptical character of the orbit is here much more pronounced than at the corresponding interval before perihelion. The aphelion distance now becomes about 16,000 A.U., as against 170,000 A.U. found for the same interval of time before perihelion.

G. VAN BIESBROECK

YERKES OBSERVATORY
February 28, 1945

[5] Amsterdam, 1940.

[1] *Pub. Kobenhavn*, No. 19, 1914.

[2] *Pub. Yerkes Obs.*, V, Part II, 31, 1927.

[3] *Ap. J.*, **99**, 58, 1944.

NOTE ON THE ECLIPSING BINARY SX HYDRAE

Velocities of SX Hydrae have been determined from 14 spectrograms taken by Dr. O. Struve at the Cassegrain focus of the 82-inch reflector of the McDonald Observatory. The star is unusual for the great depth of primary minimum, the light dropping from $m_{pg} = 8.6$ at maximum to $m_{pg} = 12.6$ during total eclipse. The photometric orbit has been computed by Mrs. M. B. Shapley,[1] who finds a period of 2.895697 days, semiduration of primary eclipse 0.171 day, semiduration of totality 0.021 day (uniform solution), and no detectable secondary minimum. Mrs. Shapley gives radii of 0.104 and 0.298 and an inclination of 79.1°. The relative intensities in photographic light are 0.965 and 0.035.

From 12 spectrograms taken at the Mount Wilson Observatory during 1934–1936, R. F. Sanford[2] has derived the approximate spectroscopic elements. Table 1 gives the

TABLE 1

RADIAL VELOCITIES OF SX HYDRAE

PLATE	DATE	U.T.	PHASE	R.V. (KM/SEC)		
				O	C	O−C
	1944					
CQ 3107.....	May 2	5^h48^m	65°	−100	−74	−26
3136.....	5	5 53	79	81	−79	−18
3176.....	8	6 11	93	81	−86	+ 5
3231.....	14	5 50	117	80	−90	+10
3063.....	Apr 30	3 39	165	62	−72	+10
3064.....	30	4 41	170	54	−68	+14
3066.....	30	7 07	183	69	−54	−15
3128.....	May 3	6 18	192	68	−44	−24
3144.....	6	5 44	202	26	−32	+ 6
3189.....	9	6 15	218	26	−17	− 9
3246.....	15	6 04	242	16	0	−16
3084.....	1	4 07	292	6	+ 5	−11
3085.....	1	5 25	299	13	+ 2	−15
3165.....	7	6 22	329	− 29	−13	−16

velocities from the McDonald spectrograms under the heading "O" and the velocities from Sanford's velocity-curve, at corresponding phases, under the heading "C." The phases are counted from primary minimum. In consideration of the wide and diffuse character of the lines in the spectrum of the primary, which is of HD type A3, the agreement is perhaps as close as might be expected. The McDonald spectrograms indicate a slightly smaller semiamplitude K than Sanford has given, but the evidence is inconclusive. The dispersion on the McDonald plates is 55 A/mm at $H\gamma$, as compared with 75 A/mm on Sanford's plates; however, the scatter of the velocities "O" in the table is no less than the scatter of Sanford's velocities, so that the computation of a new orbit has been deemed unwarranted.

Dr. Struve has also secured several spectrograms during eclipse, using a Schmidt $f/2$ camera with glass prisms. This combination gives a dispersion of about 75 A/mm at $H\gamma$. Several of the films taken during the partial phase have been measured for radial

[1] *Harvard Bull.*, No. 797, 1924.

[2] *Ap. J.*, **86**, 153, 1937; *Mt. W. Contr.*, No. 574.

velocity, but the scatter is too great for conclusions to be drawn regarding rotation. The character of the lines appears not to change with the phase. On one spectrogram, at phase 2°, the spectrum of the secondary component appears weakly. From comparison of the region of the D lines with the same region on a comparable spectrogram of β UMi, it is concluded that the type of the secondary is near K5. This result is in approximate agreement with the type implied by Mrs. Shapley's ratio of surface brightnesses (220 for the uniform solution). If the mass of the A3 star is $3\odot$, Sanford's mass function, together with Mrs. Shapley's inclination and radii, gives the unusual ratio of mean densities of 0.0018.

I wish to thank Dr. Struve for putting at my disposal the spectrograms of SX Hyd and Dr. Hiltner for securing several spectrograms of β UMi.

ARMIN J. DEUTSCH

YERKES OBSERVATORY
April 10, 1945

REVIEWS

"The Arc Spectrum of Iron (*Fe* I): Part I, Analysis of the Spectrum," by HENRY NORRIS RUSSELL and CHARLOTTE E. MOORE, and "Part II, The Zeeman Effect," by DOROTHY W. WEEKS. *Transactions of the American Philosophical Society*, **34**, Part II, 111–207, 1944. $2.25.

All astrophysicists interested in the identification of stellar lines or in the study of curves of growth will welcome this outstanding contribution concerning the atom that reveals the largest number of absorption lines in the sun and in most stars of spectral classes from F to M. Moreover, the paper will also be beneficial to astrophysics from a very different point of view. There are still many atomic spectra of astrophysical interest that await detailed analysis—as, for example, most of the doubly ionized metals and rare earths. There are good reasons to believe that elements such as *Cr* III, *Ni* III, and *Ti* III will eventually be found to play as important a role in stellar spectra as *Fe* III. But in recent years very few physicists have been willing to tackle this work on analysis, and newcomers in the field will have to be found either among the astronomers themselves or, preferably, among young students of spectroscopy. Analyzing a spectrum requires a good knowledge not only of theoretical spectroscopy but also of a number of semiempirical rules (dare I say tricks? Spectrum analysis has often been likened to an exalted crossword puzzle!) that do not appear clearly in the textbooks. In earlier publications Dr. Russell and his pupils have often mentioned helpful devices for estimating the behavior of certain terms, and other spectroscopists have also done their best. But, so far as I know, no example has ever been able to provide such a complete and clear exposition of the technique of analysis of a spectrum as does *Fe* I in the hands of Russell, Moore, and Weeks. Most certainly, many newcomers in the field will, in the years to come, turn to this paper for inspiration and help.

It is quite remarkable that a spectrum which has been observed for more than seventy years and whose first twenty multiplets were found as early as 1923 could still reveal 60 new terms to the authors in 1944. But the spectrum of *Fe* I, although quite orderly, is indeed a very complicated one. Moreover, the investigation has been delayed by political conditions, since a large number of terms (89 unpublished) found by Catalán—who in peacetime would have been a joint author, as Russell and Moore emphasize—could be communicated only after long delays. Additional progress will now require new observations. Laboratory sources may possibly be found that reveal more *Fe* I lines than the sources used thus far; this is apparent from the fact that the sun exhibits many more *Fe* I lines than any iron arc or spark. Moreover, the analysis is based on an approximate wave-number range of only 45,000 cm^{-1} (from λ 12000 to λ 1850). The spectral region covered may still be extended by about 10,000 cm^{-1} in the ultraviolet and by some 8000 cm^{-1} in the infrared, and such an extension may reveal a few new terms; the extension will be especially important in the infrared. But, on the whole, the *Fe* I spectrum is just about as completely analyzed as it can be or as its companions, *Fe* II and *Fe* III, are.

The authors list 4860 classified lines arising from combinations among 464 energy-levels. The wave lengths are the best available; yet the material is not homogeneous. While certain wave lengths have been determined very accurately for use as International secondary standards, a few are known only to 0.1 A. The situation is even worse for the intensities which are still in an extremely unsatisfactory state. It is to be hoped that the monograph by Russell, Moore, and Weeks will induce laboratory spectroscopists to work toward a more critical list of wave lengths, and especially toward a set of homogeneous intensities, extending the determination of *f*-values by R. B. and A. S. King.

Several of the latest additions to the analysis of *Fe* I were obtained by comparison with the previously published analyses of *Fe* II and *Fe* III or with the help of the Zeeman spectrograms. The principal low terms of *Fe* I arise from the configurations $3d^64s^2$ and $3d^74s$ and are thoroughly intermingled. The singlet terms belonging to $3d^64s^2$ were found by comparison with *Fe* III, in which the terms corresponding to $3d^6$ lie much lower than all others and have been identified with certainty. The comparison between d^7 of *Fe* II and d^7s of *Fe* I was similarly instructive. The assignment of certain low terms to a definite configuration was based on a comparison with other atoms in which the terms based on d^n, $d^{n-1}s$, and $d^{n-2}s^2$ are known. All along for the medium

and high terms, the analysis proceeds by frequent comparisons with other atoms having similar electron configurations. Obviously, the *Fe* I analysis contains, now, a wealth of information that will help in analyzing other spectra later on! Very few strong lines of *Fe* I observed in the laboratory remain unclassified, but a good many lines of low intensity or of poor wave lengths are still unclassified. The new value of the ionization potential is 7.858 volts, which is 0.02 volt higher than the previously accepted value and is probably reliable to 0.01 volt. At the end of page 113 the authors make the erroneous statement that *Fe* I is, up to the present, the only spectrum in which terms of four different multiplicities are known. Both *Cr* I and *Fe* III now share this privileged status with *Fe* I, which first came to possess this position when Catalán found the singlet terms.

A long section of the paper deals with the problem of the predicted iron lines in the solar spectrum. In 1928 Russell and Moore had discovered that many *Fe* I lines, predicted from the term values but not yet observed in laboratory sources, were actually present in the sun. On the basis of this example, it has now become common practice in stellar identification work to consider certain predicted permitted lines of abundant metals as well as the laboratory lines. The very complete data on *Fe* I, now available, have enabled Russell and Moore to make a thorough statistical discussion of the real and accidental coincidences of predicted and solar lines. Their discussion sets an example that should be followed in all problematical identification cases, especially when molecular bands are involved. The evidence obtained is quite decisive: there should be some 1200 lines of iron which, though not yet produced in the laboratory, should be observable in the solar spectrum between λ 2975 and λ 6600. A table is given of those predicted lines for which the evidence of presence in the region from λ 2980 to λ 11000 was adjudged to be good or fair—1254 in all. Doubtless, some accidental coincidences are present, and some real iron lines have been omitted in the rather drastic process of exclusion. Moreover, many lines (some 300 between λ 2975 and λ 6600) have perforce been omitted, owing to masking in the sun. But, with these limitations in mind, any astrophysicist will often be greatly helped by the table of predicted lines present in the sun, since the great majority of the tabular lines must be real.

The Zeeman spectrograms, obtained with the Bitter electromagnet at the Massachusetts Institute of Technology and studied by Miss Weeks, have been of great help in the analysis. The field strengths ranged from 83,000 to 87,000 oersteds; and the plates were measured upon Harrison's automatic measuring machine, which recorded on a film the wave lengths and relative photographic intensities of the components. Miss Weeks gives a table of the observed Zeeman patterns for 1038 lines and the g-values deduced from each, and another table containing the g-values for all levels for which they have been determined. A detailed comparison of observed and theoretical g-values is included. Deviations from theory, because of perturbations, are discussed. As is well known, perturbations may be anticipated between neighboring levels of the same parity and with the same J, irrespective of multiplicity, L-value, and electron configuration. In the absence of Zeeman data, perturbations are indicated by the mutual repulsion of the levels involved (interrupting the usual sequence of components of these terms) and by strong intersystem combinations. Similarly, the g-values are also conclusively affected by perturbations.

The authors must be congratulated on having combined in this memoir an abundant source of data precious to astrophysicists and a general sketch of the analysis procedure which will be an inspiration to newcomers in this field. The American Philosophical Society has spared no effort in making the monograph a beautiful piece of printing; indeed, the tables are very easy to read, compared with most spectroscopic papers. Only four minor misprints have been found in the course of work based on the tables: the word "components" is misprinted in the table headings on pages 189 and 201, and the two wave lengths λ 3820.572 (p. 155) and λ 4638.687 (p. 175) should be replaced by λ 3827.572 and λ 4628.687, repectively.

P. SWINGS

Pasadena, California

Stellar Variability, Vol. II: *Eclipsing Variables*. By D. J. MARTINOFF. (In Russian.) Moscow and Leningrad: ONTI, 1939. Pp. 150. R. 4.25.

Although this book was originally written in 1935 and 1936 and was revised in 1939, it has only recently arrived in this country. The author intended it to form the second volume in a series of monographs on variable stars by B. W. Kukarkin, P. P. Parenago, W. P. Zessewitsch, and

D. J. Martinoff. The first volume, by Kukarkin and Parenago, was devoted to the physical variables and was published in 1937. The third volume will treat a number of practical questions encountered in the study of variable stars. Martinoff's book is an introduction to the study of eclipsing variables. In the first three chapters it presents the theory of orbits of eclipsing stars and a number of new diagrams to illustrate the influence of the principal elements upon the light-curve. The treatment follows the classical theory by Russell. It does not reproduce the various tables required in actual computations (these will presumably be given in the third volume of the series) but attempts to clarify the essential points upon which the theory depends. Although much recent work in this field has not been included and the discussion is not complete in all respects, the book constitutes an unusually lucid account of the more elementary aspects of the theory and is, therefore, especially valuable as a textbook for students. Chapter iv deals with periodic and secular changes in the periods of the eclipsing variables. Chapter v, on the physical characteristics of eclipsing variables, contains some new material, as well as material published by Russian astronomers in recent years, not all of which has been available to readers who are unfamiliar with the Russian language. The last chapter, on the origin and evolution of close binaries, is quite short and limited in scope.

Although the Russian language constitutes a barrier to the effective use of this book outside of Russia, it must be recognized that there is nothing even approaching it in the English language. The original articles written by Russell and by Russell and Shapley, published in 1912, in Volumes **35** and **36** of this *Journal*, are now out of print. There is a condensed account of the simplest case of Russell's theory in Aitken's book, *The Binary Stars* (2d ed.; New York: McGraw-Hill Book Co., 1935). But there are no textbooks which treat this theory in such a manner as to enable the student to start practical work on eclipsing variables without an enormous waste in time and many sad experiences. It is important that we should realize our lack of advanced textbooks in astrophysical subjects. The astrophysical monographs sponsored by the *Astrophysical Journal* are intended to relieve this need; but there is, as yet, not enough support for this venture on the part of readers and potential authors. The principal difficulty consists in the fact that our universities and research institutions feel no responsibility in the matter of textbooks, while commercial publishers know that they cannot make a profit from advanced books and therefore prefer to publish elementary texts. Since 1936, when the late B. P. Gerasimovič edited two volumes written by a number of leading Russian astronomers,[1] B. A. Vorontzov-Velyaminav has published a *Textbook of Practical Astrophysics*,[2] 648 pages in length, and a *Collection of Problems in Astronomy*,[3] comprising nearly 200 pages—a total of 1,246 questions and their answers, together with tables, reproductions of stellar spectra, etc. Not available to me are a *Textbook of Stellar Astronomy*, by P. P. Parenago, and a book on *Variable Stars and Methods for Observing Them*, by Parenago and Kukarkin. To the extent that future progress in astronomy depends upon the training of advanced students, the Russians will have a marked advantage over other nations because of their policy to produce the necessary books. Perhaps their success in this respect will be tempered by the careless external appearance of the books: the paper is very poor, the illustrations of photographs are almost useless, and even the writing is sometimes defective (though not in the volume under review).

O. Struve

Yerkes Observatory

The Mathematics of Physics and Chemistry. By Henry Margenau and George Moseley Murphy. New York: D. Van Nostrand Co., 1943. Pp. xii+581. $6.50.

The subject matter of this book covers an unusually wide range of topics. In fact, the authors' intentions have been to present a fairly complete account of the basic mathematical techniques in modern physics and chemistry. The exposition follows a moderate level of mathematical rigor with an occasional omission of proofs. A number of problems are included.

An account is given of ordinary differential equations, with frequent applications to interesting physical problems. Special emphasis is given to second-order equations, and particularly to the common special equations in physics, together with the elementary properties of their solu-

[1] Reviewed in this *Journal*, **86**, 106, 1937.

[2] Moscow and Leningrad: ONTI, 1940.

[3] Moscow and Leningrad: ONTI, 1939.

tions. The classical partial differential equations likewise find a place in the text with applications to eigenvalue problems. Good elementary treatments of vector analysis, matrices, integral equations, and group theory are given. One chapter is devoted to numerical calculations involving interpolation, numerical integration, the theory of errors, and other questions.

In separate chapters are included topics with more specific reference to definite physical subjects. They are: (1) "Thermodynamics," (9) "Mechanics of Molecules," (11) "Quantum Mechanics," and (12) "Statistical Mechanics." In these chapters some physical background is given, in addition to the purely mathematical subject matter. The most extensive of these is the one devoted to quantum theory. Here, following a postulatory introduction, a large variety of the fundamental problems find a treatment.

The book is remarkable in the high level of clarity and general scientific quality attained in the treatment of so extensive a range of topics. One should note that this range includes much that is not found in most texts of comparable purpose and level. For these reasons it should prove a useful reference volume, in addition to its primary purpose as an introductory textbook. However, one may note that, precisely because of the book's conciseness, the student may have difficulty in appreciating the physical aspects of the subjects without a good deal of additional material in the form of supplementary reading or lectures, or without prior knowledge.

L. G. HENYEY

Yerkes Observatory

Tables for Converting Rectangular to Polar Co-ordinates. By J. C. P. MILLER. New York: Dover Publications, 1939. Pp. 16. $0.75.

This useful table was published in 1939 and is recommended for such problems as the transformation of harmonic constants a and b, obtained by harmonic analysis, to amplitude c and phase angle ϵ, in accordance with the relation

$$c \sin (nt + \epsilon) = a \sin nt + b \cos nt ,$$

or the evaluation of the magnitude and direction of a vector from rectangular components and the conversion of complex numbers from the form $x + iy$ to the form $re^{i\theta}$. The tables are intended for use with a calculating machine or a slide rule.

INDEX TO VOLUME 101

INDEX TO SUBJECTS

INDEX TO AUTHORS